Thermal and non-thermal properties of the diffuse plasma in galaxy clusters

Rémi Adam

INSTITUT POLYTECHNIQUE DE PARIS

Habilitation à Diriger les Recherches

Thermal and non-thermal properties of the diffuse plasma in galaxy clusters

Habilitation à Diriger les Recherches de l'Institut Polytechnique de Paris
préparée à l'École polytechnique (Laboratoire Leprince-Ringuet)

École doctorale n°626 École doctorale de l'Institut Polytechnique de Paris (EDIPP)
Spécialité: Physique

Soutenue à Palaiseau, le 2 décembre 2022, par

Rémi Adam

Composition du Jury :

Nabila AGHANIM Directrice de Recherches, Institut d'Astrophysique Spatiale, Orsay	Rapportrice
Céline COMBET Directrice de Recherches, Laboratoire de Physique Subatomique et de Cosmologie, Grenoble	Rapportrice
Federica GOVONI Ricercatore, Osservatorio Astronomico di Cagliari, Selargius	Rapportrice
Chiara FERRARI Astronome, Laboratoire Lagrange (OCA), Nice	Examinatrice
Miguel SÁNCHEZ-CONDE Profesor Contratado Doctor, Instituto de Física Téorica (UAM-CSIC), Madrid	Examinateur

Contents

1 Introduction

The standard model of cosmology gives us a coherent description of the evolution of the Universe since the Big Bang. Although several fundamental questions remain unanswered, such as those about the nature of dark matter, the origin of the accelerated expansion of the Universe, or the source of the primordial fluctuations in an overall homogeneous Universe, the big picture of the history of the Universe and large scale structure formation is now well understood. This tremendous achievement has been made possible thanks to major cosmological experiments that have probed the Universe at various epochs, using complementary observational means. In this sense, the last ten years or so have been astonishingly prolific.

In addition to fundamental physics issues, the last decade of observations has made it clear that pushing the limits of observational cosmology would require dealing simultaneously with complex astrophysical processes associated with galaxy evolution and the formation of large-scale structures (and also sometimes foregrounds). This is not only because ignoring these aspects would potentially lead to the misinterpretation of cosmological results, but also because this physics has proved amazingly rich in itself and it should be understood in great detail if one wants to have a complete understanding of the evolution of our Universe[1].

It is in this context that I pursued my research work over the past ten years, contributing to understanding the formation of large-scale structures at different epochs in the history of the Universe. The core of my research has been concentrated on the observations of the cosmic microwave background (CMB), the use of galaxy clusters to test cosmological models, and the study of galaxy clusters to understand the astrophysical processes involved in large-scale structure formation. This document focuses on the physics of the diffuse gas in galaxy clusters, leaving aside the observations of the CMB and cluster cosmology. The following sections should put this choice into the more general context of my past work and summarize the scientific context.

1.1 Background

I started my Ph.D. in October 2012 at the *Laboratoire de Physique Subatomique et de Cosmologie* (Grenoble, France). My work was divided along two main axes, both using data at millimeter wavelengths: 1) the measurement of the CMB polarisation with the *Planck* satellite, and in particular

[1] I.e., cosmology is certainly not just about banana plots; it would be too sad!

the treatment of systematic effects on large angular scales, with the ultimate goal of contributing to constrain cosmic inflation models and the epoch of reionization; 2) the development of the New IRAM KIDs Array (NIKA) camera at the *Institut de Radio Astronomie Millimétrique* (IRAM) 30-meter telescope and the analysis of its first observations of galaxy clusters.

After my defense, I moved to the *Laboratoire Lagrange* at the *Observatoire de la Côte d'Azur* (Nice, France) to complete my first post-doctorate, from October 2015 to October 2017, thanks to a fellowship from the *Centre National d'Étude Spatiales*. I started to work on the preparation of the *Euclid* space mission, in the optical/near-infrared, contributing to the development of the galaxy cluster cosmological probe. I was mainly involved in the estimation of the selection function via the characterization of the performances of several cluster finder algorithms, which were applied to simulated *Euclid*-like data. In parallel, I constructed and lead the multi-wavelength analysis of a sample of galaxy clusters observed with NIKA. This sample constitutes a pilot project that helped us prepare the large galaxy cluster observing program with the final camera, NIKA2.

I joined the *Centro de Estudios de Física del Cosmos de Aragón* (Teruel, Spain) in November 2017 for a second post-doctorate. While continuing to work in the *Euclid* collaboration, I got involved in the development of a new statistical tool to extract cosmological information from large-scale structure galaxy surveys, known as the angular redshift fluctuations. At the same time, I also continued working on cluster observations with NIKA and NIKA2 including the follow-up of X-ray detected clusters as part of the XXL collaboration.

It is in November 2018 that I joined the *Laboratoire Leprince-Ringuet* (Palaiseau, France), after being recruited at the *Centre National de la Recherche Scientifique*, to work on the preparation of the Cherenkov Telescope Array (CTA). This implied a significant change in my research topics, moving from observational cosmology to γ-ray astronomy, research fields that are a priori very distinct with limited interconnections. However, γ-ray astronomy has been going through a phase transition for several years, migrating from an operation close to that of particle physics to a fully-fledged sub-field of astronomy. My arrival took place at a time when more and more connections were possible, and even necessary, between the γ-ray domain and other branches of astronomy, including cosmology. I used this opportunity to take a leadership position in one of the key science projects of CTA that is dedicated to the understanding of particle acceleration at the cluster scale. Meanwhile, I also continued to invest in projects from before my recruitment, in particular in NIKA2, by exploiting new synergies between my previous and new activities.

Most of my research has been carried out in the context of large international collaborations: *Planck*, NIKA/NIKA2, *Euclid*, CTA, and XXL. In these collaborations, I took the opportunity to propose, define and lead various projects and contributed to the coordination of different working groups. Thanks to the stimulating environments I encountered, I acquired expertise in the use of astronomical data across the entire electromagnetic spectrum, which is nowadays a strong advantage, especially when studying galaxy clusters.

According to the french law, the *habilitation à diriger des recherches* (i.e., the diploma related to the present document) provides recognition of a high scientific level, the capacity to perform original research in a scientific field, the aptitude to master a research strategy in a scientific or technological domain that is sufficiently large, and last but not least, of the ability to supervise young researchers[2]. Although the core of the work presented here will focus on the scientific part, it is important for me to express my personal view regarding the last point, even if very briefly, because this is one of my main motivations for writing such a document.

The amount and quality of the fruits that are produced by a plant, let's say tomatoes for example, not only depend on the quality of the seed itself but also enormously on that of the soil (in which

[2] See *Arrêté du 23 novembre 1988 relatif à l'habilitation à diriger des recherches.*

the plant will find the necessary moisture and nutrients) and the climate. I believe that the situation is similar for students and Ph.D candidates. The difference is that the soil and the climate are replaced by the supervisor(s) and the local group (and the laboratory to some extent). We can also note that not all plants feel good and produce well in the same kind of soil and climate, but it does not necessarily mean that some are better than others. We should thus be careful to apply selection criteria that correspond indeed to the quality we want to develop. Beyond this analogy, which we could certainly push much further, it is clear that supervising Ph.D. candidates is a huge responsibility for at least two main reasons: 1) the future academic life of the students highly depends on their thesis work, but at the same time, a lot of randomness and chance is involved in the choice of where and with whom a student will end up doing a Ph.D. (i.e., the tomato seed does not truly make an informed choice of where it lands); 2) it is likely that students will not realize if something goes wrong (or at least does not go great) until a long time after the problems start, because they cannot have perspective on their own thesis which they undertake only once. Additionally, the fact that pursuing a stable academic career is getting more and more difficult nowadays is certainly increasing the amount of responsibility associated with supervision.

Having this in mind, I supervised eleven students, from license 2 to master 2, in the context of internships. In each case, I did my best to integrate the students into the respective teams and collaborations and make them work on hot research topics. I tried as much as possible to define the subjects to address specific research topics and technical issues so that the students could benefit from their internship as much as possible. In many cases, this allowed the students to contribute to publications related to their internship work. I also contributed to supervising two Ph.D. candidates for some part of their thesis, although I have not yet been the direct supervisor of any Ph.D. candidate. At the time of writing, these former students and Ph.D. candidates are now doing post-doctorates and Ph.Ds., or have got permanent research or engineering positions. Some others are still students, and I lost track of a few of them. The scientific results reviewed here will include most of the publications and works to which the students and Ph.D. contributed.

In this document, I decided to focus on the contributions that I made to better understand the physics of the diffuse intra-cluster plasma, thus leaving aside aspects of my work related to the CMB polarization or cluster cosmology in the optical / near-infrared. This choice is motivated by the fact that this topic corresponds to my longest-term research contribution since I started my Ph.D., via the use of resolved millimeter wavelength observations. Additionally, my more recent work in CTA has led me to contribute to the understanding of particle acceleration at the cluster scale and the non-thermal physical processes involved in the intra-cluster plasma. In fact, the interplay between the thermal and the non-thermal physics is now becoming clearer. As these connections are being established, studying jointly the various components at play is becoming essential to fully characterize the intra-cluster medium physics and the formation of galaxy clusters and large-scale structures. With it, and the development of future instruments, new opportunities are being brought to light. Therefore, I believe this choice is particularly timely and is also influenced by the research direction that I anticipate pursuing in the following years.

1.2 Introduction to the tempestuous life of galaxy clusters and their intra-cluster medium

About half a century ago, X-ray observations showed that clusters of galaxies were pervaded by a diffuse hot gas phase. This discovery complemented previous findings in the optical, which established that galaxies were assembled in clusters themselves. Since that time, colossal accomplishments were realized, both from theory and observations, providing the means to address the

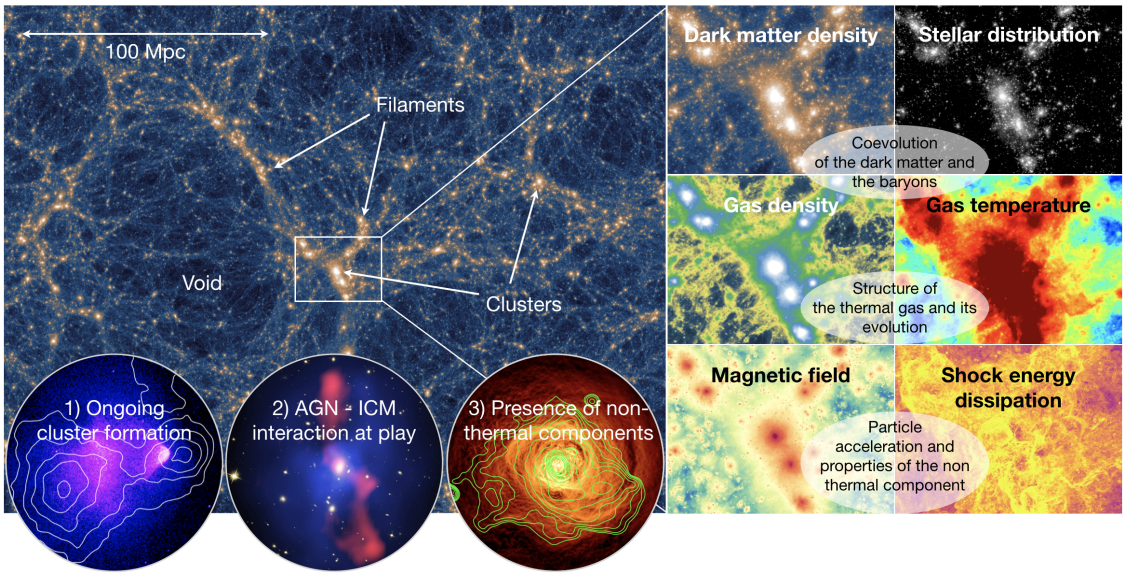

Figure 1.1: Visual summary of the scientific context. Slice of the IllustrisTNG (TNG300-1) cosmological magnetohydrodynamical simulation made with the IllustrisTNG Explorer tool. It corresponds to the nearly full box (300 Mpc across), with a depth equal to one third of the entire volume, at $z = 0$ (https://www.tng-project.org/). **Left panel**: dark matter distribution of the nearly full box. **Right panels**: zoom of the most massive halo ($M_{200} = 1.5 \times 10^{15}$ $M_\odot$) showing the dark matter, stellar distribution, gas density, gas temperature, gas magnetic field strength and shock energy dissipation. **Bottom left subplots**: illustration of relevant physical processes at play in clusters. 1) Merger event that affects the structural properties of clusters (*Chandra* X-ray view of the bullet cluster with weak lensing contours, Markevitch 2010); 2) AGN outburst interacting with the ICM (this image of the inner 700 kpc of MS0735.6+7421 combines X-ray in blue, I-band in white, and radio wavelengths in red, McNamara et al. 2009); 3) Illustration of the presence of a non-thermal component including turbulence, CR and magnetic field (Jansky Very Large Array synchrotron emission on top of the filtered X-ray image of the Perseus cluster core, Gendron-Marsolais et al. 2017).

physics of galaxy clusters and understand their intra-cluster medium (ICM). Nowadays, we know that galaxy clusters form at the intersection of cosmic filaments. They are excellent tracers of matter density peaks. Consequently, they provide incomparable astrophysical laboratories, they grant one of the most important ways to test cosmology and are used to test fundamental physics.

The observational properties of galaxy clusters are the consequence of their hierarchical formation, driven by gravitational collapse. In the first order, they are completely characterized by their masses and redshift, as self-similar objects. Yet, galaxy clusters host complex physical processes related to galaxy formation and gravity-induced dynamics. Indeed, they grow via the merging of sub-clusters and by accretion of the surrounding material. During these energetic events, the kinetic energy is dissipated into heat through turbulence and shocks but also contributes to amplifying the magnetic fields and accelerating cosmic rays (CR) up to very high energy. Additionally, the feedback from active galactic nuclei (AGNs) is expected to release energy in the ICM directly.

Whereas our global understanding of ICM physics has strongly improved during the last 10 years or so, many new issues have arisen regarding the thermal and non-thermal properties of the cluster diffuse gas phase and the way it is interconnected with galaxy and large-scale structure formation. This section aims to provide a very general overview of the recent theoretical and observational advances in understanding the ICM physical properties. Figure 1.1 presents a visual summary and Table 1.1 gives the main typical properties of the ICM. An excellent book gathering relevant reviews that fit this topic well may be found following Bykov et al. (2019).

Table 1.1: Typical main properties of the ICM for a massive ($\sim 10^{15}$ $M_\odot$) local cluster. They are meant to provide an order of magnitude indication and some quantities may show a strong radial dependence.

Mass budget				Energy budget				ICM global properties			
Dark matter	ICM	Stars	CR	Thermal	Kinetic	CR	Magnetic field	T	n_e	B	$\beta_{\rm pl}$
85%	12%	3%	10^{-6}%	83%	15%	1%	1%	1-10 keV	10^{-2}-10^{-5} cm^{-3}	1 μG	10^2-10^3

Note: CR are the cosmic rays ; T is the gas temperature ; n_e is the thermal electron density ; B is the magnetic field strength ; $\beta_{\rm pl} \equiv P_{\rm th}/P_{\rm mag}$ is the thermal to magnetic pressure.

1.2.1 Galaxy clusters as the nodes of the cosmic web

Before focusing on the ICM properties themselves, let us first consider clusters as objects embedded in the cosmic web, in a cosmological context.

1.2.1.1 From primordial fluctuations to large-scale structures

The last two decades of cosmological observations have revealed that our Universe is consistent with being very close to flat, dominated by dark energy (69%) and that the matter is mostly in the form of a cold and dark component called dark matter (26%). The remaining 5%, in the form of ordinary baryonic matter, is our (nearly) only observational window to the Universe. See Planck Collaboration et al. (2020) for recent results and a complete overview.

The matter distribution itself is highly structured, forming a network of walls, filaments, and nodes separated by large voids (Figure 1.1; Jones et al. 2009; Huchra et al. 2012). The formation of these large-scale structures was driven by the gravitational collapse of tiny primordial density perturbations that are presumably related to quantum fluctuations generated in an early inflationary phase (see Lyth and Riotto 1999; Liddle and Lyth 2000, for reviews).

This picture is supported by a solid theoretical framework (Peebles 1993; Peacock 1999) and various observational probes that are sampling different epochs of the history of the Universe. Among the main recent results are those obtained via CMB anisotropy measurements (Hinshaw et al. 2013; Planck Collaboration et al. 2020), the clustering of galaxies (Alam et al. 2017; Ata et al. 2018), type Ia Supernovae as standard candles (Betoule et al. 2014; Scolnic et al. 2018), weak lensing as a tracer of the mass distribution (Kilbinger et al. 2013; Köhlinger et al. 2017; Hamana et al. 2020), and galaxy clusters (see hereafter). These probes, among others, played a key role in establishing the concordance cosmological model, but have also revealed possible discordance and tensions[3].

1.2.1.2 As spiders on their web

Galaxy clusters occupy the node positions in the cosmic web. They are often referred to as the largest gravitationally bound structures in the Universe, forming peaks in the matter density field with a density contrast up to 10^5. Clusters assemble via smooth accretion of the surrounding material, but also via the merger of smaller groups (Voit 2005; Kravtsov and Borgani 2012), leading to roughly virialized halos. Indeed, structures are thought to have grown hierarchically so that galaxies were formed first and assembled into groups and clusters from redshift $z \sim 3$. This picture is strongly supported by the observations of distant star-forming galaxies aggregating in

[3] Although the coherence between the different cosmological probes is astonishing overall, a significant discrepancy has been observed lately between the values of the Hubble constant, H_0 (i.e., the current Universe expansion rate), inferred via the CMB fluctuations and via local measurements, e.g., based on type Ia Supernovae (Verde et al. 2019, for details). Other tensions have also been actively discussed, such as those concerning the amplitude of matter fluctuations.

proto-clusters that are likely the progenitors of massive nearby clusters (Casey et al. 2015; Wang et al. 2016; Oteo et al. 2018). Nonetheless, this early formation phase remains largely unknown and should be explored in the future with large high-z samples (Euclid Collaboration et al. 2019) and dedicated follow-ups.

Most of the mass of a cluster is in the form of dark matter ($\sim 85\%$) and the baryonic content is dominated by the ICM ($\sim 12\%$). Galaxies, typically a few hundred, account for the remaining ($\sim 3\%$). The cluster mass function is continuous, reaching a few times 10^{15} $M_\odot$ at $z = 0$, but clusters are often referred to as objects with masses larger than 10^{14} $M_\odot$ and smaller objects are considered as groups. As extended structures ($\sim$ Mpc), slowly fading out in the outskirts, the extents of clusters are defined via their enclosed spherical overdensity relative to the background Universe[4]. However, the way that they connect to the cosmic web involves complex physics and other relevant radii have been identified (e.g., splash-back or accretion radii, More et al. 2015; Anbajagane et al. 2022).

1.2.1.3 The self-similarity of galaxy clusters

While the full treatment of the hierarchical structure formation can only be numerical (e.g., Efstathiou et al. 1988, for early developments), it was soon realized that it is possible to infer statistical cluster properties under simplifying assumptions (Gunn and Gott 1972; Fillmore and Goldreich 1984; Bertschinger 1985). The large-scale matter distribution is well-described by a random Gaussian field, in which fluctuations are characterized by the amplitude and spectral index of the power spectrum over some spatial scales, following scale-free initial conditions. In these conditions, assuming a single spherical gravitational collapse (driven by dark matter) with no extra energy input into the ICM and no preferential scale involved, the density fluctuations amplitude should be a power-law function of the scale, and thus of mass. The transition at which fluctuations become non-linear when reaching a density contrast of unity introduces a characteristic scale that is a power-law function of redshift, given the mean background density evolution.

Collapsed halos are thus expected to be scaled versions of each other once renormalized accordingly in mass and redshift (i.e., self-similar; see Kaiser 1986, for the complete framework). Their observational properties should be, at first order, fully characterized by their masses and redshifts, reflecting the cluster's hierarchical formation under gravitational collapse. The results from this self-similar model have been confirmed by hydrodynamical simulations when discarding any non-gravitational heating or dissipative effects (see Borgani and Kravtsov 2011, for a review).

Yet, clusters are also affected by complex physics due to the interplay of the gas, galaxies, and dark matter. These processes, neglected at first order, should affect cluster properties to some extent.

1.2.1.4 Clusters as seen through their multi-wavelength observables

Thanks to their multiple components, galaxy clusters produce observable signals across the electromagnetic spectrum. Observations in the visible were historically used to detect and study clusters thanks to their galaxy population (latter complemented by infrared; Gal 2006, for a review). Increasing attention is now being focused on the use of the gravitational lensing of background galaxies to infer the total mass of the cluster, i.e., one of the key cluster parameters, thanks to major advances in optical facilities (Umetsu 2020)[5]. The ICM emits diffuse Bremsstrahlung radiation in

[4]The mass is defined as $M_\Delta = \rho_\Delta \frac{4\pi}{3} R_\Delta^3$, with R_Δ the corresponding enclosed radius and ρ_Δ defined as $\Delta\rho_c(z)$ or $\Delta\rho_m(z)$, based on the critical density or the mean matter density at the cluster's redshifts, respectively. The value of Δ is often taken as 500 or 200, and R_{200} is expected to approximately correspond to the virial radius.

[5]Gravitational lensing also allows to probe early stages of galaxy formation by using clusters as natural telescopes.

the X-ray (Rybicki and Lightman 1986) and leaves an imprint on the CMB that is observable in the millimeter range via the Sunyaev-Zel'dovich effects (SZ; i.e., the inverse Compton scattering of clusters' energetic electrons on the CMB, Sunyaev and Zeldovich 1970, 1972), providing direct probes of the thermal gas. The radio emission traces CR electrons (CRe) and magnetic fields (van Weeren et al. 2019). CR protons (CRp) are also expected. They should lead to γ-ray emission due to interactions with the ICM, but this signal has remained elusive so far (Wittor 2021).

Whatever the science goals, the construction of cluster catalogs using survey data is a fundamental step. In this sense, X-ray, SZ, and optical observations (and possibly radio shortly) have played a key role in modern cluster astrophysics and cosmology, establishing state-of-the-art detection techniques (Mantz et al. 2019). Catalogs are generally built from single waveband observations. However, because of the multi-wavelength complementarity, there is now rising interest in using them jointly to improve detection efficiency and obtain cleaner catalogs with better-understood selection functions and reduced systematic effects (e.g., Tarrío et al. 2018).

1.2.1.5 Cluster cosmology and fundamental physics

Galaxy clusters are privileged objects to study the growth of cosmic structure and the expansion history of the Universe (Allen et al. 2011). The most widely used cluster-based cosmological probe consists in comparing the abundance of halos predicted in a given cosmological scenario with the one observed, as a function of mass and redshift. This is challenging as it requires an accurate model (e.g., Bocquet et al. 2016; Ondaro-Mallea et al. 2022), a well-characterized selection function, and accurate mass measurements (Pratt et al. 2019). Recently, a tension was reported between cluster counts and CMB measurements on the key parameter σ_8, which measures the amplitude of the matter fluctuations within 8 Mpc (Planck Collaboration et al. 2014b, 2016d). Many solutions were proposed to solve this issue (e.g., Sakr et al. 2018), including new physics, but systematic effects in the masses or detection may be responsible. Many other cluster-based complementary probes were used to constrain cosmology recently. These includes the angular power spectrum of the SZ effect (Planck Collaboration et al. 2014c, 2016f), gas fraction measurements (Mantz et al. 2022), distance measures combining X-ray and SZ data (Bonamente et al. 2006; Kozmanyan et al. 2019), cluster clustering (e.g., Marulli et al. 2018; Lindholm et al. 2021), or measurement of the CMB temperature evolution (e.g., Hurier et al. 2014). The collision velocity of merging clusters may give another probe (Bhattacharya and Kosowsky 2007), but its measurement remains challenging.

Clusters are recognized as unique fundamental physics laboratories. For instance, they may be used to search for dark matter decay or annihilation signatures (Bulbul et al. 2014; Sánchez-Conde et al. 2011; Moliné et al. 2017). Alternatively, merging clusters are excellent targets to constrain the nature of dark matter (Clowe et al. 2006) and its possible self-interaction (Tulin and Yu 2018). Mass profiles are also sensitive to this physics (Newman et al. 2013b,a), but baryonic effects are difficult to control. The mass-observable relations, the cluster structural properties and dynamics, and their abundance are also sensitive to the nature of gravity (Cataneo and Rapetti 2018).

Today, clusters are well-established as rich and unique probes for cosmology and fundamental physics. However, this requires accurate modeling of their observational properties, which implies understanding their astrophysics in great detail, including the ICM and galaxy formation.

1.2.2 On the physical properties of the hot gas

The ICM is essentially thermal. Additionally, structure formation implies bulk and turbulent motions, which should contribute to the pressure support at 10-15%. The presence of CR and magnetic fields is also established, but they should be subdominant in terms of energetics. This section

focuses on the structural properties of the hot gas, its co-evolution with dark matter, and galaxy formation. The next section will further consider interconnections with the non-thermal components.

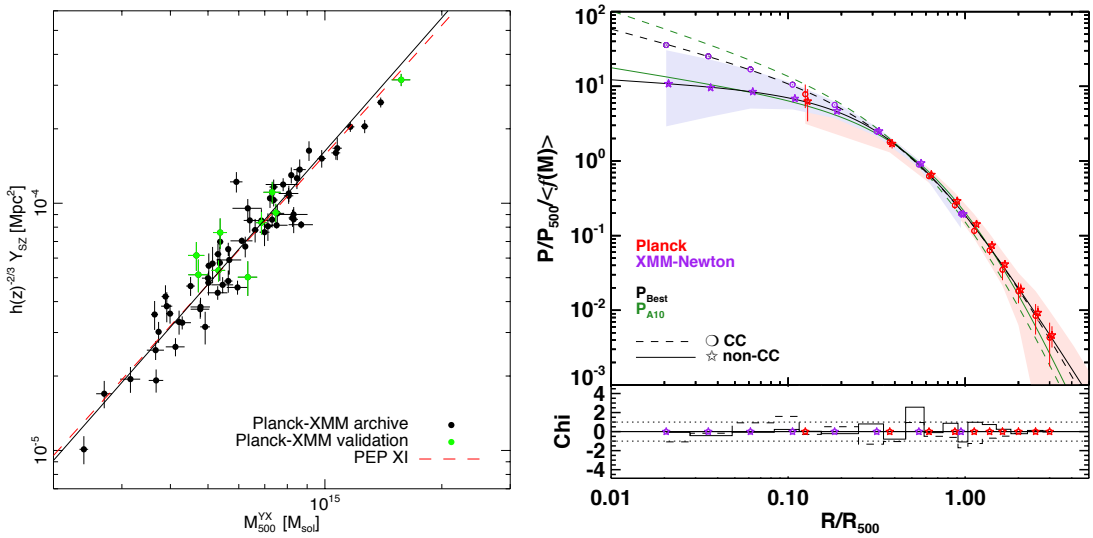

Figure 1.2: **Left:** calibration of the SZ flux - mass scaling relation used for *Planck* 2013 cluster counts cosmological constraints. Extracted from Planck Collaboration et al. (2014b). **Right:** Universal pressure profile derived from *Planck* clusters and *XMM-Newton* data. Cool-core (circles) and non-cool-core (stars) systems are presented independently. The comparison to the results from Arnaud et al. (2010) is given in green. Extracted from Planck Collaboration et al. (2013a).

1.2.2.1 Thermodynamical characterization of the ICM

The ICM gets established during the early phase of cluster formation, at $z \sim$ 2-3, and is continuously fed by the in-falling gas whose kinetic energy is converted into heat, essentially via shocks and turbulent cascades. This is expected according to numerical simulations (Bennett and Sijacki 2020) and observational evidence for virialized systems up to $z \sim 2$ is now available (Mantz et al. 2018; Gobat et al. 2019; Mantz et al. 2020; Andreon et al. 2021). Because of the high depth of the potential wells of the cluster, the gas is heated to $T \sim$ 1-10 keV and is fully ionized. It is tenuous, with electron and proton densities $n_e \simeq n_p \sim 10^{-2}$ cm^{-3} in cluster cores and drops rapidly in the outskirts so that the plasma is optically thin with a mean free path of a few kpc and behaves as an ideal gas. The atmospheres of clusters should reflect the helium abundance of the Universe, although helium sedimentation may be significant (Ettori and Fabian 2006; Bulbul et al. 2011). The plasma is nonetheless enriched in heavy elements ($Z \sim 0.3$ Z$_\odot$, Werner et al. 2013).

The hot ICM is subject to two main radiation mechanisms: 1) thermal Bremsstrahlung emission in the X-rays (Sarazin 1988; Böhringer and Werner 2010); and 2) the SZ effects observable in the millimeter (Birkinshaw 1999; Mroczkowski et al. 2019). The X-ray surface brightness, $S_X \propto \int \sqrt{T} n_e^2 d\ell$, probes mainly the line-of-sight integrated electron density. X-ray spectroscopy is used to infer the gas temperature and metallicity and may be sensitive to gas motions if sufficient spectral resolution is available. We can distinguish the thermal SZ (tSZ) effect, due to the thermal electron pressure, from the kinetic SZ (kSZ) effect, arising from the CMB Doppler shift induced by the motion of the cluster electrons. The kSZ effect is subdominant unless the gas velocity reaches $\sim$1000 km/s. The tSZ surface brightness is related to the gas pressure, $\Delta I_{\rm tSZ} \propto \int P_e d\ell$, and to the gas momentum for the kSZ, $\Delta I_{\rm kSZ} \propto \int v_z n_e d\ell$. The SZ effects surface brightness are not affected by redshift dimming since they are CMB spectral distortions. While X-ray observations have been

routinely used since the 1980's (Jones et al. 1979), tSZ observations only reached maturity in the last decade (despite early detection in the 1970s, e.g., Birkinshaw et al. 1984) and the kSZ effect was only detected recently (Hand et al. 2012; Sayers et al. 2013b; Adam et al. 2017b).

X-ray and SZ data are now commonly used to infer the ICM thermodynamics, which is fundamental to understanding cluster formation (Nagai et al. 2007; Dolag et al. 2009). Because they probe the same component in a complementary way, the joint use of X-ray and SZ is now recognized as extremely valuable (Adam et al. 2015, 2017a; Eckert et al. 2017a; Ruppin et al. 2018). They measure the thermal density, temperature, and pressure directly, but can also infer other fundamental quantities. For instance, the entropy, defined as $K_e = P_e n_e^{-5/3}$, measures the energy gain or loss in the ICM, thus recording the thermodynamical history of cluster formation (Voit et al. 2005; Cavagnolo et al. 2009; Pratt et al. 2010). The total mass profile can be measured assuming spherical symmetry and hydrostatic equilibrium (HSE). The HSE bias corrects the HSE masses relative to the true total mass. It is expected to be $b_{\rm HSE} = 1 - M_{\rm HSE}/M_{\rm true} \simeq 0.2$ (Planck Collaboration et al. 2014b). It has been extensively discussed in the literature recently, either using real data or numerical simulations (Hoekstra et al. 2015; Smith et al. 2016; Miyatake et al. 2019; Eckert et al. 2019; Biffi et al. 2016; Ansarifard et al. 2020), but its complete characterization still represents an important open issue, especially in light of the tension between cluster and CMB cosmology. The ICM also offers unique access to the baryon content of clusters (Chiu et al. 2018; Akino et al. 2022) allowing the gas fraction to be inferred and used to test cosmology.

1.2.2.2 Beyond self-similarity: the ICM as a rich astrophysical playground

The ICM is the playground for many astrophysical processes. They may be divided into gravitationally induced dynamics, plasma physics including radiative, dissipative, or transport processes, and the interaction between galaxies and the ICM. All of them are somehow interconnected and may lead to deviation from self-similarity. Here we discuss some of the most relevant processes.

Gravitationally induced dynamics Cluster formation is a 3-dimensional process. It involves asymmetric accretion and the merging of sub-structures preferentially along filaments. This drives ICM bulk and turbulent motions, it induces shocks and adiabatic gas compression, which eventually inject heat into the ICM (ZuHone and Su 2022). Sloshing can also give rise to turbulence and mixing that eventually heat cluster cores (ZuHone et al. 2010). Additionally, the gas may be preheated before accretion (Kaiser 1991) but this is likely not very significant (Iqbal et al. 2017). The characteristic timescale of this dynamical activity ($\sim$ Gyr) is comparable to that of the cluster formation. This implies that at fixed mass and redshift, scatter should affect the cluster's properties depending on the dynamical state. Accordingly, the cluster population is roughly divided into disturbed merging clusters and relaxed cold-core clusters, but this distinction is not strictly bimodal.

AGN feedback The X-ray emitting gas is radiatively cooling. By doing so, it falls in the potential well, enhancing the density and thus the flow. Catastrophic runaway cooling is thus expected in relaxed systems given sufficient time without major perturbation. However, it was realized that the star formation rate falls ~ 100 times shorter than the enhancement expected in this scenario (McDonald et al. 2018, for an update). Additionally, core entropy measurements indicate the need for heat injection to maintain the thermal equilibrium (Donahue et al. 2006; Babyk et al. 2018).

It was soon realized that supermassive black holes in AGNs located in cool-core Brightest Cluster Galaxy (BCG) were responsible for self-regulation heating processes, mostly due to the effects of episodic powerful jets, on a timescale of ~ 100 Myr (McNamara and Nulsen 2007; Fabian 2012; Hlavacek-Larrondo et al. 2022). These outbursts inject large amounts of energy into the surrounding environment and quench star formation. Their imprint in the ICM has been made quite

spectacular, thanks to the superb angular resolution of *Chandra*, that has revealed giant cavities filled with radio jets that are pushing the thermal gas, visible around many central AGNs (e.g., Nulsen et al. 2005; Wise et al. 2007; Finoguenov et al. 2008; McNamara et al. 2009; Fabian et al. 2011). See also the first SZ detection of such cavities by Abdulla et al. (2019). Today, we have solid evidence that AGN feedback can prevent catastrophic gas cooling (Rafferty et al. 2006) and that it is operating at least since $z \gtrsim 1$ (Hlavacek-Larrondo et al. 2015). However, the detailed mechanisms are not understood (accretion physics, the channel of energy release, the composition of cavities; see the review by Werner et al. 2019). The heat redistribution involves plasma micro-physics (convection, conduction, viscosity, instabilities, etc, Kunz et al. 2012; McCourt et al. 2012; Yang and Reynolds 2016a,b), which remain difficult to address (Kunz et al. 2022).

The feedback from AGNs (and star formation and supernovae to some extent) plays a crucial role in shaping the ICM structure. It is expected to induce baryon depletion in the cluster cores. As the potential well of low mass clusters and groups is more shallow, these effects should be more efficient at low mass (Eckert et al. 2021). AGN feedback is recognized as a key ingredient to galaxy and cluster formation and was considered in numerical simulations early on (Sijacki et al. 2007). It may also be important for cosmological constraints that are sensitive to the small-scale matter distribution since it induces a deficit in the power spectrum at $\gtrsim$ Mpc^{-1} (Chisari et al. 2018).

Galaxy evolution and ICM interactions Not only central AGNs interact with the ICM. In fact, clusters play a key role in galaxy evolution due to environmental effects[6] (Mo et al. 2010; Somerville and Davé 2015; Naab and Ostriker 2017). These interactions unavoidably affect the observational properties of galaxies (color, morphology, etc). On the other hand, these processes affect the ICM properties. They also provide us with observational means to characterize them since ICM – galaxy interactions depend on the ICM physics (thermal conductivity, viscosity, magnetic field; Roediger et al. 2015; Eckert et al. 2017b; Su et al. 2017). Additionally, the metals produced in galaxies are redistributed in the ICM via winds, outbursts, or ram-pressure stripping (e.g., Domainko et al. 2006). They are believed to appear early in cluster formation (Mantz et al. 2020). Understanding the ICM metallicity is still an important topic and a way to probe galaxy evolution and feedback mechanisms (Simionescu et al. 2019a). For reviews, see Mernier et al. (2018); Biffi et al. (2018).

This rich astrophysics is expected to break self-similarity to some extent. Yet, since gravity is the main driver of cluster formation, they should be reflected as a second-order effect, with various impacts depending on the physics involved. It is now important to understand to which extent it affects clusters observables depending on mass, redshift, dynamical states, and spatial scales.

1.2.2.3 The mass – observables scaling relations

The mass is a key property of clusters. The ones derived from surveys generally rely on global quantities (X-ray luminosity, SZ flux, etc) because individual measurements are expensive and generally not available (Pratt et al. 2019). Such an approach builds on the intimate relationship that cluster masses maintain with their global observable, called scaling relations. This is largely made possible thanks to the self-similarity in which the cluster's global properties follow $Q \propto H(z)^{\beta} M_{\Delta}^{\alpha}$ (Kaiser 1986), where the normalization evolves in redshift due to the change in the background density. The astrophysically induced deviations from self-similarity may affect the slope α, introduce non-trivial redshift or mass evolution, and induce scatter. On the other hand, the characterization of the scaling relation provides insight into the astrophysics at play. For these reasons, huge efforts

[6]This includes galaxy merging (Mihos 2004), ram pressure striping (Gunn and Gott 1972), harassment (Moore et al. 1996), turbulent viscous striping (Nulsen 1982), tidal compression and truncation (Merritt 1983; Byrd and Valtonen 1990), starvation (Larson et al. 1980), and thermal evaporation (Cowie and McKee 1977).

are still undergoing in this direction, especially in light of the future surveys that will reach yet unexplored regime (Giodini et al. 2013; Lovisari et al. 2021; Lovisari and Maughan 2022).

The X-ray luminosity, temperature, or gas mass were used early to study scaling relations (Edge and Stewart 1991; Henry and Arnaud 1991). Deviation from self-similarity soon indicated that non-gravitational physics was significant. Today, X-ray data expand to galaxy groups and cover a large redshift range, providing huge leverage on these relations (Bahar et al. 2022; Chiu et al. 2022). The SZ flux scales as $Y_{\rm SZ} \propto H(z)^{2/3} M^{5/3}$ in the self-similar model. As a direct measure of the thermal energy, it provides a robust and low scatter mass proxy (Figure 1.2; Nagai 2006), but merger events may still contribute to the scatter and affect its evolution (Yu et al. 2015). Its X-ray analogous, $Y_X = M_{\rm gas} T_X$ (Kravtsov et al. 2006), was also shown to be an excellent mass proxy (Vikhlinin et al. 2009). Current observations overall support well the power-law behavior predicted by self-similarity, but deviations in the slopes have confirmed the relevance of astrophysical processes, although primarily limited to cluster cores (Lovisari et al. 2015; Czakon et al. 2015; Anderson et al. 2015; Dietrich et al. 2019; Salvati et al. 2022). With the advance of SZ surveys and in light of the cluster – CMB cosmological tension (Planck Collaboration et al. 2014b), much effort has been devoted to the investigation of the $Y_{\rm SZ} - M$ relation (Bocquet et al. 2015; Mantz et al. 2016; Penna-Lima et al. 2017; Medezinski et al. 2018; Miyatake et al. 2019; Zubeldia and Challinor 2019), including with gravitational lensing. These results were used to infer $b_{\rm HSE} \sim 0.1$-0.4, although no clear consensus has emerged yet. This value is roughly consistent with expectations from numerical simulations, which are overall useful in interpreting scaling relations (Pike et al. 2014; Planelles et al. 2014; Le Brun et al. 2017; Truong et al. 2018; Pop et al. 2022a,b).

The characterization of the scaling relations is made difficult because of selection effects (e.g., Malmquist and Eddington biases, see Sereno and Ettori 2017, for discussions). Detections from a given waveband may also alter the sample representativity due to preferential selection towards specific characteristics (e.g., the cool-core bias in X-ray, due to the prominent surface brightness peak, Rossetti et al. 2017). Because SZ samples are weakly dependent on cluster astrophysics and are nearly mass-selected, they allowed considerable progress in the field. Similarly, large mass-selected upcoming weak lensing samples (independent of the ICM) should be very relevant.

1.2.2.4 Radial thermodynamical profiles

As for scaling relations, the ICM thermodynamical radial profiles should behave, at first order, self-similarly and be universal once scaled in mass/radius and redshift. Still, they reflect the imprints of astrophysics via the scatter and the non-trivial deviations from self-similarity. The knowledge of the ICM internal structure and its scatter is also important for cluster detection. For instance, the ICM pressure and density profiles are essential for cluster detection in SZ and X-ray, respectively.

Universal profiles The thermodynamical profiles can be predicted using numerical simulations. Accordingly, the entropy profile is expected to follow $K_e(r) \propto r^{1.1}$ when only gravitational processes are included (Voit et al. 2005). Radial pressure, temperature, and density profiles, that show decaying profiles towards the outskirts were also investigated depending on the considered astrophysics (Nagai et al. 2007; Pike et al. 2014; Gupta et al. 2017) and characterized using local cluster samples. For instance, Arnaud et al. (2010) and Planck Collaboration et al. (2013c) derived the pressure profile from the REXCESS sample and from *Planck* data, respectively (Figure 1.2). REXCESS was also used to study the temperature (Pratt et al. 2007) and entropy profiles (Pratt et al. 2010) of a representative population. Recently, Ghirardini et al. (2019a) derived universal thermodynamical profiles using the X-COP local sample taking advantage of large radial coverage. Overall, these profiles are most sensitive to astrophysics on small and large scales. At $0.5 \lesssim \frac{r}{R_{500}} \lesssim 1$, however, they follow remarkably well self-similarity as these scales are truly driven by gravity.

Cluster cores They are strongly affected by AGN feedback (cool-cores) or merger-induced dynamics (perturbed systems). This induces a large scatter among the population at these scales. AGN feedback implies excess entropy in cool-cores, but this remains small compared to the large entropy floor in mergers (Cavagnolo et al. 2009; Pratt et al. 2010). The temperature drops towards the center in cool cores or flatten at a high plateau in disturbed systems (Pratt et al. 2007; Leccardi and Molendi 2008). The density is also largely affected by the core physics, with cooling flows implying very peaked cores while merging systems present a flat core (Croston et al. 2008). The same trend affects the pressure, although the scatter is smaller (Arnaud et al. 2010).

Clusters outskirts They are interesting regions because they reflect how clusters connect to the cosmic web. Their physics is driven by accretion, preferentially along filaments. They are challenging to probe because they are very tenuous, such that great sensitivity and dedicated analysis techniques are required. Nevertheless, major advances in SZ and/or X-ray have been obtained recently, up to the virial radius (Walker et al. 2019; Walker and Lau 2022). Observations support the fact that outskirts are more affected by gas substructures, inhomogeneities, and clumping, which enhance the density measurements (Urban et al. 2014; Eckert et al. 2015b) and possibly lead to excess pressure compared to numerical simulations (Planck Collaboration et al. 2013c; Sayers et al. 2013a; Pointecouteau et al. 2021). The consequences are mostly reflected in the entropy, which often presents a large-scale flattening when compared to the pure gravitational collapse (Tchernin et al. 2016; Simionescu et al. 2017). In addition to these general trends, a large scatter affects the cluster population. Note that the non-thermal pressure support is expected to be higher in the outskirts, which should affect the HSE assumption (e.g., Shi et al. 2015).

Redshift evolution The evolution of the thermodynamical profiles is also of great interest for structure formation. Sayers et al. (2022) recently characterized the mass and redshift evolution up to intermediate redshift ($z \leqslant 0.6$) with SZ and X-ray data. The use of SZ selected sample plus X-ray follow-up with *Chandra* or *XMM-Newton* proved very powerful at high-z. For instance, Ruppin et al. (2021) have shown that the fraction of cool-core clusters is remarkably stable, $\sim 1/3$, even up to $z \gtrsim 1$. Ghirardini et al. (2021) tested the ICM evolution of massive clusters out to $z \sim 1.8$. They found that the thermodynamic properties in the outskirts are similar to that of low-z clusters and follow self-similar evolution. However, increased scatter and strong deviation from self-similarity was observed in the core. Current observations seem to converge to the fact that no non-standard evolution is detected, at least out to $z \sim 1.5$ (see also McDonald et al. 2014; Sanders et al. 2018; Bartalucci et al. 2017; McDonald et al. 2017; Bartalucci et al. 2019). This implies that the physics that drives the ICM properties, at least for high mass systems, is already in place early on.

While the cluster thermodynamical radial profiles are well characterized in the local Universe, their evolution in mass and redshift remains an important topic for cluster astrophysics and cosmology. A detailed understanding of the co-evolution of the baryonic and dark matter, up to high-z and low mass, is mandatory to properly use them as a strong cosmological probe in the future.

1.2.2.5 Internal gas dynamics and substructures

The cluster's inner structure and energetics are largely driven by the interaction within and between dark matter and the hot gas. The characterization of substructures is an excellent way to probe these physics, provided sufficient sensitivity and angular resolution are available. With the advances of X-ray observatory such as *XMM-Newton* and *Chandra*, this is readily performed out to intermediate-z. In the SZ, the instrumental advances of high-resolution instruments such as MUSTANG2 (Dicker et al. 2014) or NIKA2 (Adam et al. 2018a) allow us to probe the detailed gas pressure structure.

The 3D shape of clusters Dark matter halos are expected to be triaxial rather than spherical. The gas should be rounder, but its structure is still driven by the dark matter collapse. Combining SZ, X-ray, and lensing is sensitive to the line-of-sight elongation, thanks to their different ICM sensitivities. Using this method, Morandi et al. (2012) measured a minor to major axis ratio ~ 0.6 in Abell 1835 (see also Limousin et al. 2013; Sereno et al. 2017). Sereno et al. (2018) measured the shape of halos and found consistency with N-body simulations, which supports the standard cosmological model. BCGs were also shown to align with the surrounding matter up to $z = 1.8$, implying an intimate connexion with cluster formation since early time (West et al. 2017).

ICM discontinuities In addition to the smooth ICM profiles, several remarkable features arise during violent events such as mergers (Sarazin 2002). We can distinguish shocks (i.e., a pressure discontinuity) from cold fronts for which the denser side of the edge is colder than the other, but in pressure equilibrium (Markevitch and Vikhlinin 2007; Zuhone and Roediger 2016).

The superb angular resolution of *Chandra* has played a critical role in studying discontinuities in a large number of shocks and cold fronts (e.g., Markevitch et al. 2002, 2005; Botteon et al. 2018). In this sense, instrumental advances in the millimeter have also been critical to studying shocks since the SZ directly measures the pressure (e.g., Korngut et al. 2011; Basu et al. 2016; Adam et al. 2018b; Di Mascolo et al. 2019). The relatively low resolution of *Planck* was still enough to study shocks in the Coma cluster (Planck Collaboration et al. 2013b; Erler et al. 2015).

Recently, Walker et al. (2022) reported the presence of a large-scale cold-front near the virial radius of the Perseus cluster, indicating that they may also be significant in the outskirts. Cluster shocks are also expected in the periphery of clusters. The detection of a strong shock in the outskirt of Abell 2319 was reported using *Planck* SZ data and interpreted as the first detection of an accretion shock (Hurier et al. 2019). Discontinuities in the stacked profiles of 516 South Pole Telescope clusters were also investigated, leading to the tentative detections of several features (Anbajagane et al. 2022).

Gas motions The kSZ effect can probe the gas dynamics since it is sensitive to its momentum. However, it requires high angular resolution and high sensitivity to distinguish the faint individual cluster components. Such conditions were achieved only recently by Mroczkowski et al. (2012) who found hints of kSZ signal in the merging system MACS J0717.5+3745. This was confirmed by Sayers et al. (2013b). Latter, Adam et al. (2017b) were able to map the kSZ signal in the same cluster. See also (Sayers et al. 2019) who applied similar techniques to a sample of ten clusters.

Future X-ray missions will surely probe the gas velocity, but Sanders et al. (2020) already obtained evidence for gas motion in Coma thanks to a novel *XMM-Newton* calibration technique (see also Gatuzz et al. 2022, for AGN driven gas motions). Thanks to its unprecedented spectral resolution, *Hitomi* was used to measure the gas velocity dispersion in the Perseus core, finding ~ 150 km/s, before the satellite was lost (Hitomi Collaboration et al. 2018). ICM turbulence also induces X-ray and tSZ surface brightness fluctuations, which can be used to infer the gas dynamics and plasma microphysics. This was performed in the X-rays (e.g., Schuecker et al. 2004; Churazov et al. 2012; Zhuravleva et al. 2015, 2018), although it was recognized that several processes may contribute to the signal. Recently, Khatri and Gaspari (2016) directly measured pressure fluctuations in the Coma cluster using *Planck* SZ data and deduced a core HSE bias $b_{\rm HSE} \sim 0.15$, in line with expectations (see Simionescu et al. 2019b, for a review on ICM motions).

ICM – galaxies interactions give an indirect probe of gas motions. For example, the distortions of AGN jets embedded in the ICM tell us about internal motion (Mendygral et al. 2012; Garon et al. 2019). Ram-pressure stripped tails of infalling cluster galaxies may provide similar information.

1.2.2.6 The baryons beyond galaxy clusters

The baryons commonly observed in the local Universe account for only half of the total compared to CMB measurements. This discrepancy is known as the missing baryon problem, and the remaining ones should be in the form of a warm-hot diffuse gas in filaments. The observations of filaments between pairs of individual systems were first made using *XMM-Newton* (Werner et al. 2008). This is now achieved readily in SZ (e.g., Planck Collaboration et al. 2013c; Hincks et al. 2022) or X-ray (e.g., Eckert et al. 2015a; Reiprich et al. 2021), and in the radio (Govoni et al. 2019). More recently, the first detections of filamentary gas over-densities were reported in the X-ray (Tanimura et al. 2020, 2022) and SZ (de Graaff et al. 2019; Tanimura et al. 2019), using the correlation with luminous red galaxies that are good tracers of the large scale structures. Using a similar technique, diffuse radio emission from stacked filaments was reported in Vernstrom et al. (2021), although not confirmed by Hodgson et al. (2022) with deeper data. Such results provide the first thermodynamical characterization of these low-density regions and support the prediction that $\sim 50\%$ of the baryons are in the form of a warm-hot gas in filaments.

1.2.3 Particle acceleration and non-thermal diffuse emission from galaxy clusters

The ICM is a very active environment. The shocks and turbulent motions are believed to accelerate particles up to very high energies and amplify the magnetic field. However, CR and magnetic fields are entangled, difficult to probe directly, and subject to very complex physics, which makes them challenging to characterize both observationally and theoretically. This Section focuses on particle acceleration at the cluster scale and discusses the associated problematics.

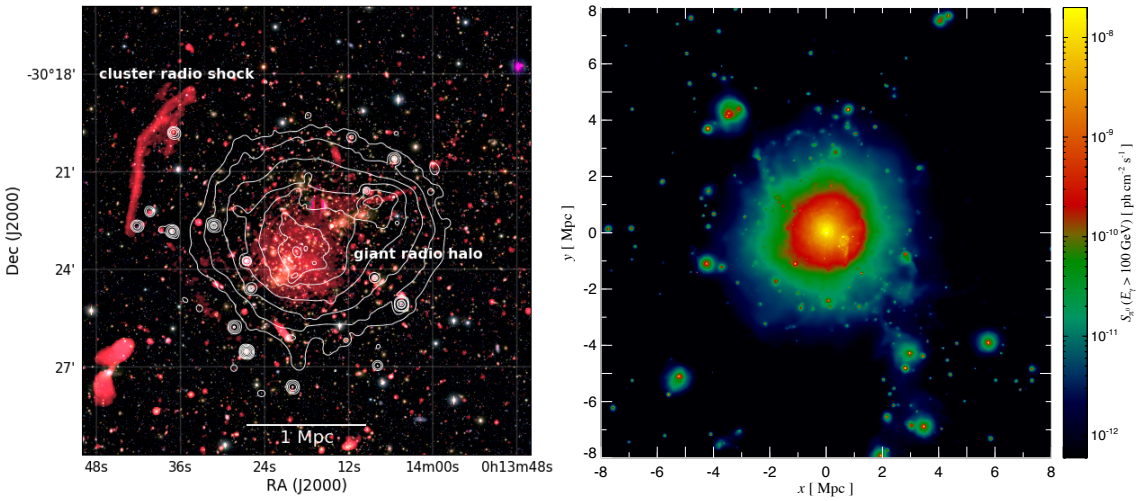

Figure 1.3: **Left:** 1-4 GHz Very Large Array image of Abell 2244, showing a giant radio halo coincident with the thermal gas density (X-ray, white contours), and a radio relic (shock) in the periphery. Extracted from van Weeren et al. (2019). **Right:** hadronically induced diffuse γ-ray signal expected for a simulated Coma-like cluster, above 100 GeV. Extracted from Pinzke and Pfrommer (2010).

1.2.3.1 Diffuse radio emission from galaxy clusters and implications

The radio signal from clusters was detected early on (Ryle et al. 1950; Baldwin and Elsmore 1954; Seeger et al. 1957; Large et al. 1959). It was rapidly thought to be due to synchrotron emission (Burbidge 1958) and was shown not to be directly associated with individual galaxies, but rather

diffuse (Willson 1970), providing evidence for a non-thermal ICM component including $\sim$GeV electrons and $\sim\mu$G magnetic field (see Rybicki and Lightman 1986, for the radiative process).

Today, the presence of CRe and magnetic fields in galaxy clusters is well established (Ferrari et al. 2008; Feretti et al. 2012; van Weeren et al. 2019). We can distinguish between radio halos, which are spatially coincident with the thermal gas in massive clusters, and relics believed to trace shock acceleration at the periphery of clusters (van Weeren et al. 2010). See also Figure 1.3. Relics are strongly polarized, implying an ordered magnetic field on large scale, and present spectral index gradient across their width due to CRe aging. Radio halos are further divided between giant and mini-halos. The formers are $\sim$Mpc scale sources found in mergers (Cassano et al. 2010). The latter, much more compact (few hundreds kpc), are found in cool-core clusters (Giacintucci et al. 2017). Despite these differences, the distinction between giant and mini-halos is not always clear (Ferrari et al. 2011; Bonafede et al. 2014; Savini et al. 2019).

CRe should lose their energy quickly by inverse Compton scattering and synchrotron losses, within $\lesssim 100$ Myr for GeV electrons. On the other hand, the distance over which they can travel within a radiative lifetime falls far shorter than the Mpc scales required even when considering transport (Bagchi et al. 2002, for discussions), implying in-situ acceleration.

Theoretically, the modeling of CR acceleration and propagation in the ICM is very challenging. It requires dealing simultaneously with $\gtrsim$Mpc scales, on which CR acceleration happens, and very small scales at which the microphysics is effective ($\sim 10^{-6}$ pc for the gyroradius of GeV protons), but far below the resolution limit of numerical simulations. Additionally, the small-scale processes that couples the CR and the thermal gas via the magnetic field imply very complex plasma physics (Brunetti and Jones 2014, for a review). However, since pioneering works by Miniati et al. (2001), cosmological simulations including CR have been used to make quantitative predictions for the associated observables, albeit with many simplifying assumptions and recipes (e.g., Dolag and Enßlin 2000; Pfrommer et al. 2007, 2008; Skillman et al. 2008; Vazza et al. 2009; Pinzke and Pfrommer 2010; Wittor et al. 2017). In terms of energetics, a CRp to thermal energy ratio of about 1% provides a typical scale of what can be expected in clusters, but their spatial and spectral distribution are nearly unconstrained.

1.2.3.2 Large scale intra-cluster magnetic field

The diffuse radio emission implies cluster scale magnetic fields (Donnert et al. 2018). They remain poorly known despite their importance for particle acceleration or ICM microphysics (strength, topology). Cluster's magnetic fields are thought to result from the amplification of seed fields. However, it is still unknown whether these fields have a primordial origin (Planck Collaboration et al. 2016b for constraints; Subramanian 2016 for a review) or were produced along with galaxy formation and injected in the ICM (Kronberg et al. 1999; Bertone et al. 2006; Donnert et al. 2009).

The structure formation processes are expected to amplify the magnetic fields (Donnert et al. 2018) and it is common to express its strength as $|\overrightarrow{B}| \propto n_e^{\eta_B}$. For instance, pure adiabatic compression, where the field is frozen into the plasma and the magnetic flux is conserved, implies $\eta_B = 2/3$, but simulations show that it is difficult to reach a few μG by compression only. Alternatively, we expect $|\overrightarrow{B}| \propto P_e^{1/2}$ for constant magnetic to thermal energy ratio. Additionally, the turbulence kinetic energy is converted into magnetic energy via dynamo effects due to field stretching and folding, leading to amplification until the back reaction becomes important. CRs also interact with the magnetic field and various plasma instabilities may lead to its amplification. Shocks and cold fronts may result in field compression, turbulence, stretching, and magnetic draping.

Faraday rotation measures (Burn 1966), i.e., the rotation of the light polarization of background sources when propagating in a magnetized medium as a function of wavelength, is used to measure magnetic fields. This was used to infer a central value of about 25μG (Taylor et al. 2006) and 5 μG

(with $\eta_B \sim 0.5$, Bonafede et al. 2010) in the Perseus and Coma clusters, respectively, and a turbulence coherent scale of ~ 10 kpc is expected (van Weeren et al. 2019). See also (Vacca et al. 2012; Bonafede et al. 2013; Vacca et al. 2016; Govoni et al. 2017; Stuardi et al. 2021). However, Faraday rotation measures are affected by large inherent uncertainties (Johnson et al. 2020). Alternatively, the study of a Kelvin-Helmholtz instability in the Perseus cluster allowed Walker et al. (2017) to infer a thermal to magnetic pressure of about 200. Inverse Compton emission should show up as a tail in hard X-rays and might help disentangle the CRe from the magnetic field in radio data. However, such a signal is difficult to measure because of the large, mainly thermal Bremsstrahlung, background. Mernier et al. (2022) claimed the first robust detection of such signal, obtaining a rather high magnetic field in a galaxy group (1.9 μG), and complementing previous lower limits (few tens of μG, e.g., Wik et al. 2014). Moreover, the magnetic field of distant clusters was found to be as high as for local ones from the diffuse radio signal (Di Gennaro et al. 2021) and Faraday rotation measures (Xu and Han 2022), which may challenge current models.

1.2.3.3 Particle acceleration

Several mechanisms have been proposed to explain CR acceleration, involving AGN feedback, shocks, turbulence, or hadronic interactions (Brunetti and Jones 2014; Bykov et al. 2019). They could occur simultaneously, be entangled, and may explain the variety of observed radio sources.

Injection from cluster galaxies High energy particles can be injected into the ICM via the powerful jets induced by AGNs (Mathews and Brighenti 2007; Guo and Oh 2008; Sijacki et al. 2008; Fujita and Ohira 2012; Yang et al. 2019). This is obvious for BCGs in cool-cores clusters, but may be relevant for lower luminosity AGNs. However, it is not clear how these CR mix and age in the ICM. AGN jets may also induce ICM turbulence and shocks capable of accelerating particles indirectly (Randall et al. 2011, 2015). Alternatively, star formation activity may generate CR. They can then be redistributed in the ICM via galactic winds or ICM – galaxy interactions (Völk et al. 1996; Völk and Atoyan 2000; VERITAS Collaboration et al. 2009; Acero et al. 2009; Abdo et al. 2010). In turn, measuring the CR content of clusters gives a way to estimate the integrated AGN and star formation activity over cosmic history, provided that transport is sufficiently understood.

Shock acceleration Diffusive shock acceleration is a well-known mechanism that can accelerate CR up to very high energy. Given the huge energy release involved in structure formation shocks ($\gtrsim 10^{64}$ ergs, Sarazin 2002), a significant population of CR may be produced even for relatively low acceleration efficiency. We can distinguish between merger-induced shocks and peripheral shocks due to large-scale inflows. The formers are located close to cluster cores and are relatively weak (Mach numbers $\mathcal{M} \sim$ 2-3), although they get stronger when traveling outwards (Zhang et al. 2019). The latter are quasi-stationary, much stronger ($\mathcal{M} \gtrsim 10$), but in low-density regions.

Particles can be trapped in shocks if they diffuse on smaller scales than the shock thickness, and eventually escape (Brunetti and Jones 2014). The power-law slope of the resulting spectrum builds on the competition between energy gain and escape rate. It is related to the shock strength as $\delta_{\rm inj} = 2\frac{\mathcal{M}+1}{\mathcal{M}-1}$. Nonetheless, the acceleration physics depends on the shock structure (magnetic field orientation, amplification, interaction with CR) and the energy distribution of the injected particles, involving complex microphysics. Contrary to the protons, thermal electrons cannot be efficiently accelerated because their gyroradius is not large enough to cross the shock transition layer width and pre-acceleration mechanisms are often invoked (Kang et al. 2012; Vink and Yamazaki 2014). Additionally, the resulting spectrum reflects the competition between energy gain and losses.

ICM shock acceleration is not well constrained both from theory and observations. Numerical simulations and subsequent predictions are impacted by sub-grid modeling. In particular, the in-

jected CR energy relative to the total dissipated energy is key (e.g., Pinzke and Pfrommer 2010). See Ackermann et al. (2014) for γ-ray observational constraints on this parameter.

Turbulent (re)acceleration Turbulence may play a major role in cluster scale acceleration (Brunetti and Jones 2014, for a review). The energy injected as large-scale motions cascades down to small scales. It is eventually dissipated into heat, but may also be efficiently transferred to the CR in a stochastic way. As for shocks, thermal particles are much more difficult to accelerate than pre-accelerated CR. Turbulence is thus mostly considered a possible reacceleration mechanism. Modeling turbulent reacceleration requires computing the change in the CR population induced by interactions with the turbulent field. Because protons-ICM interactions generate secondary CRe, the evolution of CRe and CRp are coupled in addition to the fact that they are both accelerated via the same turbulence. Over the last two decades, many theoretical efforts have been devoted to the turbulence reacceleration of CR in clusters (Brunetti et al. 2001; Petrosian 2001; Brunetti and Lazarian 2007, 2011). Such models were also constrained by confrontation to observations (Brunetti et al. 2017; Pinzke et al. 2017; Nishiwaki et al. 2021). Because the underlying physics is very complex, with many assumptions and parameters involved, the predictions remain somehow qualitative. For instance, it involves the cascading of turbulence down to the smallest scales, its time evolution, and its interaction with the CR, all of these being very challenging to model. However, it is now clear that turbulence is key to the non-thermal properties of clusters.

Hadronic interactions CRp interact hadronically with the ambient gas. These interactions lead to γ-ray, electron, positron, and neutrino emission, mainly through the production of pions (e.g., Figure 1.3). This CRe production mechanism is referred to as the hadronic model (Dennison 1980; Blasi and Colafrancesco 1999; Dolag and Enßlin 2000). The interaction rate is given by the proton-proton cross-section, which is measured from particle physics accelerator data, and the density of CRp and thermal gas. Hadronic interactions are expected to inject secondary particles into the ICM according to the energy spectrum of the primary CRp. The spatial distribution of the injected particles follows the interaction rate, which reflects the CRp to thermal gas overlap. The secondary CRe, accounting for their evolution in the ICM may contribute to the seed population reaccelerated in shocks and turbulence (Brunetti and Lazarian 2007, 2011; Adam et al. 2021).

Energy losses CR are affected by energy losses that limit their lifetime. In the case of CRe, the main channels are synchrotron radiation, inverse Compton scattering, Coulomb, and ionization (Sarazin 1999). Synchrotron and inverse Compton dominate in the core and the periphery, respectively, at $E \gtrsim 100$ MeV. Coulomb losses largely dominate below ~ 10 MeV. The main channel for CRp losses is hadronic interactions for $E > 1.2$ GeV, the interaction threshold. At lower energies, they are dominated by Coulomb and ionization losses. CR of sufficiently high energy may escape the cluster, but this is expected to be significant only at $E \gtrsim$ PeV (Blasi et al. 2007). CR may also be affected by energy gain or loss during transport, e.g., due to adiabatic expansion.

Because of these losses, CRe should accumulate at $E \sim$10-100 MeV provided that the injection of fresh particles is sufficiently continuous. Such a population may serve as the pre-accelerated seed for merger-induced transient re-acceleration via shocks and turbulence. Relativistic protons, on the other hand, should accumulate over the cluster formation history because their lifetime is larger than the age of the Universe. In this sense, CRp should provide an integrated measurement of the total particle acceleration over the cluster's formation history.

Transport The transport physics of CR affects their spatial distribution, and thus the interaction mechanisms they are suffering from. The magnetic field forces CR to travel in helical orbits along

the field lines. Therefore, their transport is strongly controlled by its properties. We can list three main ways to transport CR (Enßlin et al. 2011, for a dedicated study): 1) advection, in which case CR are passively transported together with the magnetic field that is frozen in the ICM, by gas motion; 2) diffusion, for which CR travel mainly along the field lines in a random walk scattering on plasma waves ; 3) streaming, for which a net CR flux is induced by a strong gradient in their spatial distribution. CR advection in the turbulent ICM-driven motion should enhance the profiles towards the center. On the other hand, diffusion and streaming are expected to flatten CR profiles. Therefore, the spatial CR distribution strongly depends on the dominant transport mechanism. Yet, very little is known about CR transport in clusters despite the major consequences it may have on their observational properties (Wiener et al. 2013; Zandanel et al. 2014).

1.2.3.4 Non-thermal cluster scale emission and connection with the dynamical state

Galaxy clusters host a large variety of radio sources. Here, we discuss recent observational results and their most accepted interpretation focusing on radio halos and relics.

Giant-halos in mergers Two main mechanisms have been considered to explain giant radio halos: 1) hadronic models, where CRe are secondary particles resulting from hadronic interactions (Dennison 1980; Blasi and Colafrancesco 1999; Dolag and Enßlin 2000; Miniati et al. 2001) ; 2) turbulent (re)acceleration (Brunetti et al. 2001; Petrosian 2001; Brunetti and Lazarian 2007, 2011).

On the one hand, the presence of a giant radio halo correlates with the cluster's dynamical state (Giovannini et al. 1999; Buote 2001; Cassano et al. 2010): nearly all giant halos are found in mergers. This bimodality implies a mechanism that can switch on/off the CRe population quickly. Moreover, the radio emission correlates with the X-ray luminosity and mass (in agreement with CRe acquiring part of the merger energy) and with X-ray surface brightness fluctuations (Eckert et al. 2017c). These observational facts cannot be explained in the pure hadronic model, but naturally arise in turbulent reacceleration. On the other hand, turbulent acceleration requires pre-accelerated CRe. Such population could arise from hadronic interactions, AGNs, or shocks, but their necessary spatial and spectral distribution is not obvious to obtain (Pinzke et al. 2017).

The presence of CRp implies high energy γ-rays, but the associated signal was never unambiguously detected. Upper limits were used to rule out the pure hadronic model in the Coma cluster (Brunetti et al. 2017). However, these results rely on the knowledge of the magnetic field that is affected by large uncertainties.

Today, turbulent re-acceleration is the most widely accepted scenario to explain giant radio halos. Nevertheless, only indirect evidence is available and CRp may be important in generating the seed CRe population (Brunetti and Blasi 2005; Brunetti and Lazarian 2011; Adam et al. 2021)

Mini-halos in cool-cores The possible origins of the mini-halos are similar to that of the giant-halos. However, the turbulence may be sourced by AGN feedback or sloshing motion, instead of a major merger. The central AGNs outbursts are natural candidates to provide fresh CR.

Contrary to giant halos, the compact morphology of mini-halos agrees well with the hadronic model expectations. The dense cool-cores provide huge quantities of target material for CRp provided they do not considerably leak outside the core (ZuHone et al. 2015, for simulations). γ-ray observations did not rule out the hadronic scenario (Aleksić et al. 2012; Ahnen et al. 2016). This is also because central AGNs are often γ-ray emitters such that the search for a diffuse signal is difficult, especially with low angular resolution. Nevertheless, several results indicate that gas motions could be connected with the structure of mini-halos. For instance, (Mazzotta and Giacintucci 2008) have shown that mini-halos might be confined by cold-fronts (ZuHone et al. 2013, for simulations).

Recent results from the observations of the cluster MS 1455.0+2232 obtained at radio frequencies could also indicate that neither simple hadronic nor turbulent reacceleration models can explain the data well (Riseley et al. 2022). Again, it might point to the fact that the underlying CR and magnetic fields result from a complex combination and entanglement of several processes (e.g., Zandanel et al. 2014, for the proposed connection between giant and mini halos).

Radio relics at shocks Radio relics are associated with shocks (Ensslin et al. 1998; Roettiger et al. 1999) and their properties suggest that CRe originate from diffusive shock acceleration (van Weeren et al. 2019). Numerical simulations support this idea (e.g., Nuza et al. 2017), which is also reinforced by the detection of several double radio relics as expected for head-on binary mergers (e.g., Hoang et al. 2018). Additionally, the spectral index gradients seen along relic width support the CRe being accelerated at shock fronts and smoothly losing energy afterward.

The shock Mach number can be measured independently in the radio and X-ray (or SZ), using the particle injection spectrum and the Rankine-Hugoniot jump conditions, respectively. However, significant tension has been found in several clusters when comparing the two (e.g., Akamatsu et al. 2017). While these measurements are difficult to make, and possibly affected by systematics, it might also point to the simple diffusive shock acceleration picture being incomplete (van Weeren et al. 2019, for discussions). By comparing results from simulations at shocks and *Fermi-LAT* observations, Vazza et al. (2016) inferred a limit on the CR acceleration efficiency that is below the radio requirement (see also Vazza and Brüggen 2014; Vazza et al. 2015): the simple shock picture cannot explain simultaneously the bright radio emission and the lack of hadronically induced γ-rays. Again, this might show that a revision of the simple shock acceleration picture is needed.

Given these issues, the understanding of radio relics is an active topic and various solutions are being investigated. For instance, the radio versus X-ray disagreement could be due to geometrical effects, in which case SZ data could provide an interesting complementary view. Numerical simulations have shown that shock obliquity could impact the acceleration of CR, reducing the tension between γ-rays and radio observations. It has also been suggested that merger-induced gas motions could turn AGN bubbles into radio relics (ZuHone et al. 2021).

The detailed understanding of particle acceleration at the cluster scale remains a hot topic 70 years after its discovery. Improvements in both theory and observations, including radio, high energies, but also the multi-wavelength combination, appear necessary to characterize the underlying physics.

1.2.4 Hot topics and main issues

In the scientific context depicted here, the global theoretical framework that describes the formation of large-scale structures is well established. The detailed physical mechanisms at play, however, are still uncertain or even poorly known. Complex dynamics are obvious in merging systems, but even in the clusters that are a priori the most relaxed, tumultuous activity is unavoidable. It is clear that the different facets related to the physical properties of the ICM (thermal and non-thermal), but also galaxy evolution, are fully interconnected, and it becomes difficult to focus on a specific aspect without considering clusters in their entirety. Despite these difficulties, the field of cluster astrophysics and cosmology has evolved quickly in the last years. While many more fundamental and astrophysical issues related to the thermal and non-thermal properties of the ICM remain, this document is structured around the following questions, that I have contributed to addressing in the past years, or that constitute a thoughtful perspective work.

- What is the thermodynamical state and internal structure of the hot gas in clusters and how does it evolve in mass, redshift, and as a function of the dynamical state? Answering this question

would shed light on the co-evolution of the dark matter, that shapes structure formation, and the baryons that are responsible for the complex physics including feedback mechanisms. It requires characterizing gravitational and non-gravitational physics across cosmic history and mass scale. The detailed description of the scaling relations that are used to connect global quantities and the cluster mass is also intimately connected to this issue, which in turn, is fundamental for cluster cosmology as soon as the ICM is involved.

- What are the mechanisms that accelerate and transport high-energy particles at the cluster scale? Theoretically, this problem is extremely complex due to its multi-scale nature, the many unconstrained free parameters, and assumptions involved, such that reliable predictions are difficult to obtain. Answering this question would require understanding the detailed physical properties of turbulence and shocks and how their energy is transferred into CR, which involves the microphysics of the ICM. It is also connected to our understanding of how AGNs interact with the ICM, and in particular what is the CR content of AGN outburst cavities. From an observational point of view, the γ-ray band is a unique channel to probe directly the CRp and measure their spectral and spatial distribution to address this question. On the other side of the electromagnetic spectrum, it also relates to the longstanding issue of the origin of relativistic electrons that emit diffuse radio synchrotron emissions in the magnetized ICM.
- What are the quantitative contributions to the non-thermal pressure support in clusters and how does it shape their observational properties? The presence of non-thermal components in the form of CR, magnetic fields or turbulence, and bulk motion in galaxy clusters is now well established. However, they are difficult to measure directly and are presumably interconnected such that very little is known about them. While they are thought to be subdominants, they may nonetheless have a significant influence on cluster formation. Characterizing these components could help understand particle acceleration in the ICM, better interpret scaling relations and address issues related to the HSE mass bias that is fundamental for cluster cosmology.

While it is clear that these topics are interconnected, they can be addressed somewhat individually thanks to dedicated analysis, observations at different wavelengths, and their combination.

1.3 Aims and organization

This document aims at depicting the key role of galaxy clusters in our understanding of large-scale structure formation, but also as marvelous astrophysical laboratories. It focuses on the physics of the ICM, considering on the one hand the internal structure of the thermal component and its evolution, and on the other hand the acceleration of CR on clusters scales and the search for the associated diffuse γ-ray emission from the ICM. This document is organized as follows.

Chapter 2 reviews the role of high angular resolution observations at millimeter wavelengths as a key observable mean to probe the thermal properties of the cluster's hot gas phase and its evolution. It focuses on the achievements that have been obtained with the NIKA camera at the IRAM 30m telescope in the context of the observations of galaxy clusters via the SZ effects. Still, ongoing observing programs with the final NIKA2 camera are also discussed.

In Chapter 3, the focus is made on the search for diffuse γ-ray emission from galaxy clusters. As such observations can potentially probe the CR population, they provide a unique window onto the non-thermal components via the physics of particle acceleration at the cluster scale. The latest observational results using the *Fermi-LAT* satellite data are discussed, as well as the ongoing preparation for future CTA observations.

Perspectives are discussed in Chapter 4. Highlights are made on possible ways to further exploit the CTA data to constrain cluster CR physics. The opportunities of probing the non-thermal cluster component from the joint use of radio and resolved millimeter data are also discussed.

2

Measurement of the thermodynamical properties of galaxy clusters along their formation history

Contents

Contrary to their local counterparts, the ICM state of mid to high-redshift clusters is poorly known. Yet, this is where structure formation becomes more efficient and cluster counts more sensitive to cosmology. Accordingly, the detailed investigation of the evolution of the thermodynamics of the ICM is very relevant. Their structural properties and scaling relations tell us a great deal about the astrophysics associated with large-scale structure formation, and this knowledge is crucial to use clusters as reliable cosmological probes, especially in the context of the current tensions between CMB and probes of the more local Universe. Such investigations are also particularly pressing given starting/forthcoming surveys such as *eROSITA*, LSST, *Euclid* or CMB-Stage4, that aim at pushing cluster cosmology to the next step and for which the multi-wavelength complementarity is highly valuable.

As directly sensitive to the thermal pressure, the Sunyaev-Zel'dovich (SZ) effect is recognized as a powerful probe of the ICM and an excellent way to study how the matter is structured in the Universe. It is appealing to investigate the thermodynamics of distant clusters because it does not suffer from redshift dimming. After its theoretical description about 50 years ago (Sunyaev and Zeldovich 1970, 1972) and early detections, its observation by the *Planck* satellite and other CMB experiments have strongly improved our understanding of galaxy clusters. For instance, they have allowed characterizing the universal pressure profile (Planck Collaboration et al. 2013a; Pointecouteau et al. 2021), studying individual nearby systems in detail (Planck Collaboration et al. 2013c,b, 2016e), providing large cluster catalogs (Bleem et al. 2015; Planck Collaboration et al. 2016c; Hilton et al. 2021), extracting large Compton parameter sky maps (Planck Collaboration et al. 2016f; Aghanim et al. 2019), and obtaining major cosmological results (de Haan et al. 2016; Planck Collaboration et al. 2014b, 2016d).

Despite these unprecedented advances, distant clusters ($z \gtrsim 0.5$) are not resolved in such surveys. This prohibits investigating their SZ structure and the underlying astrophysics, which is very relevant in light of the cluster-CMB cosmology tension (Planck Collaboration et al. 2014b), since systematics induced by uncontrolled cluster physics may play a significant role. For these reasons, dedicated high angular resolution follow-ups are needed to better characterize clusters up to high redshifts. In fact, following the work of pioneering instruments (e.g., at IRAM or Nobeyama, Pointecouteau et al. 2001; Komatsu et al. 2001), the age of SZ imaging has now entered a new era. With the advances of new facilities such as MUSTANG2 (Dicker et al. 2014), NIKA2 (Adam et al. 2018a) and precursors, high-resolution SZ observations are now becoming very mature. It opens new opportunities to deeply address the ICM physics, but also requires new analysis techniques.

This chapter discusses the advances that have been made in our understanding of galaxy clusters thanks to resolved observations of the SZ effects in galaxy clusters. The new methods that were developed, the challenges to face, and the results obtained at the IRAM 30m telescope with the NIKA and NIKA2 cameras are highlighted. Prospects are also presented in light of the ongoing observing program.

2.1 Resolving galaxy clusters at millimeter wavelengths

2.1.1 The Sunyaev-Zel'dovich effects and their X-ray counterpart

The SZ effects (Sunyaev and Zeldovich 1972, 1980) results in the spectral distortion of the CMB due to the inverse Compton scattering of CMB photons off energetic electrons in galaxy clusters. Accounting for both the tSZ (thermal electron population) and kSZ (electrons bulk motion) effects, the signal surface brightness ΔI_ν reads

$$\frac{\Delta I_\nu}{I_0} = f(\nu, T)\, y_{\rm tSZ} + g(\nu, T, v_z)\, y_{\rm kSZ}, \tag{2.1}$$

where I_0 is the CMB intensity. The characteristic spectral dependencies, f and g, depend on the temperature only in the relativistic regime ($T \gtrsim 10$ keV). We have implemented the work by Itoh and Nozawa (2003) to account for it. The amplitude of the tSZ and the kSZ signal are given by

$$y_{\rm tSZ} = \frac{\sigma_{\rm T}}{m_e c^2} \int P_e d\ell \tag{2.2}$$

and

$$y_{\rm kSZ} = \sigma_T \int \frac{-v_z}{c} n_e d\ell. \tag{2.3}$$

They are sensitive to the electron pressure P_e and the line-of-sight velocity v_z, respectively. The kSZ effect is subdominant and is generally neglected unless the velocity reaches $\gtrsim 1000$ km/s.

In comparison, the X-ray surface brightness is sensitive to the gas electron density, n_e, as

$$S_{\rm X} = \frac{1}{4\pi\,(1+z)^4} \int n_{\rm e}^2 \Lambda(T, Z)\; d\ell, \tag{2.4}$$

where Λ is the cooling function and Z the metallicity. X-ray spectroscopy can be used to infer the gas temperature and metallicity when sufficient statistics is available.

X-ray and SZ observations are independent probes of the same cluster component. They are thus highly complementary, especially since they suffer from different systematics and limitations. As we shall see, their combination may be used to provide detailed thermodynamical investigations of the ICM. This is particularly the case at high redshift because the SZ surface brightness is not affected by redshift dimming, provided sufficient sensitivity and resolution are available.

2.1.2 Measuring the Sunyaev-Zel'dovich signal at high angular resolution

The SZ effects (Mroczkowski et al. 2019, for a review) are observable around millimeter wavelengths. The angular size of distant ($z \gtrsim 0.5$) clusters is of the order of a few arcmin so that subarcmin resolution is required to reveal their inner structure. At these frequencies, this is only achievable from the ground either with interferometers[1], or large aperture single dish telescopes[2] on which we focus here.

The telescopes are equipped with cameras made of arrays of cryogenic detectors, which scan the target sky regions to modulate the signal in time. The mapping performance of SZ imagers is driven by the number of detectors and their sensitivity, the size of the field of view, and the angular resolution. The atmospheric fluctuations are generally the main contribution to the noise (Adam et al. 2014). The atmosphere also induces absorption of the astrophysical signal that has to be corrected using dedicated methods (Catalano et al. 2014).

The necessary removal of the atmospheric noise, inherent to SZ imagers, is made by combining the time domain signal from the different detectors, which all see the same common atmospheric fluctuations, but different regions of the sky. Such methods imply filtering of the astrophysical signal on scales larger than the instrument field of view[3] and the associated transfer function has to be accounted for in the scientific analysis. In addition, correlated noise residual propagates

[1] See, e.g., the Sunyaev-Zel'dovich Array (SZA, e.g., Muchovej et al. 2007), the Combined Array for Research in Millimeter-wave Astronomy (CARMA, e.g., Plagge et al. 2013), the Arcminute Microkelvin Imager (AMI, e.g., AMI Consortium et al. 2012; Rumsey et al. 2016) or The Atacama Large Millimeter/submillimeter Array (ALMA, e.g., Kitayama et al. 2016) for past and current interferometers observing the SZ effect.

[2] See, e.g., the MUSTANG2 at the Green Bank 100m telescope with a 9 arcsec resolution at 90 GHz, or NIKA2 at the IRAM 30m telescope with 12 and 18 arcsec resolution at 260 and 150 GHz, respectively.

[3] Multi-frequency time-domain analysis were attempted taking advantage of the atmospheric spectral dependence to avoid this issue (Adam et al. 2014), but with mitigated results.

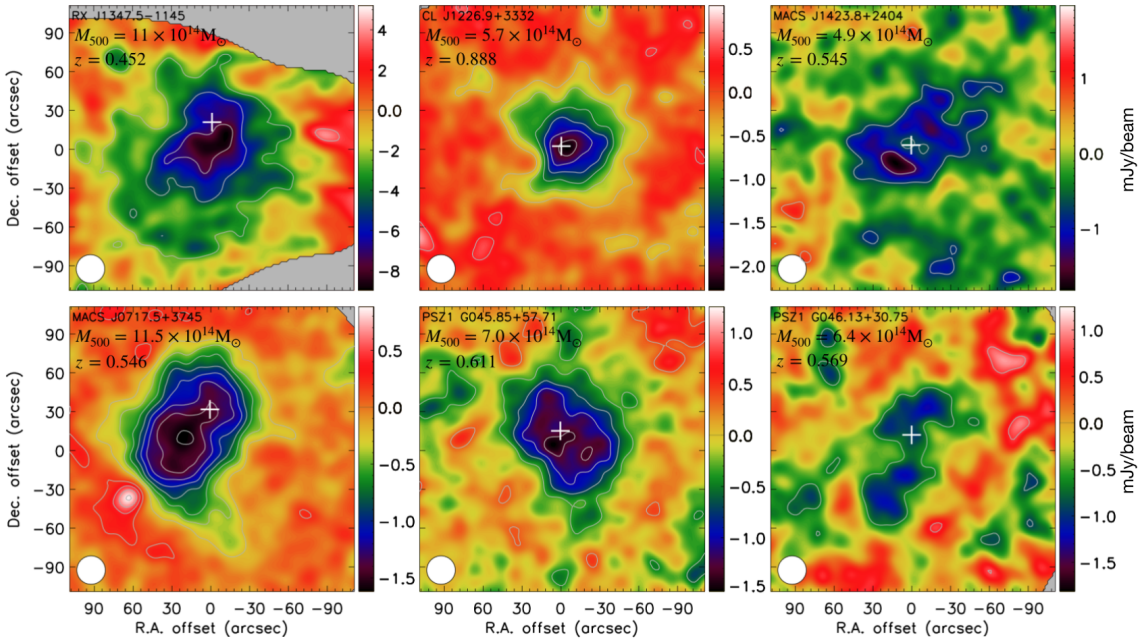

Figure 2.1: Surface brightness images of the NIKA cluster sample at 150 GHz. From Adam et al. (2018b).

to the maps so that large scales fluctuations may affect the data and should be considered when interpreting the results. In the case of diffuse SZ emission, the characterization of the beam is critical because it tells us how the sky signal is convolved by the optical chain, but also because it enters into the calibration procedure together with the instrument spectral bandpass. For more details, we refer to Adam (2015) and Ruppin (2018) in which the framework was developed and the computation of the data products necessary for scientific exploitation are described.

2.1.3 The NIKA cluster sample: a pilot project for NIKA2

NIKA2 has been installed at the IRAM 30m telescope since the end of 2015. It observes the sky with state-of-the-art detector sensitivity, at 150 and 260 GHz. The beam full-width at half-maximum is about 18 and 12 arcsec, respectively, and the field of view of 6.5 arcmin diameter (Adam et al. 2018a), so that it is well designed for SZ mapping up to high redshift. The NIKA pathfinder camera was similar but with a reduced field of view of 2 arcmin (Catalano et al. 2014). As a reward for the construction of NIKA2, the collaboration was awarded guaranteed-time observations, among which that of the SZ Large Program (LPSZ). This project aims at observing about 45 clusters at 150 and 260 GHz with the NIKA2 camera. Its goal is to investigate the structural properties of a representative galaxy cluster sample and its impact on the mass-observable scaling relation at redshift $0.5 < z < 0.9$.

To prepare the scientific outcomes of the LPSZ, and more generally of NIKA2 SZ observations, we have built a sample of six galaxy clusters with the NIKA pathfinder camera. They have been selected by sampling different configurations: very bright and well-known, high-redshift, extremely disturbed major merger, relaxed cool-core, or *Planck* selected clusters. The scientific exploitation of this sample is summarized in the following and the 150 GHz images are shown in Figure 2.1. The corresponding data and products have been made publicly available[4].

[4]The data have been released at http://lpsc.in2p3.fr/NIKA2LPSZ/nika2sz.release.php

2.2 Astrophysical contamination

Several kinds of astrophysical sources may contribute to the observed signal in the millimeter range. Since early observations of the SZ effect, they have been recognized as major contaminants (e.g., Cooray et al. 1998; Lin et al. 2009; Muchovej et al. 2010; Sayers et al. 2013b). As the instrument's sensitivity increases and the measurements get more precise, it has become very important to develop methodologies and tools to account for them.

2.2.1 Diffuse backgrounds and foregrounds

Diffuse astrophysical emission, including the CMB primary anisotropies, the cosmic infrared background (CIB), or Galactic foregrounds (dust, synchrotron, and free-free) should induce an extra source of noise that cannot be reduced by increasing the observing time.

The Galactic emission depends on the sky location. It can be estimated on an individual basis by extrapolating *Planck* data (Planck Collaboration et al. 2016a) spatially and spectrally. For instance, Adam et al. (2016) found that this background was by far negligible for MACS J1423.8+2404 (69 deg above the Galactic plane), which generally applies to most cases.

The level of CMB anisotropies is estimated according to its power spectrum computed given a set of cosmological parameters (using standard tools, e.g., Lewis et al. 2000). It is expected to be negligible because of the steep decline of the power with angular scale (Adam et al. 2016).

Finally, the CIB contributes to the noise via the clustering of dusty star-forming galaxies and the shot noise from both dusty star-forming galaxies and radio sources. We have developed a framework that extrapolates the clustering power spectrum measured by Planck Collaboration et al. (2014d) and models the shot noise using the results from Béthermin et al. (2012) in the case of dusty star-forming galaxies and Tucci et al. (2011) for radio sources. The shot noise dominates by a factor of about 5 over the clustering term. It can be significant. For instance, in deep NIKA observations of MACS J0717.5+3745, the noise is boosted by 15 and 22% at 150 and 260 GHz, respectively, due to the CIB (Adam et al. 2017b). Thus, the CIB appears as a very relevant diffuse astrophysical noise contribution and constitutes an irreducible sensitivity floor. The current precision on such a background is about 20%, but we note that another NIKA2 program should improve a lot on its characterization. See also Ruppin et al. (2018) in which this methodology was applied to NIKA2 and the different noise contributions are shown in terms of their power spectrum.

2.2.2 Unresolved infrared and radio sources

Strong individual sources, if blended in the SZ signal, may introduce a bias in the recovered morphology, as highlighted in Adam et al. (2015, 2016, 2017b, 2018b), Kéruzoré et al. (2020) and Dicker et al. (2021). NIKA(2) observes simultaneously at 150 and 260 GHz. This allows us to identify infrared contaminants, such as dusty-star-forming galaxies. For radio sources, on the other hand, we have to rely on lower frequency observations that are not always available.

Beyond the point source identification, we have developed a methodology that combines NIKA or NIKA2 with external data (e.g., *Herschel* or radio surveys) to provide a prior on the flux of the contaminants, assuming a given model. The model is usually a power law for radio sources and a modified black body for dusty star-forming galaxies (DSFGs). This was shown to be critical when recovering the morphology and pressure profile of galaxy clusters (Adam et al. 2016). This methodology was later used in many analyses (Adam et al. 2017b; Ruppin et al. 2017, 2018; Kéruzoré et al. 2020)

Given these results, we have argued that the bias induced by infrared sources can be mitigated since they are identified at 260 GHz and do not strongly correlate with the target signal such that on

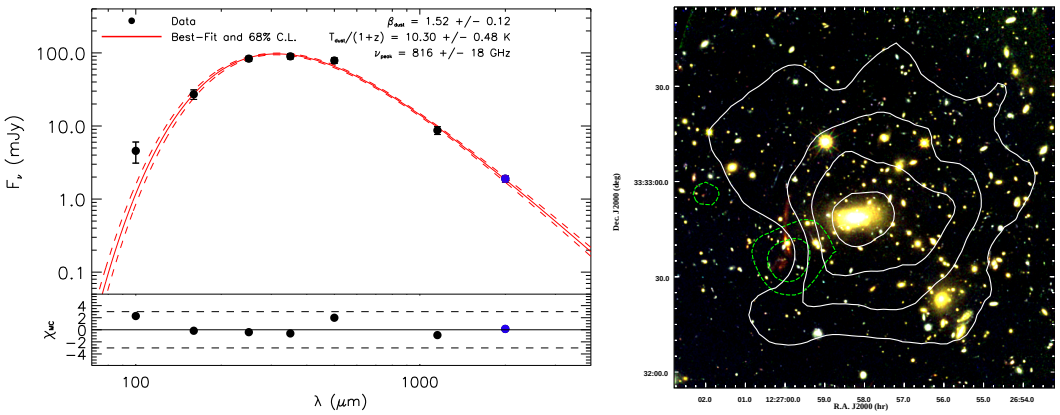

Figure 2.2: **Left:** Spectral energy distribution (SED) of one of the lensed galaxy candidate in the field of CL J1226.9+3332 (left). **Right:** Multi-wavelength view of the field of CL J1226.9+3332: 150 GHz SZ contours in white, 260 GHz contours in green, and *Hubble* color image. A giant red arc is visible at the 260 GHz peak. Extracted from NOEMA (W16DL) and EMIR (193-16) proposals (Adam, Beelen et al., 2016).

average, they should not introduce misinterpretations. Radio sources, on the other hand, are mostly found in the BCG of cool-core relaxed clusters, such that their presence correlates strongly with the dynamical state. They cannot be well-removed using lower frequency data because it implies a large extrapolation that is often not reliable.

2.2.3 Clusters as telescopes to probe galaxy formation in the distant Universe

While they are a contaminant to the SZ signal, the detection of DSFGs around clusters may appear as an opportunity to test galaxy formation at high redshift. Indeed, high-redshift DSFGs play a fundamental role in galaxy formation and evolution. In the quest for probing these distant objects, galaxy clusters can serve as giant telescopes, thanks to the lensing magnification they produce, to observe galaxies that would be inaccessible otherwise (see recent results by Sun et al. 2022).

In this context, we have attempted the follow-up of several high-redshift candidates with IRAM facilities (EMIR and NOEMA), as highlighted in Figure 2.2 in the case of a $z = 2.4$ source lensed by CL J1226.9+3332. These observations aimed at performing CO redshift searches, checking for source multiplicity, obtaining a high signal-to-noise (S/N) ratio and accurate position, and thus identifying counterparts at other wavelengths, to obtain a detailed view of the physics of DSFGs at high redshift, using a multi-wavelength approach. Unfortunately, these observations were not successful yet (non-detection and not observed) but others are ongoing[5].

In addition to the interest in individual sources, we expect CIB dimming due to the cluster-induced gravitational lensing (Zemcov et al. 2013). This was not investigated with NIKA nor NIKA2 and may provide an interesting way to measure the integrated total intensity of the CIB.

Once astrophysical contaminants are identified and well-characterized, whether they are scientifically interesting on their own or not, they can be accounted for as requested. They can either be accurately subtracted or masked so that the remaining SZ signal can be used to study the ICM.

[5] Another group performed the observations of one of our target with similar goals, revealing a low metalicity together with a high dust content, which may challenge our current picture of early dust formation (Pope et al. 2017).

2.3 Unveiling the dynamical state of high-redshift clusters

The dynamical state is one of the most important attributes of galaxy clusters and key information to studying other cluster properties. However, it is still unclear how much it affects the scatter and biases that arise in the mass-observable relations and how it evolves across mass and redshift. This section reviews the two main ways that have been explored to unveil the dynamical state of galaxy clusters: via the analysis of features in the tSZ images, and the reconstruction of the gas velocity using the kSZ effect.

2.3.1 Morphology and substructures from thermal Sunyaev-Zel'dovich imaging

The dynamical state of galaxy clusters is reflected in the inner structure of the ICM, which is thus a valuable way to understand how clusters form and assess connections with the astrophysics at play. In principle, this information can be accessed via resolved tSZ imaging because the thermal pressure is sensitive to shocks, the presence of substructures, and disturbances in the ICM.

To investigate the sensitivity of NIKA-like observations to the cluster pressure morphology and substructure, dedicated tools were developed in Adam et al. (2018b). We focused on the gaussian gradient magnitude (GGM) and the difference of gaussian (DoG) filtering. The former is defined as the magnitude of the gradient map, smoothed with a Gaussian kernel over some scale G_{θ_0} (see Sanders et al. 2016, for application in the X-rays),

$$M_{\rm GGM} = \sqrt{(\mathcal{D}_{\rm x} * [G_{\theta_0} * M])^2 + (\mathcal{D}_{\rm y} * [G_{\theta_0} * M])^2}, \tag{2.5}$$

where M is the input map, and where the filter, along the axis x and y, is

$$\mathcal{D}_{\rm x} = \mathcal{D}_{\rm y}^{\rm T} = \frac{1}{8\Delta\theta} \begin{pmatrix} -1 & 0 & 1 \\ -2 & 0 & 2 \\ -1 & 0 & 1 \end{pmatrix}. \tag{2.6}$$

The GGM filter allows for the identification of discontinuities in the pressure (i.e., shocks) or compression. The latter is simply the difference of tSZ maps smoothed at two different scales (similar to unsharp-masking, as used in X-ray analysis, see e.g., Fabian et al. 2003),

$$M_{\rm DoG} = G_{\theta_1} * M - G_{\theta_2} * M, \tag{2.7}$$

which captures the ICM substructures within the range of scales $[\theta_1, \theta_2]$. These filters were applied to the NIKA cluster sample, to toy models, and to synthetic tSZ maps extracted from the RHAPSODY-G hydrodynamical simulations (Wu et al. 2013; Hahn et al. 2017) to test the behavior of these new tools and interpret the results. This was also the opportunity to build a first mock sample associated with NIKA data (see also Ruppin et al. 2019, for similar developments with other simulations, in another context). The simulations were also used to carefully investigate the amplitude and impact of possible systematics, among which: the residual contamination from compact sources, the filtering implied by the NIKA data processing, and the propagation of the spatially correlated noise. The application of the GGM and DoG filters is illustrated in Figure 2.3 both on a RHAPSODY-G cluster and a comparable NIKA cluster. In both cases, the cluster is made of a main structure undergoing a merging event with a subgroup. A discontinuity and an extension are visible, as indicated in the images.

Thanks to these developments, it was shown that the quality of resolved tSZ data is now sufficient for detailed investigation of the ICM even at high redshift. They have a huge potential for investigating cluster formation in distant systems. The GGM and DoG filters revealed features that

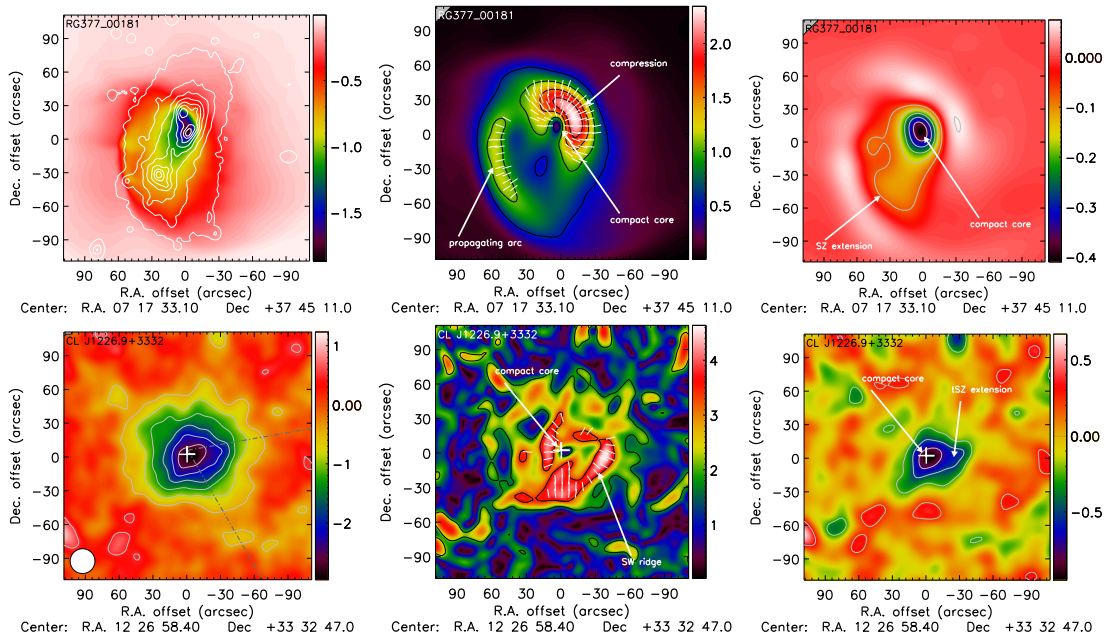

Figure 2.3: Application of the GGM and DoG filter on a RHAPSODY-G (top) and NIKA (bottom) cluster. The RHAPSODY-G mock data does not account for noise or instrumental response. **Left:** surface brightness images. Dark matter surface density contours are also reported in white for the RHAPSODY-G cluster. **Middle:** GGM filtered maps highlighting discontinuities and compressions. **Right:** DoG maps highlighting substructures. Figure extracted from Adam et al. (2018b).

correspond to compressions and shocks related to merger events, as also indicated by the comparison with hydrodynamical simulations. Nevertheless, high S/N ratio data ($\gtrsim 10$ at the tSZ peak) are necessary to detect significant features and only half of the NIKA cluster present reliable detections. It was also shown that the clean subtraction or identification of point sources is important, but the corresponding filtered images are distinct from that of tSZ substructures. The effect of the data reduction processing is minor because of the characteristic scale of the features, at least for the NIKA sample. The tools developed here are not unique and other methodologies may help to push further the investigation of the ICM dynamical state (e.g., centroid shift, concentration, etc, as used in X-ray).

In the end, we have developed and characterized a new set of tools, which can be used to study merging events and infer the cluster structural properties from resolved tSZ data. In turn, this information can be used to study the thermodynamical distribution of scaling relations, e.g., in dedicated sectors, and infer the role of the dynamical state on scaling relations. These tools have been commonly applied to help subsequent analysis of NIKA2 clusters (e.g., Ricci 2018; Ricci et al. 2020; Ruppin et al. 2018)

2.3.2 Imaging the gas velocity with the kinetic Sunyaev-Zel'dovich effect

The collision velocity of clusters is extremely valuable as it tells us about the merger kinematics, but also hydrodynamical interactions, and the relation between the dark matter and the baryons. The statistical properties of the large-scale matter velocity field, including clusters, also provides a way to test cosmology and probe structure formation (in particular dark energy and modified gravity models, Kaiser 1987; Bhattacharya and Kosowsky 2007). The study of the cluster's internal velocities is possible via the optical spectroscopy of its member galaxies (e.g., Ferrari et al. 2005),

but is affected by fundamental degeneracies between the peculiar velocities and the expansion of the Universe. The subtraction of the Hubble flow with independent distance measures (e.g., Tully and Fisher 1977) limits such measurement to the local Universe. The kSZ effect provides a unique and direct probe of the gas momentum, and thus its velocity, with the CMB as a fixed reference frame. It is difficult to measure because it requires high sensitivity, the control of systematic effects, and high resolution if one wants to image the signal. The first statistical detection of the pairwise kSZ signal was reported in Hand et al. (2012) using the joint analysis of Atacama Cosmology Telescope and the Baryon Oscillation Spectroscopic Survey data. Later, Mroczkowski et al. (2012) reported the hint of the presence of a kSZ signal in MACS J0717.5+3745 using Bolocam data at 140 and 268 GHz. The improved reanalysis of the augmented Bolocam data by Sayers et al. (2013b) led to the first significant kSZ detection in an individual cluster.

MACS J0717.5+3745 is part of the NIKA sample. As a striking example of a very massive triple merging system at $z = 0.55$, it is indeed very well-suited for kSZ searches. On the other hand, NIKA (and NIKA2) is well-suited to search for the kSZ effect in clusters due to its high sensitivity, high resolution, and dual-band photometer capabilities. After a careful treatment of point source contamination, we used the NIKA data for a detailed kSZ investigation (Adam et al. 2017b). The kSZ signal was separated from the tSZ one by inverting equation 2.1 using the combination of the two NIKA bands (that observes at $\nu_{1,2} \equiv \{150, 260\}$ GHz), as

$$y_{\rm kSZ} = \frac{f(\nu_1, T)\Delta I_{\nu_2} - f(\nu_2, T)\Delta I_{\nu_1}}{I_0 f(\nu_1, T) g(\nu_2, T) - I_0 f(\nu_2, T) g(\nu_1, T)}. \tag{2.8}$$

The constraints on the tSZ and kSZ spectra as integrated in different regions of the cluster are shown in the left panel of Figure 2.4. We also used equation 2.8 to extract an image of the kSZ signal, and thus the map of the gas momentum in MACS J0717.5+3745, as reported in Figure 2.4, right panel and compared to other wavelengths. The image presents a bipolar structure, reflecting the pre-merger between the two main groups oriented nearly along the line-of-sight. The detection reaches 5.1 and 3.4 σ at the peaks. The extraction of the velocity itself implies to disentangle the kSZ signal from the ICM optical depth (see equation 2.3), which requires an extra information on the ICM such as its temperature. We developed a modeling framework that accounted for the four sub-clusters, fitting the NIKA maps in the two bands simultaneously, informed from the *XMM-Newton* derived isothermal spectroscopic temperatures in each group, as

$$\frac{\Delta I_\nu^{\rm model}}{I_0} = \sigma_{\rm T} \sum_i f(\nu, T_{\rm X}^{(i)}) \frac{k_B T_{\rm X}^{(i)}}{m_e c^2} \int n_e^{(i)} d\ell + \sigma_T \sum_i g(\nu, T_{\rm X}^{(i)}, v_z) \frac{-v_z^{(i)}}{c} \int n_e^{(i)} d\ell. \tag{2.9}$$

In this case, $T_{\rm X}^{(i)}$ and $v_z^{(i)}$ are scalar quantities. This allowed us to derive the following velocities for the three main groups (see Figure 2.4): $v_z^{(B)} = 6607^{+3212}_{-2409}$ km/s, $v_z^{(C)} = -4106^{+1594}_{-1104}$ km/s, $v_z^{(D)} = 150^{+1510}_{-1208}$ km/s. However, the posterior likelihood revealed large remaining degeneracies between the optical depth and the velocity, leading to large uncertainties. We thus used X-ray imaging data to add an extra prior on the gas density, especially for sub-cluster B, leading to a much better constraint of $v_z^{(B)} = 2058^{+486}_{-447}$ km/s, although more sensitive to modeling assumptions. Finally, the recovered best-fit model allows us to compute a map of the optical depth, which we used together with equation 2.3 to extract a map of the line-of-sight velocity of the ICM, albeit model dependent. In this very hot cluster, relativistic corrections to the SZ effects are important and we derived an X-ray spectroscopic temperature map to correct for it. Note that another NIKA cluster, CL J1226.9+3332, was used to search for the kSZ signal using a similar method. We reported a measurement of $v_z = -445 \pm 461$ km s^{-1} compatible with no kSZ signal.

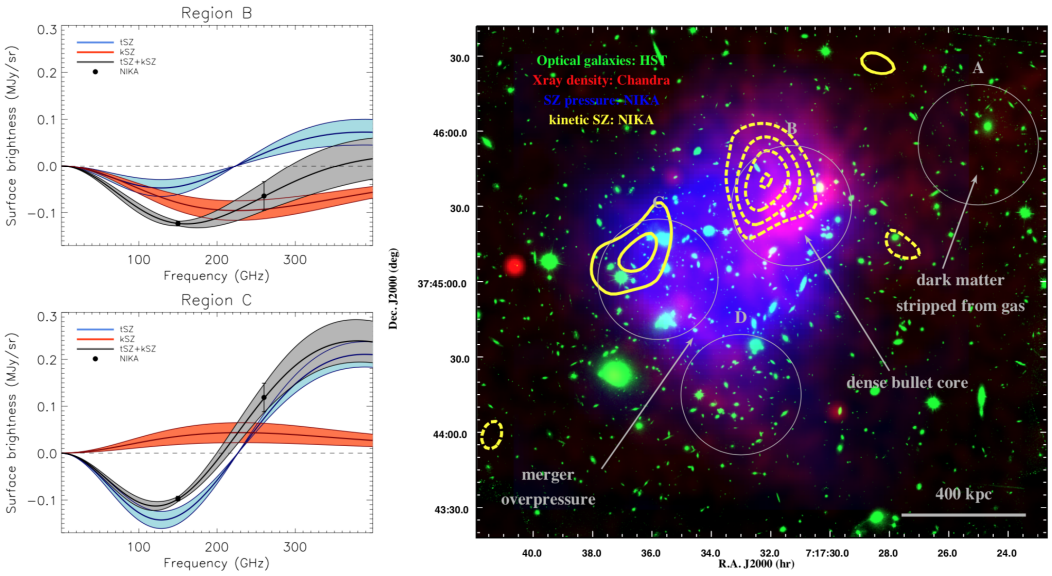

Figure 2.4: **Left:** tSZ and kSZ amplitude constrained by NIKA data in region B (top) and C (bottom). Extracted from Adam et al. (2017b). **Right:** multi-wavelength view of MACS J0717.5+3745, including the kSZ imaging contours in yellow. The different groups are indicated in grey. Extracted from the press release.

The work discussed here provided an important milestone in kSZ searches because it is the first time that imaging of the kSZ effect was reported. Although model-dependent, we also derived for the first time a map of the gas velocity, via the kSZ effect. This effort proved very important to understand the ongoing merger in MACS J0717.5+3745, showing the strength of kSZ imaging for cluster physics. Because it relies on the 260 GHz NIKA band, where the contribution from sub-millimeter galaxies is important, this work has shown that point source subtraction is critical and that the CIB is likely to be a limiting factor for future kSZ mapping at high angular resolution. More recently, Sayers et al. (2019) studied the kSZ signal in 10 massive clusters observed by Bolocam, including three NIKA clusters, but no further significant detection was reported. Nonetheless, other well-known mergers could be ideal targets for kSZ searches with the higher NIKA2 angular resolution, possibly complemented by the 90 GHz band of MUSTANG2.

2.4 Thermodynamical properties of distant galaxy clusters

The ICM is essentially thermal. The characterization of its thermodynamical properties is thus important to understand how clusters form and connect their observational properties to underlying cosmological and astrophysical models. This section reviews the methodological development, challenges, and results obtained regarding the measure of the pressure profile in distant clusters over the last few years, as one of the most fundamental properties of the ICM. X-ray observations provide complementary information, which allows us, in combination with tSZ, to unveil nearly all the thermodynamical properties of the ICM, as also summarized hereafter.

2.4.1 The thermal pressure profile of galaxy clusters up to high redshift

The thermal pressure profile of the ICM is a fundamental tracer of the matter distribution in galaxy clusters. It is intimately related to the underlying potential well, shaped by the dark matter because the gas is compressed by gravity. Additionally, it is sensitive to astrophysical processes such as AGN feedback and dynamical activity that provide another energy input. It can be directly ac-

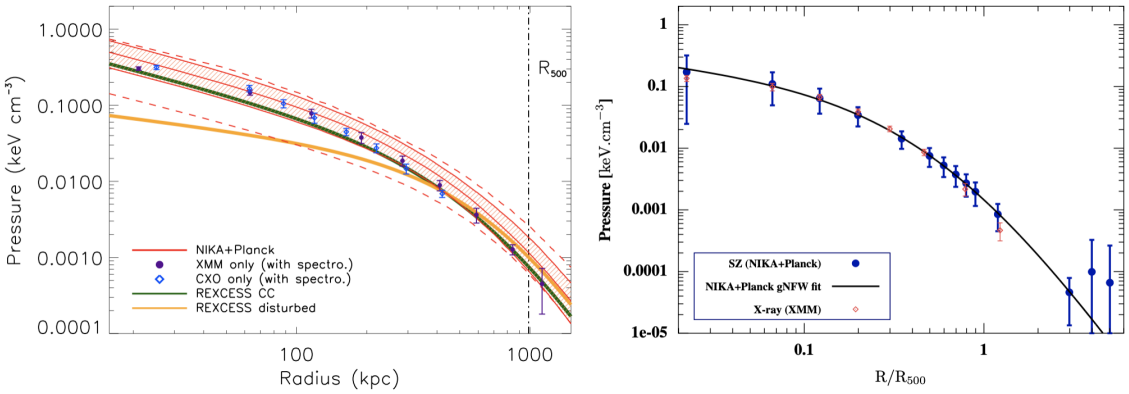

Figure 2.5: The pressure profile of galaxy clusters observed by NIKA. **Left:** parametric generalized Navarro-Frenk-White model fit to the NIKA data for MACS J1423.8+2404 plus the *Planck* total flux prior and comparison to expectations from the REXCESS sample (Arnaud et al. 2010) for cool-core and disturbed clusters. **Right:** parametric and non-parametric fit to the NIKA+*Planck* data for PSZ1 G045.85+5771. In both cases, the recovered pressure is compared to the one derived from X-ray only data. Figure extracted from Adam et al. (2016) and Ruppin et al. (2017).

cessed through resolved tSZ observations if enough sensitivity is available. Its characterization is also particularly relevant for cluster detection in the tSZ, which usually relies on match filtering assuming a given pressure model.

Over the last years, we have developed different methods to extract the pressure profile from resolved NIKA and NIKA2 tSZ data, but also in combination with other observations from MUSTANG and Bolocam, or *Planck* data. The most standard technique that we have used consists of the forward modeling and fitting of the NIKA map, together with a prior on the total flux inferred from *Planck* data (Adam et al. 2015, 2016; Ruppin et al. 2017, 2018; Ricci et al. 2020; Kéruzoré et al. 2020; Ruppin et al. 2020). The pressure model (usually generalized Navarro-Frenk-White profile) is projected along the line-of-sight, the resulting map convolved with the data processing transfer function and beam, and converted into surface brightness accounting for spectral responses and data calibration. Markov Chain Monte Carlo (MCMC) fitting is used to sample the model parameters, either with the originally developed packages (`IDL`-based, Adam 2015) or using `Python`-based packages such as `emcee` (Foreman-Mackey et al. 2013). The necessity to account for the data processing transfer function was realized and implemented early on (Adam et al. 2015). Later, we also accounted for the noise residual correlations by computing the noise covariance matrix including the CIB contribution (Adam et al. 2016). The implementation of non-parametric fitting was developed in Ruppin et al. (2017), using the power-law interpolation between pressure values binned in radius. We also developed new methods to combine data from different instruments in Romero et al. (2018). This proved very useful to sample the pressure profile from the core to its outskirt. Later, the tools evolved into the `PANCO2` software (Pipeline for the Analysis of NIKA2 Cluster Observations, Ruppin 2018; Kéruzoré 2021; Kéruzoré et al. 2022b, see also Section 2.4.2). Note that tSZ observations alone can be used to recover the pressure only in the case where relativistic corrections are negligible. In practice, however, the X-ray density is used jointly to compute the temperature, which enables accounting for the corrections in the fitting procedure (see Section 2.4.2). Other similar softwares have been developed and applied to the NIKA data by external teams (e.g., Castagna and Andreon 2019, 2020). In Figure 2.5, we illustrate the reconstruction of the pressure profile for two clusters of the NIKA sample, using different versions of the tools we developed.

The cluster pressure profile can also present features in the cluster periphery related to gas

accretion in the outskirts (Molnar et al. 2009). While NIKA2 is not sensitive enough to image the tSZ signal on very large scales, this can be attempted with *Planck* in the direction of high S/N ratio resolved nearby clusters. In Hurier et al. (2019), we reported the detection of a discontinuity, in the pressure profile of Abell 2319 at $R = 2.93 \pm 0.05 R_{500}$ (8.6σ significance). We interpreted this feature as the accretion shock and constrained its Mach number to $\mathcal{M} > 3.25$, consistently with expectations from numerical simulations. By combining the location of the shock with theoretical results and the tentative discontinuity seen in the galaxy density profile, we also inferred the mass accretion rate of the cluster to $\dot{M} = (1.4 \pm 0.4) \times 10^{14}$ $\mathrm{M}_{\odot}$ Gyr^{-1} and the gas adiabatic index $\gamma_g = 1.65 \pm 0.02$, consistently with the expected value of $\gamma_g = 5/3$ (see also Shi 2016, for details).

The detailed characterization of the cluster pressure profile has been achieved at low redshift, even up to the accretion shock for some sources, and these results are widely used in the community (Arnaud et al. 2010; Planck Collaboration et al. 2013a; Sayers et al. 2013a; Ghirardini et al. 2019a). To push its investigation at higher redshifts, we have developed dedicated tools that allow us to recover the pressure distribution from ground-based observations such as those obtained by NIKA and NIKA2. So far, mostly individual studies have been reported on specific targets such that no general conclusions can be firmly established for the cluster population. Nonetheless, all of them agree with the pressure profile expected from the extrapolation of the one measured for low redshift samples, even at low mass and for highly perturbed systems. This also seems to agree with the cluster properties following standard evolution at least out to $z \sim 1.5$ (see Chapter 1). Interestingly, a remarkable agreement has been obtained with the pressure inferred from X-ray only, showing that no major uncontrolled systematic effect is at play on both sides. Obviously, this should be confirmed and further investigated in a systematic way with well-characterized samples (see Section 2.5).

2.4.2 The thermodynamical radial properties of clusters from Sunyaev-Zel'dovich and X-ray photometry

The tSZ effect directly measures the thermal pressure. The X-ray emission is mainly sensitive to the thermal gas density squared and can be used to infer the spectroscopic temperature if sufficiently deep observations are available. These two observables are therefore sensitive to the same cluster component but in a complementary way. Over the last few years, we have explored new methodologies to extract information related to the thermodynamics of the ICM and the matter distribution in galaxy clusters, using the joint analysis of resolved tSZ and X-ray data.

The methodology discussed in Section 2.4.1, to recover the pressure profile, was early incremented to jointly constrain the gas density profile derived independently from X-ray data. Consequently, the temperature can be inferred from the pressure and density taking advantage of the ideal gas law,

$$k_{\rm B}\, T_e(r) = P_e(r)/n_e(r) \equiv k_{\rm B}\, T_{\rm gas}(r). \tag{2.10}$$

Similarly, the entropy is given by

$$K_e(r) = \frac{P_e(r)}{n_e(r)^{5/3}}. \tag{2.11}$$

Assuming the HSE and spherical symmetry, the enclosed mass is given by

$$M_{\rm HSE}(r) = -\frac{r^2}{\mu_{\rm gas} m_p n_e(r) G} \frac{dP_e(r)}{dr}, \tag{2.12}$$

and is connected to the total mass (and overdensity contrast) via the HSE mass bias as

$$M_{\rm tot}(r) = \frac{M_{\rm HSE}(r)}{(1 - b_{\rm HSE})}. \tag{2.13}$$

The X-ray density tells us about the enclosed gas mass,

$$M_{\rm gas}(R) = 4\pi \int_0^R \mu_e m_p n_e(r) r^2 dr. \tag{2.14}$$

which can be used to derive the gas fraction,

$$f_{\rm gas}(r) = \frac{M_{\rm gas}(r)}{M_{\rm tot}(r)}. \tag{2.15}$$

On the other hand, the tSZ integrated flux, often used to track the cluster mass, can be obtained by direct integration of the y-map, in a cylindrical way, as

$$Y_{500,\rm cyl} = \int_0^{R_{500}} 2\pi r y dr, \tag{2.16}$$

or by spherical integration of the recovered pressure profile,

$$Y_{500,\rm sph} = \frac{\sigma_{\rm T}}{m_e c^2} \int_0^{R_{500}} 4\pi r^2 P_e dr. \tag{2.17}$$

Similarly, its X-ray analog, Y_X, is given by

$$Y_{X,500} = M_{\rm gas}(R_{500}) T_{\rm X}. \tag{2.18}$$

Using the simultaneous MCMC sampling of the density and pressure, it is straightforward to propagate the constraints on all the thermodynamical and matter properties described above, as illustrated in Figure 2.6. This methodology was used in many NIKA/NIKA2 publications (e.g., Adam et al. 2016; Ruppin et al. 2018; Kéruzoré et al. 2020). It is also implemented in the `PANCO2` software (Kéruzoré et al. 2022b). In Ricci et al. (2020), we also use it to calibrate the relation between the two mass proxies $Y_{X,500}$ and Y_{500} as a function of radius. Note that a similar methodology was used by other projects, such as X-COP in the case of nearby clusters combining *Planck* with *XMM-Newton* (Eckert et al. 2017a).

Thanks to the combination of resolved tSZ data and X-ray photometry, we can recover all the radial thermodynamical properties of galaxy clusters. Under the assumption of spherical symmetry and using the HSE, we have access to the mass and the gas fraction. On the other hand, the tSZ (and X-ray) imaging provides complementary information about the dynamical state of clusters, and the integrated tSZ signal, Y_{500} can be recovered as a powerful mass proxy. This allows us to study the cluster properties in different regions and as a function of the reference center to investigate the implications of the underlying physics and assumptions on the cluster global properties (see also Section 2.5).

2.4.3 Mapping the hot gas temperature in galaxy clusters combining X-ray and Sunyaev-Zel'dovich imaging

The structure of the gas temperature is fundamental for several reasons. The temperature informs us about shock-heated gas undergoing merging events, it is connected to turbulence, and may help study cold-front and sloshing events. It is thus an excellent diagnosis for the gas dynamics and a key observable to understand cluster formation and to interpret scaling relations. Precise temperatures are also crucial for inferring cluster masses under the HSE hypothesis such that they are key for cluster cosmology as long as X-ray is involved. Temperatures are traditionally derived by fitting an isothermal model to the X-ray spectra. Unfortunately, they suffer from two main systematic effects.

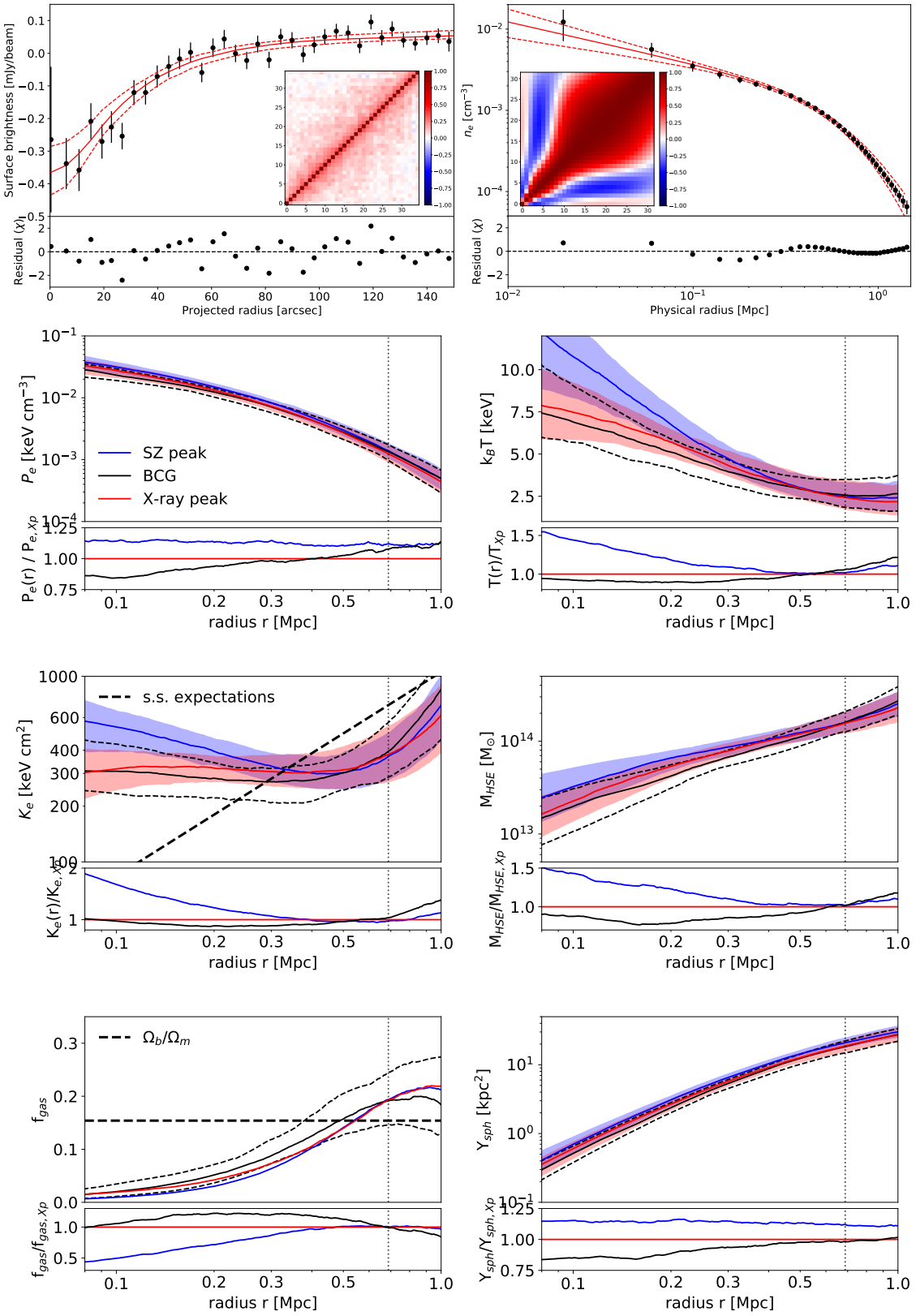

Figure 2.6: Thermodynamical profiles of XLSSC 102 ($z = 0.97$, $M_{500} \sim 2\times10^{14}$ M$_\odot$). The top row shows the tSZ surface brightness (left) and the X-ray density (right) profiles with their covariance matrices. The six bottom panels give the pressure, temperature, entropy, HSE mass, gas fraction, and integrated Compton parameter derived with the different centers given in the legend. Extracted from Ricci et al. (2020).

The former is related to the fact that temperatures are directly affected by the energy calibration of X-ray instruments. In fact, *XMM-Newton* temperatures are generally lower than those of *Chandra*, by up to 20% (e.g., Schellenberger et al. 2015). The latter arises because the X-ray emission is weighted by the gas density so that denser and cooler regions dominate, and thus clumping affects X-ray temperatures (Mazzotta et al. 2004; Rasia et al. 2014). Last but not least, X-ray spectroscopy becomes very challenging with increasing redshifts, but also at very high temperatures given the spectral responses of the main current instruments.

We proposed a new method for mapping the gas temperature distribution in galaxy clusters using tSZ imaging in combination with X-ray photometry (Adam et al. 2017a). Indeed, the tSZ and X-ray imaging are sensitive to the projected gas pressure and density squared, respectively, such that their combination can be used to map the temperature. We used MACS J0717.5+3745 as a test case because this cluster is very hot, providing huge temperature leverage, and very deep data were available. The so-called SZX temperature is defined as follows,

$$k_{\rm B}T_{\rm SZX} \equiv \frac{\int P_e d\ell}{\int n_e d\ell} = \frac{1}{\sqrt{\ell_{\rm eff}}} \frac{m_{\rm e}c^2}{\sigma_{\rm T}} \sqrt{\frac{\Lambda\left(T_e, Z\right)}{4\pi\left(1+z\right)^4 S_{\rm X}}} y_{\rm tSZ}, \tag{2.19}$$

with $\ell_{\rm eff} = \left(\int n_e d\ell\right)^2 / \int n_e^2 d\ell$ an effective line-of-sight length of the ICM. Unlike the spectroscopic temperature, the $T_{\rm SZX}$ map is an estimate of the gas mass-weighted temperature. It is affected by different systematic effects, in particular: the 3D geometry of the cluster via $\ell_{\rm eff}$, the absolute NIKA (or others) calibration uncertainty and data processing transfer function, and kSZ contamination in some specific cases such as MACS J0717.5+3745. Relativistic effects are negligible because they can be dealt with iteratively. Note that entropy mapping is also available in the same way. The $T_{\rm SZX}$ map of MACS J0717.5+3745 is reported in Figure 2.7, where we can see exceptionally high temperatures, reaching up to 25 keV. The hot gas bar arises from adiabatic compression in this extreme merger. The comparison with X-rays shows a good morphological agreement. *XMM-Newton* spectroscopic temperatures are about 10% lower and the *Chandra* temperatures about 10% higher than our gas mass-weighted temperature, but this should not be overinterpreted in a single cluster and given the uncertainties. We find an intrinsic scatter of about 1 keV in both cases. The uncertainties of the $T_{\rm SZX}$ map are significantly lower than that of the X-ray spectroscopic ones, especially at high temperatures, but it is obtained with a factor of three smaller observing time.

Our new method provides an alternative to purely X-ray spectroscopic-based techniques. While the geometry of the cluster limits our results, the application on a larger sample would enable us to disentangle the systematic instrumental calibration with the effects related to the intrinsic properties of the clusters. This method is excellent for high-redshift and/or high-temperature systems, where X-ray spectroscopy is challenging. It was already applied to another system, MOO J1142+1527, at $z = 1.2$, where a low-entropy core was found at the X-ray peak surrounded by high temperatures on the south and west (Ruppin et al. 2020).

2.5 Towards a census of the thermal state of the cluster population and its evolution

The analysis of the NIKA sample and the first NIKA2 observations proved very useful to explore the capability of deep SZ imaging to study galaxy clusters, in combination with other wavelengths. However, these data were obtained, by design, for specific individual targets selected because of their typical characteristics known from other wavelengths. They are thus likely to be biased with respect to the underlying cluster population. Therefore, it is now time to apply the methodology and

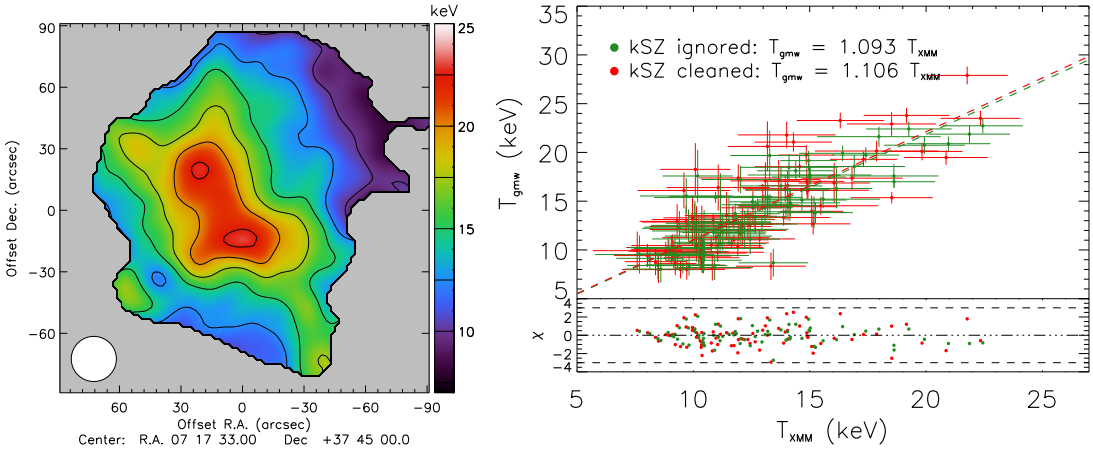

Figure 2.7: **Left:** $T_{\rm SZX}$ temperature map of MACS J0717.5+3745 computed from combining NIKA tSZ mapping and *XMM-Newton* surface brightness. **Right:** pixel-to-pixel comparison and fit of the $T_{\rm SZX}$ and *XMM-Newton* spectroscopic temperature map. Figure extracted from Adam et al. (2017a).

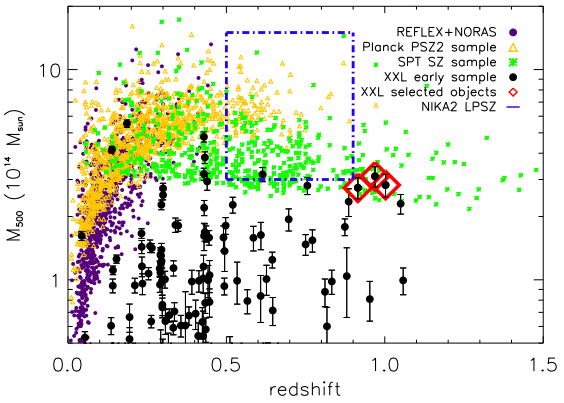

Figure 2.8: NIKA2 LPSZ and XXL follow-up selection region compared to relevant tSZ and X-ray samples. Figure reproduced from the *NIKA2 SZ follow-up of XXL clusters at* $z \sim 1$ proposal (Ricci, Adam et al., 2020).

analyses developed over the last few years to statistical cluster samples with well-defined selection functions so that conclusions can be obtained for a representative cluster population. This section discusses the still ongoing projects aiming at doing so. The focus is made on the NIKA2 SZ large program and the follow-up of XXL clusters, but we note that other NIKA2 and MUSTANG2 projects are also being pursued in that direction (e.g., the follow-up of Massive and Distant Clusters of *WISE* Survey targets at high redshift, Dicker et al. 2020; Ruppin et al. 2020, 2022).

2.5.1 The NIKA2 Sunyaev-Zel'dovich Large Program

The LPSZ program consists in the follow-up of about 45 clusters at intermediate/high-redshift ($0.5 < z < 0.9$) with masses $M_{500} > 3 \times 10^{14}$ $M_\odot$ (Mayet et al. 2017; Macias-Pérez et al. 2017; Perotto et al. 2018; Mayet et al. 2020; Perotto et al. 2022). Target sources were selected based on tSZ samples from *Planck* (Planck Collaboration et al. 2014a, 2016c) and ACT catalogs (Hasselfield et al. 2013), as also illustrated in Figure 2.8. Although the selection is based on the ICM, which is the object of study by the LPSZ, tSZ catalogs are currently the best ones to ensure the most reliable representativity with respect to the underlying cluster population. X-ray data are already available for most of the clusters and follow-ups are in progress for the remaining ones, to

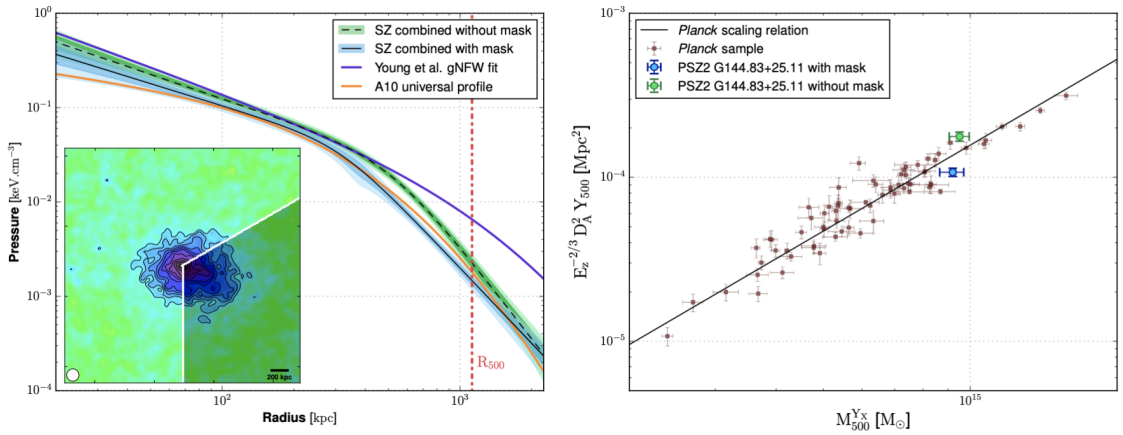

Figure 2.9: **Left:** Pressure profile of MACS J0647+7015 computed with and without a mask of the disturbed region. This region is indicated on the map as the lower right quadrant. **Right:** Location of MACS J0647+7015 on the mass - tSZ scaling relation depending on the masking or not of the disturbed region and comparison with the *Planck* scaling relation. Figure reproduced from Ruppin et al. (2018).

ensure full thermodynamical studies. A total of 300 hours of guaranteed time have been granted to complete the LPSZ, distributed over the sample to provide homogeneous data quality (S/N ratio larger than 3 on the profile at R_{500}). So far, a large fraction of the sample was already observed and its analysis is ongoing.

An excellent illustration of what could be achieved with the LPSZ is shown in Figure 2.9. It represents the pressure profile and the location on the mass - tSZ flux scaling relation of MACS J0647+7015, a $\sim 8 \times 10^{14}$ M$_\odot$ cluster at $z = 0.58$, observed for 11 hours during the science verification phase (Ruppin et al. 2018). The unprecedented tSZ mapping, over more than 1 Mpc extent and reaching 13σ at the peak allows us to identify a disturbed region in the southwest. The comparison of the analysis when masking or not this region has shown that the disturbance induces significant deviations in the shape of the pressure profile, and could lead to a boost of more than 60% on the tSZ flux and 80% on the recovered mass. In the context of the LPSZ, the analysis of one of the ACT-selected clusters at higher redshift was also published recently (Kéruzoré 2021). It highlights the LPSZ's capabilities in obtaining high-quality thermodynamical estimates in the most challenging situation. See also the early analysis of a merging system of the LPSZ by Artis et al. (2022). In addition to the data analysis of individual galaxy clusters, the development of new tools aiming at coherently inferring the statistical properties of the LPSZ sample is important. For instance, Kéruzoré et al. (2022a) presented a new Bayesian hierarchical modeling framework to constrain the Y$_{500}$ - M$_{500}$ scaling relation that enables taking into account a large panel of systematic effects.

The LPSZ should allow us to perform an in-depth study of the ICM of a representative sample of galaxy clusters at $0.5 < z < 0.9$. According to early results, it will provide an important test of the redshift evolution of the ICM state and the scaling relations that it follows. Thanks to the resolved nature of the observations, the dependence on the cluster dynamical state will be addressed. In turn, this will provide important ingredients that should allow us to obtain more reliable cosmological constraints from galaxy clusters.

2.5.2 NIKA2 follow-up of XXL clusters: focus on low-mass systems at $z \sim 1$

Due to their shallow potential wells, low-mass clusters are more affected by gas stripping, shock heating, or turbulence that are caused by merging events as well as AGN feedback. Therefore, they

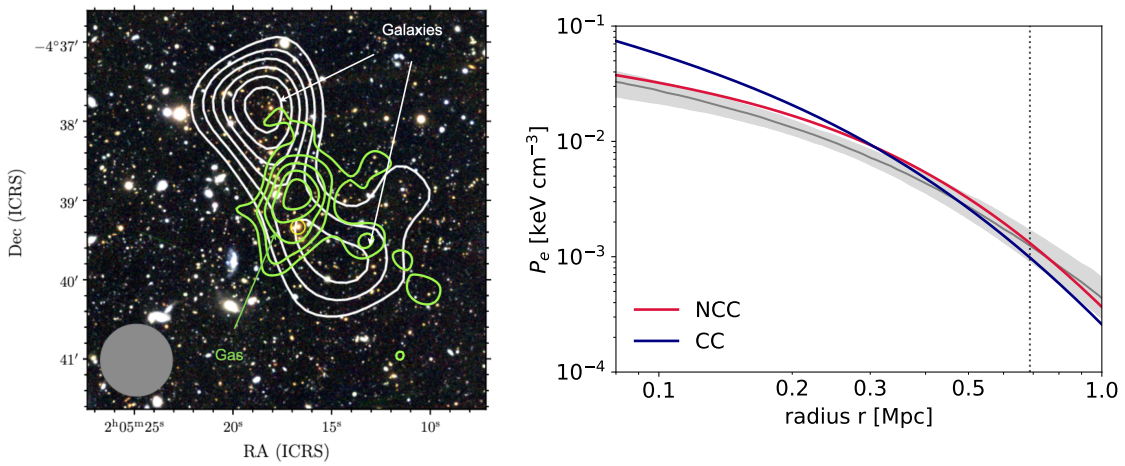

Figure 2.10: Thermal pressure distribution in XLSSC 102. **Left:** comparison between the galaxy distribution (color and white contours) and the gas pressure (green), traced by the tSZ signal. The grey circle gives the resolution of the galaxy overdensity contours. **Right:** constraints on the pressure profile of XLSSC 102 (grey). The blue and red lines give the cool-cores (CC) and morphologically disturbed (NCC) expectation assuming extrapolation from the REXCESS sample at lower redshift and higher mass (Arnaud et al. 2010). The vertical dashed line corresponds to R_{500}. Figure reproduced from Ricci et al. (2020).

may follow scaling laws that deviate from self-similarity, in particular at high redshift, where those effects are more efficient (Le Brun et al. 2017; Pop et al. 2022a,b). These targets are of course more challenging to observe, but they will strongly contribute to the detections of future/ongoing surveys such as *Euclid* (Euclid Collaboration et al. 2019), LSST (LSST Science Collaboration et al. 2009), CMB-Stage4 (Abazajian et al. 2016) or *eROSITA* (Pillepich et al. 2012), which makes them important to characterize early on. Thanks to its design and depth, the XXL program, performed in the X-ray with *XMM-Newton*, allows us to explore high-redshift clusters down to low mass (Pierre et al. 2016). It comes with extensive multi-wavelength coverage and thus represents an excellent pathfinder for future X-ray and optical/near-infrared missions. Despite its importance, low-mass high-redshift clusters are still unexplored using high-resolution SZ observations due to the lack of dedicated instruments and the observational challenge, while such data would provide unique insight into the physical properties of these objects.

For these reasons, and as part of the XXL collaboration, we proposed the follow-up of three XXL clusters detected independently in the optical (see Figure 2.8): XLSSC 102 ($z = 0.97$), XLSSC 100 ($z = 0.92$), and XLSSC 072 ($z = 1.00$) with masses estimated to $\sim 2 \times 10^{14}$ M$_\odot$. This open-time project complements well the LPSZ at lower masses and higher redshifts. All the data have been collected by now and we have obtained significant detections for the three sources (peak S/N $\sim$ 7-10). The analysis of the first target, XLSSC 102, was published in Ricci et al. (2020) where we combined the NIKA2, *XMM-Newton* and optical data. Despite the limited S/N ratio in each band, the multi-wavelength comparison allowed us to characterize the dynamical state of this highly perturbed system. As shown in Figure 2.10, the large offset between the two galaxy clumps and the gas likely indicates that XLSSC 102 is a bullet-like cluster at $z \sim 1$. The X-ray/tSZ comparison also revealed a good morphological agreement on the large scale, but an offset of the peak (as well as the BCG) that is typical of merging systems. The application of the tools described in Section 2.4, in different sectors and with different centers defined according to the morphological analysis, allowed us to characterize the full radial thermodynamical properties of the cluster. XLSSC 102 was confirmed to be a disturbed system, and we characterized the impact of the merger on the thermodynamical profiles. Despite its extreme nature (low-mass, high-redshift,

highly disturbed), we found that the pressure profile of XLSSC 102 is in line with extrapolation from low redshift relations (Arnaud et al. 2010), as shown in Figure 2.10. We find that XLSSC 102 does not deviate significantly from the scaling relation extrapolated from higher mass and lower redshifts, given the statistical and systematic uncertainties (e.g., the choice of the center).

This analysis of XLSSC 102 is unique given the location of the cluster in the mass-redshift plane. The fact that the cluster agrees with standard extrapolation is an important result for future surveys that will explore further this regime. Moreover, this allowed us to test the NIKA2 capabilities of imaging the tSZ signal down to the detection limits of upcoming large X-ray and optical/near-infrared missions, showing that even with a limited S/N ratio, the multi-wavelength comparison provides an excellent way to understand the cluster dynamics. The analysis of the full sample is ongoing. Although currently limited in the number of sources, it should already prove useful to test further this yet barely explored region of the mass redshift plane with resolved tSZ data.

2.6 Conclusion and outlook

The era of mature millimeter imaging instruments, capable of producing deep high-resolution mapping of the SZ effect in galaxy clusters, has started. Pathfinder experiments such as NIKA allowed us to build cluster samples that were used to test the scientific outcomes, develop new analysis techniques and address the limitations of such observations. This has already proved extremely powerful in studying distant clusters, in complement to more traditional X-ray data and other wavelengths.

Despite being essentially limited to test case clusters, the data exploitation of SZ imaging has already provided many relevant results, among which:

- Point source contamination is both a challenge and an opportunity. In particular, radio sources in cool-core BCG are likely to significantly affect the study of statistical samples. The detection of lensed galaxies, on the other hand, opens an interesting window to the far Universe.
- So far, the pressure profile of distant clusters is in line with standard evolution, although this should be confirmed and investigated in-depth with statistical samples.
- Pressure substructures are likely very common and affect the mass-SZ scaling relation.
- Joint X-ray photometry plus SZ studies are extremely powerful, and unique given existing facilities, in measuring the thermodynamics of clusters up to high redshift. Noteworthy, they allowed us to reveal the presence of extremely high gas temperatures, up to 25 keV.
- The mapping of the kSZ effect is now at reach via multi-band photometry. Its measurement is very challenging but provides unique insights into the dynamics of cluster assembly.
- Joint X-ray, SZ, and optical analysis allows us to extract much more information than that available when summing individual contribution, even at a low S/N ratio.

In general, high S/N ratio data have proved extremely rich, especially since they opened an unexplored view of cluster physics. While it depends on the scientific case, observing fewer clusters with a high S/N ratio is likely more fruitful than observing many weakly detected objects, in the same amount of time, because the strength of NIKA and NIKA2 truly rely on their mapping capabilities.

It is now time to perform these observations and apply similar techniques using well-defined statistical samples, as planned for example with the NIKA2 SZ Large Program. This will allow us to answer how the physical properties of the cluster population and the scaling relations evolve with redshift, and what is the impact of the dynamical state. Alternatively, other ways to understand the ICM physics may be explored with high-resolution SZ measurements. For instance, the study of the small-scale SZ structures in local systems was not truly attempted yet, while it may be extremely useful in understanding the physics of shocks and turbulence in the ICM. Some studies have started

exploring the structure of filaments and interacting clusters (Hincks et al. 2022), the energetics of AGN bubbles (Abdulla et al. 2019; Orlowski-Scherer et al. 2022), or how resolved SZ combined with lensing may give insights into the HSE mass bias (Ferragamo et al. 2022; Muñoz-Echeverría et al. 2022a,b). The resolved measurement of gas temperature from relativistic corrections, using SZ alone, may also be soon achieved (Ruppin et al. 2022). In this context, upcoming spectroscopic experiment (e.g., Concerto Collaboration et al. 2020) are likely to play a very significant role shortly. Finally, the exploitation of the numerous sub-millimeter galaxies detected around SZ clusters is still waiting. While such dedicated projects have been performed at higher frequencies (Egami et al. 2010), the data are available and may allow us to push high-redshift galaxy formation studies one step further.

3

The quest for the diffuse γ-ray emission from galaxy clusters

Contents

The growth of cosmic structures necessarily implies the release of powerful shock waves into cosmic plasmas and the development of turbulence. These processes eventually dissipate most of the kinetic energy into heat, but they are also expected to accelerate charged particles up to very high energy and amplify magnetic fields (Brunetti and Jones 2014; Bykov et al. 2019). Compact sources, and in particular AGNs are also recognized as important sources of energy via feedback mechanisms, especially in cluster cores, and may directly inject CR into the ICM (Fabian 2012; Werner et al. 2019).

The detection of diffuse radio emission from galaxy clusters has proved the presence of CRe and magnetic fields in the ICM. Nevertheless, about 70 years after the first detections, the origin of CRe is still not well understood due to the complex physics involved and the entanglement between

different components, although major advances have been made during the last decade or so (Ferrari et al. 2008; Feretti et al. 2012; van Weeren et al. 2019, for reviews). Diffuse γ-ray emission, on the other hand, is expected to provide a univocal diagnosis for the physics of CRp in the ICM (Blasi et al. 2007; Wittor 2021). Indeed, CRp should accumulate over the cluster formation history, since they do not suffer major losses, and lead to diffuse γ-ray emission when interacting with the thermal gas. Despite many searches, for over more than two decades, either from space (e.g., Sreekumar et al. 1996; Reimer et al. 2003; Huber et al. 2013; Prokhorov and Churazov 2014; Zandanel et al. 2014; Ackermann et al. 2014, 2015, 2016, at about 30 MeV - 300 GeV) or from the ground (e.g., Aharonian et al. 2009; Aleksić et al. 2010, 2012; Arlen et al. 2012; Ahnen et al. 2016, at 50 GeV - 10 TeV energies), this signal has never been unambiguously detected so far. The non-detections started to challenge our understanding of the CR acceleration mechanisms, and/or how CRp get stored in the ICM (see Bykov et al. 2019, for a review).

Galaxy clusters have also been considered prime targets for indirect dark matter searches. Indeed, the decay or annihilation of dark matter particles could cause γ-ray emission. Galaxy clusters are excellent objects to search for dark matter decay since the signal scales linearly to the dark matter reservoir. Considering annihilation, clusters are competitive targets when accounting for substructures (see Sánchez-Conde et al. 2011; Moliné et al. 2017). Over the last decade, many constraints on the dark matter were produced using clusters (e.g., Ackermann et al. 2010; Aleksić et al. 2010; Arlen et al. 2012; Abramowski et al. 2012; Combet et al. 2012; Cadena 2017; Acciari et al. 2018). Although it is well beyond the aim of this document, some of the work reviewed in this chapter has been made in close collaboration with groups aiming at constraining the nature of dark matter. Indeed, considering simultaneously the signal arising from CR and dark matter is becoming relevant in the context of future observations.

This chapter reviews the latest advances made regarding the search for diffuse γ-ray emission from galaxy clusters. This effort aims at understanding the spatial and spectral properties of CRp in the ICM, which is intimately connected to their acceleration mechanisms and transport physics. It discusses the modeling of the expected signal from a multi-wavelength approach, the state-of-the-art constraints obtained with the ongoing *Fermi-LAT* satellite, and prospects for future CTA observations.

3.1 `MINOT`: a framework for modeling the diffuse thermal and non-thermal emission from galaxy clusters

The diffuse γ-ray emission from galaxy clusters may arise from two main channels (Brunetti and Jones 2014): 1) the inverse Compton interaction between CRe and the ambient radiation field (mainly the CMB); 2) the decay of particles produced in hadronic interactions between CRp and the thermal target gas. The modeling of this γ-ray emission is essential for constraining the cluster scale CR physics using existing data, predicting the expected signal during the construction phase of future γ-ray facilities such as CTA, and also providing easy ways to compute the expected background associated with the ICM in dark matter searches towards clusters. Here, we review the methodology employed to fulfill these goals, via the development of the `MINOT` package (Modeling the Intra-cluster medium (Non-)thermal content and Observable prediction Tools, Adam et al. 2020).

3.1.1 Motivations and general overview

The γ-ray modeling requires describing the CR population and the particle interactions, but other cluster components that are accessible from other wavelengths also enter into the computation.

Because they relied on heterogeneous data and literature results, diffuse γ-ray constraints obtained during the last decades were not always obtained in a self-consistent way (e.g., combining fluxes measured in different apertures). In practice, most of them directly model the photon spectrum and their spatial distribution, but the results are difficult to connect to the underlying particle distributions. Alternatively, they may also present large uncertainties associated with particle interactions that are not characterized or may suffer from large extrapolations (e.g., of core properties to the virial radius). This implies that current constraints are often affected by large systematic uncertainties that are not always well-characterized.

`MINOT` is a coherent multi-wavelength modeling framework. It relies on state-of-the-art well-characterized particle interaction models. It aims at computing easily the diffuse γ-ray emission given a cluster model, as well as observable at other wavelengths, in a self-consistent way. This can be used to calibrate models, perform joint multi-wavelength analysis, or at least estimate underlying systematic effects related to the modeling. `MINOT` does not aim at modeling the microphysics related to particle acceleration. Instead, it provides a framework to describe the physical state of the ICM. While the physical description is made simple, assuming smooth spherically symmetric distributions, the code is unique in its self-consistent multi-wavelength nature.

A general overview of the different components involved in the code is presented in Figure 3.1. The first step consists in describing the involved physical properties via their radial profile and energy distributions: we consider the magnetic field strength, the CRe and CRp, and the thermal pressure and density of the gas. The relevant processes taking place in the ICM are then modeled to obtain the emission rate at the considered wavelengths. This includes a description of hadronic interactions using accelerator and Monte Carlo data to obtain the production of secondary particles ($e^{\pm}$, γ, ν). We consider energy losses of the secondary electrons, but the code does not include reacceleration or transport mechanisms. Finally, the observable signal is calculated according to the sky coordinates and distance of the object by integrating the emission rates on the line-of-sight. The absorption of γ-rays during their propagation is also included. The code makes it possible to quickly calculate the observables in the radio, tSZ, X-ray, γ-ray, and even neutrinos.

3.1.2 Input modeling

The input modeling may be divided into three main ingredients: 1) global cluster properties, 2) spectral and spatial description of the state of the ICM components, and 3) sampling parameters. The code makes use of the `unit` module from `astropy` to simplify the user interface and secure the input definition. The input ingredients are briefly summarized below. Overall, they are established so that a quick, easy and secured cluster definition can be made to provide nearly immediate outputs accordingly.

Global properties Several parameters control the global cluster properties, such as the mass M_{500}, the redshift, the sky coordinates, etc. These variables are generally involved when computing observables or radiation processes from the physical state of the ICM. This also includes the choice of some particle physics interaction or propagation models to be used. The code deals with the entanglement between the parameters such as redshift and distances, given a cosmological model.

Spatial and spectral distributions The spatial and spectral energy distributions of the relevant physical properties of the cluster are the key ingredients of `MINOT`: magnetic field strength, CRp and primary CRe, and thermal gas pressure and density (see Figure 3.1). A library of standard predefined radial and spectral models is available and may be used to select them via dedicated functions (e.g., β-profile, power-law spectrum), but it is possible to define any arbitrary distribution. Dedicated functions are also available to deal with the scaling between different properties. For instance,

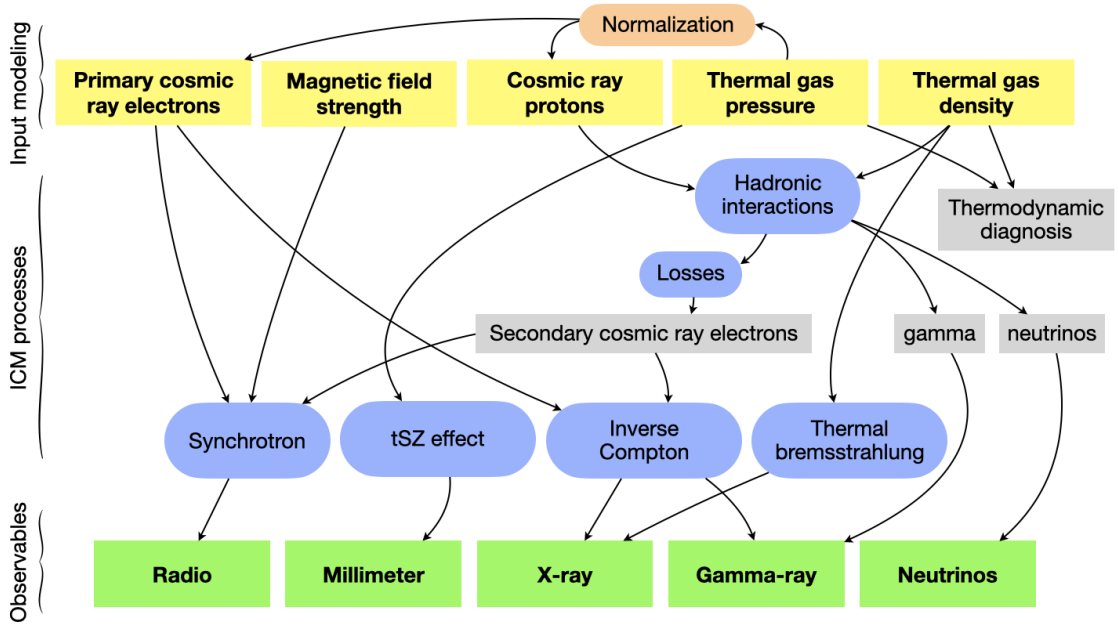

Figure 3.1: Overview of the `MINOT` input modeling, the considered physical processes at play in the ICM, and the observables that are computed. The interdependences are shown by the black arrows. Extracted from Adam et al. (2020).

the CR or magnetic field profiles can be defined relative to the thermal gas density/pressure according to a scaling parameter (e.g., $|\vec{B}(r)| \propto n_e(r)^{\eta_B}$). Similarly, the thermal profiles can be quickly set to their universal expectation according to various results from the literature and given the global cluster properties. This is particularly useful when predicting observables for large catalogs for which only global quantities are available.

The thermal model relies primarily on the thermal gas electron density and pressure profiles, motivated by the fact that X-ray and tSZ observations are sensitive to these components. Given these inputs, the code can derive the thermodynamical diagnosis that is very useful in itself when studying the thermal properties of clusters: pressure, density, temperature, entropy, HSE mass, gas fraction, thermal energy profiles, etc (see also Section 2.4.2 for more details). Currently, the input CRp and primary CRe are described as

$$J_{\rm CR} \propto f_1(r) \times f_2(E), \tag{3.1}$$

where $f_1(r)$ and $f_2(E)$ are the radial and spectral distributions. At this stage, the shape of the spectral energy distribution is assumed constant over the cluster volume, but more complex distributions are intrinsically easy to implement. As it will be the case in Section 3.2 and 3.3, the CRp spectrum is often assumed to be a power-law with spectral index $\alpha_{\rm CRp}$ and the profile is often written as scaled to the thermal electron profile as $n_{\rm CRp}(r) \propto n_e(r)^{\eta_{\rm CRp}}$. The normalization is defined according to the ratio between the CRp and thermal energy, $X_{\rm CRp}(< R) = \frac{U_{\rm CRp}(<R)}{U_{\rm th}(<R)}$, computed within a chosen aperture R.

Sampling Finally, several parameters allow the user to control the numerical precision when sampling the physical distributions, something which also affects the computing time. More importantly, these parameters define the sky map projection (generally small sky patches, but `healpix` projections are also available). A given header may be fed directly to `MINOT`. This is particularly

useful when doing a point-to-point comparison between a model and the data that are already projected onto some grid.

3.1.3 Intra-cluster medium processes

The ICM processes that are accounted for in `MINOT` are illustrated in Figure 3.1. They include hadronic interactions, the energy losses of secondary electrons, synchrotron emission, the tSZ effect, inverse Compton emission, and thermal bremsstrahlung. Some of these processes are modeled following the `Naima` software (Zabalza 2015) and some other use the `Xspec` code (Arnaud 1996).

Hadronic interactions `MINOT` was originally developed to compute the hadronically induced γ-ray emission. It essentially happens via the production of pions and their decay through proton-proton interactions,

$$\begin{cases} p + p \longrightarrow & \pi^0 + \pi^- + \pi^+ + \text{others} \\ & \pi^0 \longrightarrow 2\gamma \\ & \pi^\pm \longrightarrow \mu^\pm + \nu_\mu/\bar{\nu}_\mu \longrightarrow e^\pm + \nu_e/\bar{\nu}_e + \bar{\nu}_\mu/\nu_\mu. \end{cases} \tag{3.2}$$

In addition to the particle distribution function, the production rate of secondary particles ($e^\pm$, γ, ν) depends on 1) the interaction cross-section, 2) the number of secondary particles produced in a collision per unit energy as a function of the initial CRp energy. These ingredients are modeled following the prescriptions of Kelner et al. (2006), Kamae et al. (2006), and Kafexhiu et al. (2014), which are obtained by fitting parametric functions to accelerator data and Monte Carlo simulations. In practice, we also include helium nuclei, which contribute significantly to the total flux, and metals, although they are negligible. The comparison between the different parametrizations (`Pythia8`, `SIBYLL`, `QGSJET`, or `Geant4`) is used to quantify the modeling uncertainty ($\sim 30\%$).

Energy losses Once produced, secondary electrons and positrons suffer energy losses. In principle, they could also be reaccelerated via shocks and turbulence, but this is not currently included in `MINOT`. Given the general ICM properties, the main losses are synchrotron radiation, inverse Compton interaction, Coulomb losses, and Bremsstrahlung radiation. They are computed following Blumenthal and Gould (1970), Gould (1972), and Longair (2011), and depend on the energy and the radial distance.

Assuming a steady state, i.e., the equilibrium between the injection and the losses, `MINOT` can compute the expected distribution of secondaries as

$$\frac{dN_{\rm CRe}}{dEdV}(E, r) = \frac{1}{\ell(r, E)} \int_E^\infty q(\epsilon, r) d\epsilon, \tag{3.3}$$

where $q(\epsilon, r)$ is the production rate of secondaries per unit volume, energy and time, and the losses $\ell(r, E) \equiv -\sum_i \frac{dE}{dt}\big|_i$ with i the loss contributions label. This is often referred as the pure hadronic model for secondary electrons.

Radiation processes Once the final particle distributions are known, `MINOT` use them to compute the emission rate per unit volume and energy/frequency, $Q(r, E)$, according to the relevant radiation processes:

- The thermal X-ray emission depends on the thermal gas density, temperature, and abundances. It is computed using the `Xspec` software.

- The tSZ signal is computed given the thermal gas pressure. Relativistic corrections are implemented following Itoh and Nozawa (2003). They account for the temperature dependence that is significant above $\sim$ 10 keV, depending on the observing frequency.
- The inverse Compton emission depends essentially on the CRe distribution and the CMB temperature at the redshift of the cluster. `MINOT` uses the analytical prescription from Khangulyan et al. (2014) to compute it.
- The synchrotron emission depends on the CRe distribution and the magnetic field. We use the results of Aharonian et al. (2010), which assumes the orientation of the magnetic field to be randomized. This implies that `MINOT` focuses on radio halos and relics are left aside.

The `MINOT` implementation of all these radiative processes has been well-characterized and validated. Their precision is generally negligible compared to other sources of uncertainties.

3.1.4 Propagation and observables

For any observable[1], the emission rate is integrated along the line-of-sight to obtain the differential flux per unit energy (or frequency), area, time and solid angle

$$\frac{dN}{dEdSdtd\Omega} = \frac{D_A^2}{4\pi D_L^2} \int_{-R_{\rm trunc}}^{R_{\rm trunc}} Q(r) d\ell, \tag{3.4}$$

with D_A and D_L the angular and luminosity distances to the cluster, respectively. $R_{\rm trunc}$ is a global parameter, which defines the cluster boundary. The energy or frequency change induced by the redshift is accounted for, or switched off upon request.

Note that γ-rays of sufficiently high energies, either from hadronic interaction or inverse Compton, are affected by extragalactic background light absorption (Dwek and Krennrich 2013). This is included as $\frac{dN}{dEdSdtd\Omega} \longrightarrow \frac{dN}{dEdSdtd\Omega} \exp\left(-\tau(E)\right)$, where $\tau(E)$ is obtained using `ebltable`[2].

In the end, `MINOT` can use the differential flux to output integrated fluxes, maps, spectra, and profiles. The computing time is sufficiently low so that the code can be coupled to MCMC fitting, or loop over large cluster catalogs to compute sky maps over large solid angles.

3.1.5 Applications and advertisement

`MINOT` is a `Python`-based package that is well-documented, easy to install and quick to use[3]. Apart from the X-ray emission that relies on the external `Xspec` software (optional), the code uses essentially standard `Python` libraries. The detailed description of the code, its working principle, structure, and underlying physical modeling was presented in the dedicated publication by Adam et al. (2020). We provided applications to existing datasets, discussed the limit and performance of the code, and released publicly available examples.

While relatively recent, the code is already used as the baseline framework for modeling the diffuse γ-ray emission in galaxy clusters as part of the dedicated CTA key science project (see Section 3.3). Application to *Fermi-LAT* data was done in the case of the Coma cluster (see Section 3.2) and other targets are currently under investigation. Even though the code was originally developed in the context of cluster CR physics, it has already proved useful in other contexts. For instance, it was used to prepare tSZ observations, and to analyze NIKA2 data (see Section 2.5). Because of its multi-wavelength completeness and user-friendliness, the code has also proved an excellent pedagogical tool for students, Ph.D., and postdocs.

[1] Because it is a spectral distortion, this does not strictly apply to the tSZ signal (see Adam et al. 2020, for details).

[2] `Python` package that interpolates extragalactic background light tables from the literature, https://github.com/me-manu/ebltable/

[3] https://github.com/remi-adam/minot

`MINOT` is still growing up. Several requests have been made to include new features such as X-ray cavities/radio bubbles, shocks, or triaxiality.

3.2 The first intra-cluster medium detection in the γ-rays?

As a massive and nearby object, the Coma cluster is one of the best targets to search for diffuse γ-ray emission. It is a disturbed merging system and hosts one of the best-studied giant radio halo, which attests to the presence of particle acceleration. Additionally, the Coma cluster is nearly located at the galactic north pole so that diffuse foregrounds are minimal and no strong γ-ray source has been identified around the cluster.

Several groups have investigated the γ-ray emission in the vicinity of the Coma cluster (Perkins 2008; Aharonian et al. 2009; Arlen et al. 2012; Prokhorov 2014; Zandanel and Ando 2014). In 2016, an excess was reported after 6 years of *Fermi-LAT* observations, but it was too faint for a detailed investigation (Ackermann et al. 2016). Later, Xi et al. (2018) reported the first significant detection towards the cluster. In 2020, a source named 4FGL J1256.9+2736, within θ_{500}, was included in the 4FGL catalog (Abdollahi et al. 2020; Ballet et al. 2020). The question of whether the γ-ray excess is attributed to the ICM or not is still open. Whatsoever, the Coma cluster is an ideal test case to constrain the cluster scale CR physics. For instance, Brunetti et al. (2017) and Nishiwaki et al. (2021) used γ-ray limits together with radio data to constraint particle acceleration models.

To constrain the CR physics of clusters, we have developed dedicated tools for the *Fermi-LAT* analysis of galaxy clusters, together with external data. This was used for the detailed investigation of the γ-ray emission observed in the direction of the Coma cluster (Adam et al. 2021). In this section, we summarize this effort, focussing on the Coma cluster as the most interesting case and an excellent illustration of the methodology and limitations we face.

3.2.1 Modeling the Coma cluster at γ-ray energies

The investigation of the CR physics relies on the modeling of the Coma cluster for addressing the detection level of the γ-ray signal we target, but also to derive physical constraints on the CR population a posteriori. Two main strategies were employed. 1) The use of a physically motivated spectral and spatial model constructed via the `MINOT` framework. 2) The use of a spectral model derived from `MINOT`, but with spatial templates computed from different wavelengths. Although not used for CR constraints, this second option captures possible deviations from spherical symmetry and possibly tracks the γ-ray contribution from different components.

`MINOT` modeling The thermal gas was modeled using the electron density profile measured by Briel et al. (1992) and the pressure from Planck Collaboration et al. (2013b). They are kept fixed given their negligible uncertainties. The Coma cluster is one of the rare system for which the magnetic field has been measured. It is necessary when considering radio synchrotron emission and its strength profile was modeled using the best-fit from Bonafede et al. (2010). Still, it is important to keep in mind that statistical uncertainties are large and that Faraday rotation measures are difficult to perform (Johnson et al. 2020). CRp are modeled as

$$\frac{dN_{\rm CRp}}{dEdV} \propto E^{-\alpha_{\rm CRp}}\, n_e(r)^{\eta_{\rm CRp}}, \tag{3.5}$$

and the CRp to thermal energy ratio within R_{500} is used to describe the normalization, $X_{\rm CRp}(R_{500})$. Because of the limited angular resolution of the *Fermi-LAT*, the parameter $\eta_{\rm CRp}$ is not fitted to the

data, but varied as $\eta_{\rm CRp} \in \{0, 0.5, 1\}$ to test its impact on the results. Primary CRe are relevant when considering the radio data. They are modeled in a similar way, as

$$\frac{dN_{\rm CRe1}}{dEdV} \propto f_{\rm CRe1}(E)\, n_e(r)^{\eta_{\rm CRe1}}, \tag{3.6}$$

but different spectral models, i.e., $f_{\rm CRe1}(E)$, are used to account for losses: exponential cutoff power-law, initial injection, and continuous injection (see Adam et al. 2020). The choice of the CR models was motivated by the minimal number of parameters involved. The systematic effects associated with this choice were estimated by varying the relevant components of the models, but are subdominant given the statistical uncertainties.

Construction of multi-wavelength templates We built five different spatial templates based on other wavelengths. A galaxy density map was derived from the Sloan Digital Sky Survey data to track γ-ray emission associated with unresolved galaxies spread over the cluster volume. We used the *ROSAT All Sky Survey* data to trace the thermal gas density squared, which should match the target signal if the CRp spatially coincide with the thermal gas. The *Planck* y-map was used to track the thermal gas pressure, which should match the γ-ray emission if CRp follow the temperature. Westerbork Synthesis Radio Telescope (WSRT) data were used to directly trace the CRe acceleration sites and both radio halo and radio relic templates were derived.

3.2.2 The γ-ray emission towards the Coma cluster as seen with *Fermi-LAT*

The *Fermi-LAT* satellite has been collecting all-sky γ-ray data at energies from about 20 MeV to more than 300 GeV since June 2008. The Coma analysis presented in Adam et al. (2021) used nearly 12 years of data selected within a radius of 10 degrees from the cluster center. Beyond the Coma cluster itself, we also modeled the whole region of interest as seen by *Fermi-LAT* using a dedicated pipeline based on `Fermipy` (Wood et al. 2017) and standard data selection and analysis. Only events between 200 MeV and 300 GeV were used as a compromise between count statistics and robustness of the results since systematic effects increase at low energy.

3.2.2.1 *Fermi-LAT* analysis

The sky model includes the diffuse backgrounds (isotropic and galactic interstellar emission) and the compact sources identified in the field of view based on the 4FGL-DR2 catalog (Ballet et al. 2020). The source 4FGL J1256.9+2736 could correspond to the Coma cluster itself, but may also be associated with AGNs. Therefore, it was decided to 1) remove 4FGL J1256.9+2736 and replace it with ICM models, and 2) keep 4FGL J1256.9+2736 in addition to ICM models.

We developed an iterative maximum likelihood fit of the sky model, introducing free parameters step by step based on the detection level of the sources. This insured the stability of the results given the large number of free parameters involved. When included, 4FGL J1256.9+2736 was strongly degenerate with the cluster model, in agreement with the source being possibly associated with the ICM. We compute the test statistics (Mattox et al. 1996), $\mathrm{TS} = -2\,(\ln\mathcal{L}_0 - \ln\mathcal{L})$ to compare the different models and measure the source detection significance[4].

We confirmed earlier finding that significant γ-ray emission is observed towards the Coma cluster. ICM models match the data better, but the difference with other models is not large enough to firmly exclude that it is due to a single point source. `MINOT` models gave TS $\sim$25-27 (depending on $\eta_{\rm CRp}$), multi-wavelength templates TS $\sim$29-35 (excluding the radio relic template), with the highest value for galaxy and tSZ based models, and 4FGL J1256.9+2736 alone (as a point source)

[4] $\mathcal{L}_0$ is the maximum likelihood value for the null hypothesis, and $\mathcal{L}$ the maximum likelihood with the extra source.

TS $\sim$25. Many tests were carried out on the spectral energy distribution, the radial profile, and the peak position of the excess to try to discriminate the possible origin of the signal. We also checked the light curve of the source to be consistent with a steady emission, as expected for the ICM. In the end, the nature of the source remains uncertain, although we obtain excellent agreement with an ICM origin associated with hadronic interactions. The excess significance should not increase sufficiently to change the situation within the next few years given the large amount of observing time already available. No detection was obtained towards the other cluster we investigated.

The *Fermi-LAT* analysis of weak extended sources is difficult and affected by various systematic effects. The tests performed have shown that even in the case of the Coma cluster, near the galactic north pole, the diffuse background modeling largely dominates the systematic effect budget and can lead to changes in the total flux up to 40%. This implies that follow-up studies in the direction of other targets are likely to be limited by the background modeling. Other sources of systematics were considered and quantified, such as the energy threshold and binning, the size of the region of interest, or the event selection, but they were subdominant.

3.2.2.2 Multi-wavelength comparison

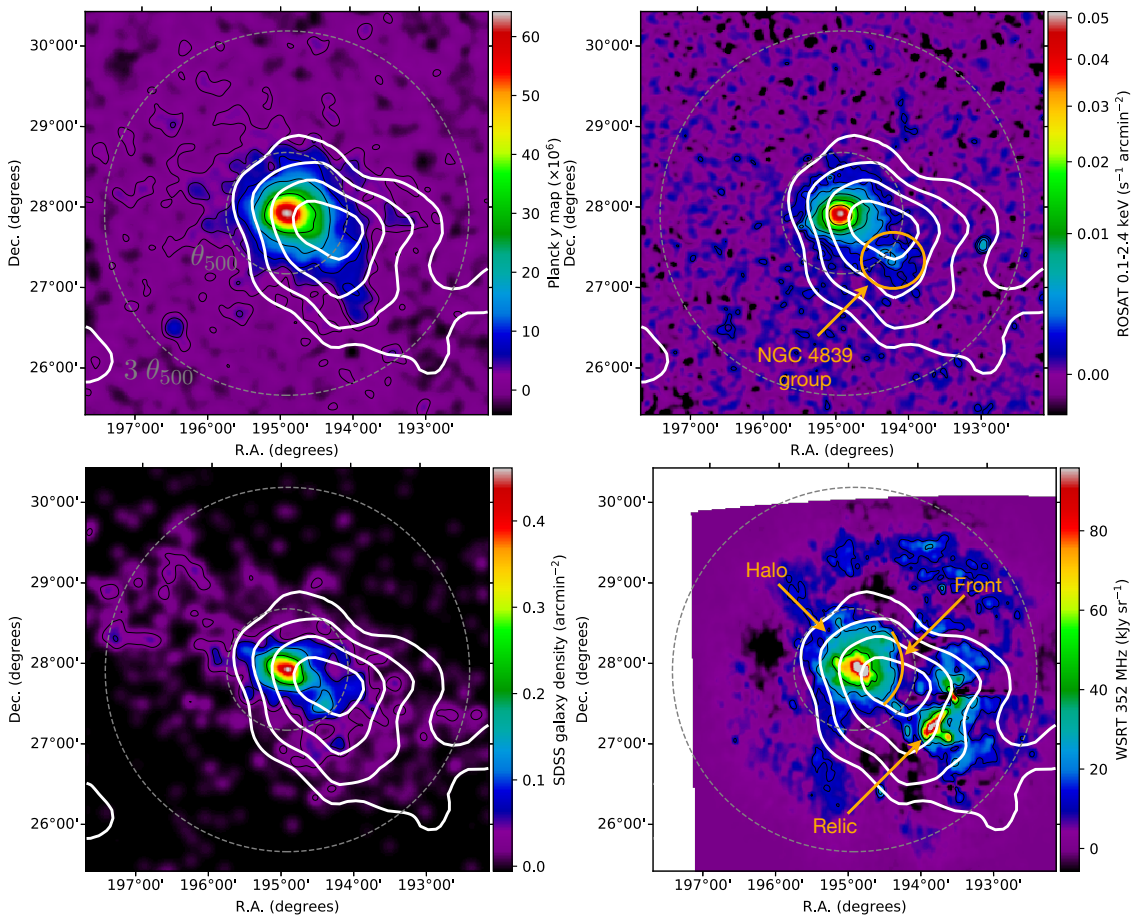

Figure 3.2: Multi-wavelength comparison of the Coma cluster signal to the *Fermi-LAT* TS map (white contours at 4, 9, 16 and 25). **Top left**: *Planck* tSZ. **Top Right**: *ROSAT* X-ray. **Bottom left**: galaxy density. **Bottom right**: WSRT 352 MHz radio signal. Extracted from Adam et al. (2021).

The *Fermi-LAT* excess is compared with data at other wavelengths in Figure 3.2. The northeast-southwest elongation, visible at all wavelengths, agrees well with the γ-ray. The best match is ob-

served with the tSZ map, indicating that if the excess is attributed to hadronic processes in the ICM, the CRp distribution should match the gas temperature well and be rather flat. The coincidence with both the radio halo and relic could also be a hint that part of the signal arises from inverse Compton emission near the relic, where the target gas density required for hadronic interactions is low. However, we cannot exclude other origins of the signal. For instance, the galaxy density, which should trace the contribution from unresolved sources, correlates well with the γ-ray.

3.2.3 Implication for the cosmic ray content of the Coma cluster

While the origin of the γ-ray signal is still uncertain, diffuse cluster scale emission is expected, and ICM models are favored. It is therefore fundamental to test the consequences of the *Fermi-LAT* detection for the cluster CR physics. We have shown that inverse Compton should not contribute significantly to the observed signal at *Fermi-LAT* energies. A purely hadronic origin of the emission is thus assumed and `MINOT` models are used to constrain the CR population.

3.2.3.1 The cosmic-ray proton population

Assuming a hadronic origin of the signal, the *Fermi-LAT* data directly depend on the CRp population (Figure 3.1). A dedicated pipeline was constructed to constrain the underlying parameter space according to a `MINOT` model and a γ-ray SED. Given a fixed spatial model, the flux of the source was extracted in each energy bin together with its likelihood scan to produce the SED accounting for the instrument response function. MCMC fitting was performed to sample the posterior distribution of the normalization $X_{\rm CRp}(R_{500})$ and slope $\alpha_{\rm CRp}$. This is illustrated in Figure 3.3.

We obtained a quantitative measurement of the CRp content in a cluster, for the first time, by direct constraint to the data, assuming a hadronic origin of the signal. The CRp normalization is slightly lower, but in line with expectation: about 1% of the thermal energy within R_{500} (e.g., Pinzke and Pfrommer 2010). For diffusive shock acceleration processes, this parameter is related to the injection efficiency, which increases with Mach number. On the other hand, a high value of the CRp spectral slope is favored ($\alpha_{\rm CRp} = 2.79^{+0.69}_{-0.13}$ for the reference model) compared to optimistic values that are usually assumed ($\alpha_{\rm CRp} \sim 2.1 - 2.3$, e.g., Arlen et al. 2012; Zandanel et al. 2014), although with large uncertainties. If confirmed, this could indicate that shock acceleration was dominated by Mach numbers that are overall smaller than usually expected. Including 4FGL J1256.9+2736 in the sky model naturally reduces the amplitude, but does not significantly affect the slope. Nor are these findings significantly affected by the choice of the CRp spatial distribution given the limited *Fermi-LAT* angular resolution and the flat core of the Coma cluster. The parameter degeneracy is limited because *Fermi-LAT* probes the peak of the hadronic emission at energies slightly lower than the proton-proton collision energy threshold (~ 1.2 GeV).

3.2.3.2 Implication for the diffuse radio emission

The presence of CRp implies the production of secondary CRe, which unavoidably leads to synchrotron emission in the ambient magnetic field. Investigating the contribution of the secondaries to the radio emission might thus help understand the still debated origin of the giant radio halos.

To do so, a dedicated procedure was built to fit simultaneously the radio halo spectrum and profile, and the *Fermi-LAT* data. We quantify 1) the ratio of primary to secondary CRe, as a function of radius and energy, assuming two distinct populations, 2) the boost needed for the secondary CRe to explain the radio data, relative to the pure hadronic model, assuming that the whole radio flux arises from the reaccelerated secondary CRe. We find that even if all the *Fermi-LAT* signal arises from hadronic interactions in the ICM, either another CRe population is needed, or secondary CRe should be reaccelerated. Moreover, the radio profile being very flat implies a nearly constant CRe

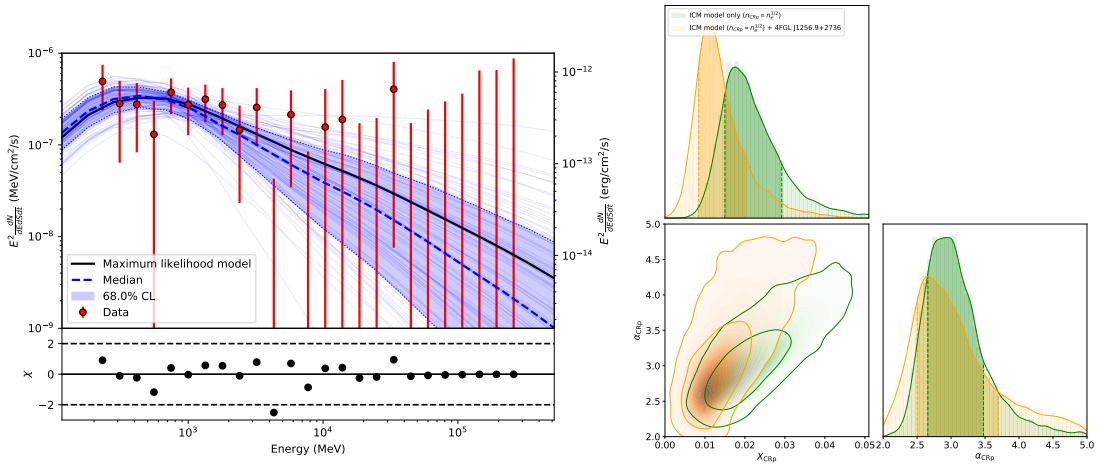

Figure 3.3: **Left**: Total SED recovered from the *Fermi-LAT* and MCMC constraint. **Right**: MCMC constraints on the model parameters when 4FGL J1256.9+2736 is excluded from the sky model (green) or included (orange). Figure extracted from Adam et al. (2021).

spatial distribution. This can be reached with secondary CRe only if CRp present an inverted profile. Alternatively, this could imply that the reacceleration of the secondary CRe increases with radius, relative to the expectations in the pure hadronic scenario, even for a flat CRp profile.

We compared the *Fermi-LAT* constraints with the turbulent reacceleration model from Brunetti and Lazarian (2011), as illustrated in Figure 3.4. It shows that the secondary CRe obtained assuming the pure hadronic model agrees very well with the seed population (i.e., when reacceleration is switched off) that is needed in the turbulent reacceleration model to explain the radio spectrum. This comparison reinforces the turbulent reacceleration model and indicates that secondary CRe could play a critical role in the required seed population.

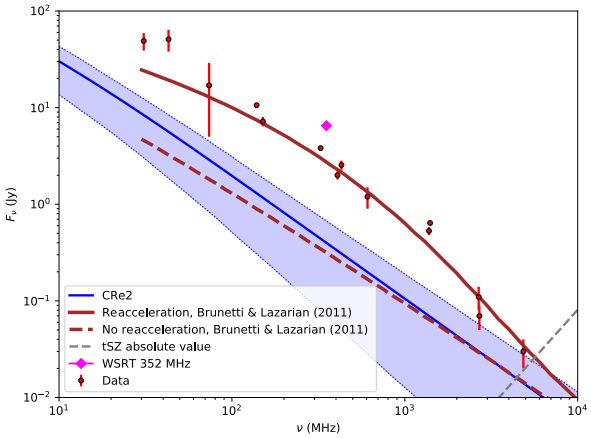

Figure 3.4: Comparison between the secondary CRe induced synchrotron spectrum to the reacceleration model developed by Brunetti and Lazarian (2011), in the case of a flat CRp population. The solid brown line corresponds to the full reacceleration model, while the dashed brown line corresponds to the case where reacceleration is switched off (see Brunetti and Lazarian 2011, for details). Figure from Adam et al. (2021).

3.2.3.3 Implications for the origin of the Coma giant radio-halo

The *Fermi-LAT* signal is not sufficient to explain the radio emission in the pure hadronic model. This confirms the results of Brunetti et al. (2017) based on γ-ray upper limits and implies that the pure hadronic model is ruled out unless the magnetic field is significantly lower than expected. Additionally, the radial profile and spectrum of the Coma giant radio halo are very flat and present curvature, respectively. This is an extra challenge for the pure hadronic model. Although it agrees with the *Fermi-LAT* data, it would imply a flat CRp and/or magnetic field profile to explain the signal (Planck Collaboration et al. 2013b; Zandanel et al. 2014). Moreover, the pure hadronic models should lead to radio power-law spectra (Schlickeiser et al. 1987), unlike what is observed in the Coma cluster. Our results provide a step forward in the understanding of the origin of the diffuse radio emission in giant radio halos. While we might expect a similar origin for all giant-halos, it is likely not transferable to mini-halos whose origin might be different and for which the pure hadronic model remains plausible.

3.3 Preparation of the CTA galaxy cluster Key Science Project

The Cherenkov Telescope Array (CTA, Cherenkov Telescope Array Consortium et al. 2019) is a new generation ground-based instrument made up of around 100 telescopes to be installed at two sites, in the northern (La Palma, Spain) and southern hemisphere (Paranal, Chile). It will observe by imaging the Cherenkov light created by high-energy showers in the atmosphere from 20 GeV to 300 TeV and with a few arcmin angular resolution. The construction of the telescopes has already started for the northern site. CTA should make it possible to explore with great precision the most extreme phenomena in the universe, including those causing the acceleration of particles in clusters.

The observation of the γ-ray emission in galaxy clusters is one of the 10 key science projects carried out by the CTA Consortium. A total of 300 hours of observations towards the Perseus cluster are planned for this purpose. The scientific preparation of this project is divided into two parts, with distinct goals, but taking place in a joint working group. The first one aims at using clusters to constrain the nature and the distribution of dark matter via annihilation or decay (see Pérez-Romero 2022). The other one is to address the physics of CR in clusters via the detection of the associated diffuse γ-ray emission. This includes the measurement of the CRp content of clusters, the understanding of the acceleration mechanisms, propagation and confinement, and the investigation of the origin of the diffuse radio emission in clusters. This section discusses the prospects for the search for a diffuse γ-ray signal in the Perseus cluster with CTA.

3.3.1 Predicting the expected γ-ray emission towards the Perseus cluster

Target selection Because CTA aims at obtaining the first unambiguous detection of the diffuse γ-ray emission from galaxy clusters, we focus on a single target, selected as the best candidate, to be observed for a long time. The hadronic γ-ray luminosity should scale as $L_\gamma \propto n_{\rm gas} n_{\rm CRp} R^3$. Assuming standard scaling relations and a universal CRp to thermal energy ratio, the γ-ray flux should scale as $F_\gamma \propto L_X^{1.2}/D_L^2$. Although this does not reflect the impact of the inner structure, it was used to extract a short list of relevant targets, using X-ray luminosities from Piffaretti et al. (2011). The best candidates, ranked by preference, are well-known nearby systems: the Virgo, Perseus, Ophiuchus, Coma, Centaurus, and the Norma clusters.

Additional selection criteria are related to the observations and instrument. The target signal should be significantly smaller than the CTA field of view (5-9 deg, depending on the energy) such that systematics associated with the background are limited. On the other hand, the signal should be sufficiently extended so that it can be clearly distinguished from AGNs.

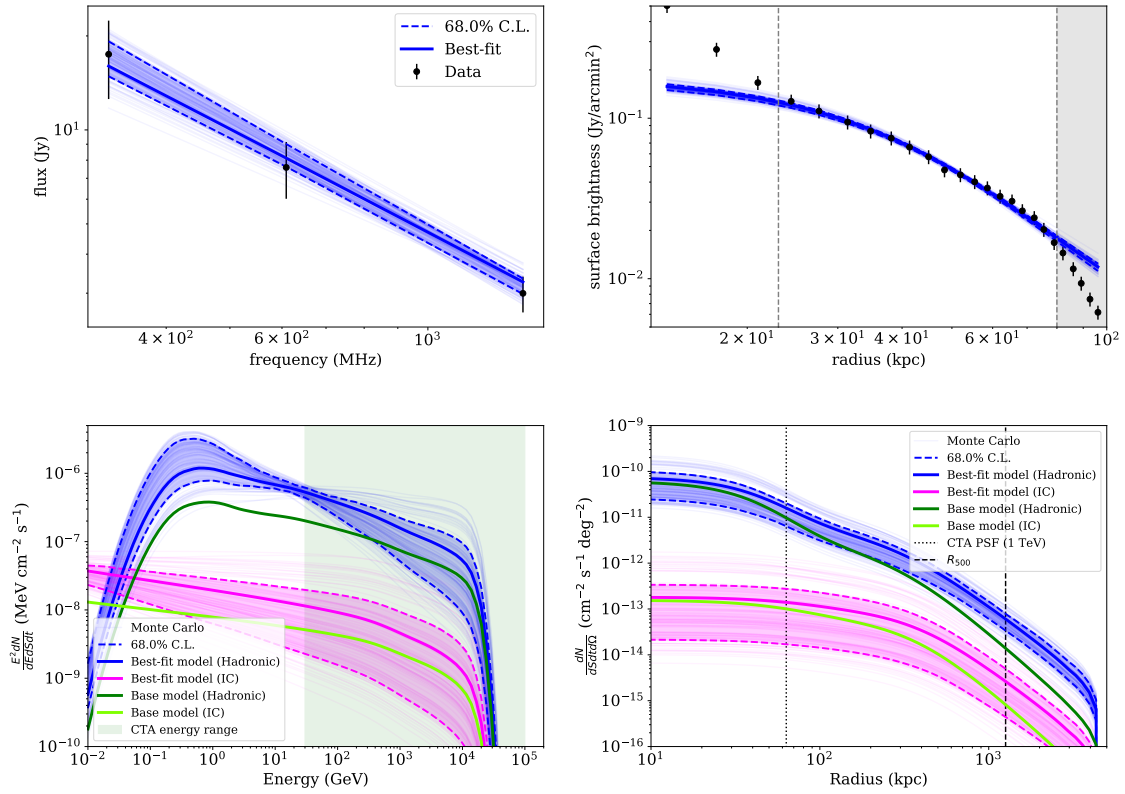

Figure 3.5: Constraints on the radio and γ-ray observables in the case of the pure hadronic model (blue and magenta) and baseline model (dark green and chartreuse). **Top left**: radio spectrum within a 15 arcmin diameter (from Gitti et al. 2002). **Top right**: radio profile at 1380 MHz (from Pedlar et al. 1990). Following Zandanel and Ando (2014), the grey area is discarded due to contamination from NGC 1275 and possible issues with large scale flux recovery. **Bottom left**: γ-ray spectrum within θ_{500}. **Bottom right**: γ-ray projected profile in the range 150 GeV - 50 TeV. Adapted from CTA collaboration (forthcoming).

Accordingly, the Perseus cluster is arguably the most promising target. This is due to its short distance ($z = 0.017$), its high mass ($M_{500} \sim 6\times10^{14}$ M$_\odot$) and appropriate angular extent ($\theta_{500} \simeq 1$ deg). Its very dense core, as the archetype of a relaxed cool-core cluster, ensures a large amount of target material for hadronic interactions. As the host of a very bright radio mini-halo, particle acceleration is already established in the Perseus cluster. Two γ-ray bright AGNs, NGC 1275 and IC 310, prevent *Fermi-LAT* from establishing reliable constraints on the Perseus diffuse emission but this should be mitigated by the much better angular resolution of CTA. The detailed modeling of a few relevant targets confirmed that Perseus is by far the best target for CTA.

Model definition and calibration The Perseus mini-halo is still compatible with the pure hadronic model. The prediction of the signal is thus very important to address the capabilities of CTA to distinguish between different scenarios and inform us about particle acceleration and transport. Two approaches were employed: 1) constraining the CRp distribution, and thus the γ-ray emission, assuming the pure hadronic model and using radio data; 2) calibrating the CRp distribution according to numerical simulations. In both cases, the CRp population was modeled as in Section 3.2, with parameters related to CR acceleration and transport physics (Pinzke and Pfrommer 2010).

The thermal gas modeling, from the core to the outskirt, was made based on the literature

(Ettori et al. 1998; Jones and Forman 1999; Churazov et al. 2003, 2004; Urban et al. 2014) and validated with *ROSAT* and *Planck* data. Its uncertainties are negligible for our purpose. When considering the radio signal in the pure hadronic scenario, a model of the magnetic field strength is necessary. Since barely any direct measurement exists for the Perseus cluster (see Taylor et al. 2006, for the core value of 25 μG), different scaling assumptions were considered, leading to the dominant systematic uncertainty (about a factor of two). The joint fit of radio synchrotron profiles and spectra from Pedlar et al. (1990) and Gitti et al. (2002), respectively, allowed us to constrain the model parameters and propagate it to the γ-ray prediction at CTA energies. Alternatively, as a baseline, the values $X_{\rm CRp}(R_{500}) = 10^{-2}$, $\alpha_{\rm CRp} = 2.3$ and $\eta_{\rm CRp} = 1$ were used according to numerical simulations expectations (Pinzke and Pfrommer 2010).

Our work gives a first quantitative prediction of the expected signal in the pure hadronic model, including thorough estimates of the modeling uncertainty. See Figure 3.5 for an illustration. Upcoming radio data are expected to provide significantly better coverage in terms of angular scale and observing frequency. This should considerably improve the statistical and systematic errors that affect our current prediction. Moreover, direct constraints on the Perseus magnetic field cluster would reduce the dominant source of systematics. On the way, we discovered that the thermal model used in Ahnen et al. (2016) overestimates the pressure by a factor of a few, which directly translates into their upper limit on CRp that is too optimistic by a similar amount.

3.3.2 CTA sensitivity to cosmic ray physics in the Perseus cluster

With the γ-ray models in hand, the CTA sensitivity to cluster CR physics can be estimated by accounting for the instrument response function and the expected background.

Simulation and analysis framework To test CTA observations and measure their sensitivity to the underlying target physics, we have developed the publicly available `Python` code `KESACCO` (Keen Event Simulation and Analysis for CTA Cluster Observations[5]). It uses the `ctools` software (Knödlseder et al. 2016), especially for convolving the sky model with the instrument response. `KESACCO` allows the users to define a sky model, the observation setup, and the analysis parameters. It runs the event simulation. In classical imaging atmospheric Cherenkov telescopes On-Off analysis, the background is estimated from the data themselves by defining an On (source) and Off (background) region. Alternatively, the full region of interest may be modeled and fit all together (template fitting) to extract the relevant information, as done with *Fermi-LAT*. `KESACCO` can perform both methods. The analysis computes data preparation files (binning, stacking, On-Off definitions, etc, depending on the requested analysis), runs likelihood fits, extracts upper limits, and performs spectral/spatial/spectral-imaging sampling of model parameters.

Observation setup `KESACCO` was used to address the CTA observation strategy to maximize the chances of detection. Given the expected azimuthal symmetry of the target, in addition to point sources, the main parameter to be optimized is the pointing offset relative to the cluster center (needed in On-Off analysis). Template fitting and On-Off methods were tested. The S/N ratio obtained in the latter depends on the number of Off regions available, the size of the On region, and the point source mask size, all of these depending on the pointing offset. In the end, the results were weakly depending on the signal itself and an offset of about 1 deg was favored.

Sensitivity to cosmic ray physics The application of `KESACCO` to the Perseus key science project was also used to test the degeneracies between the sky components (e.g., the diffuse emission and

[5] https://github.com/remi-adam/kesacco

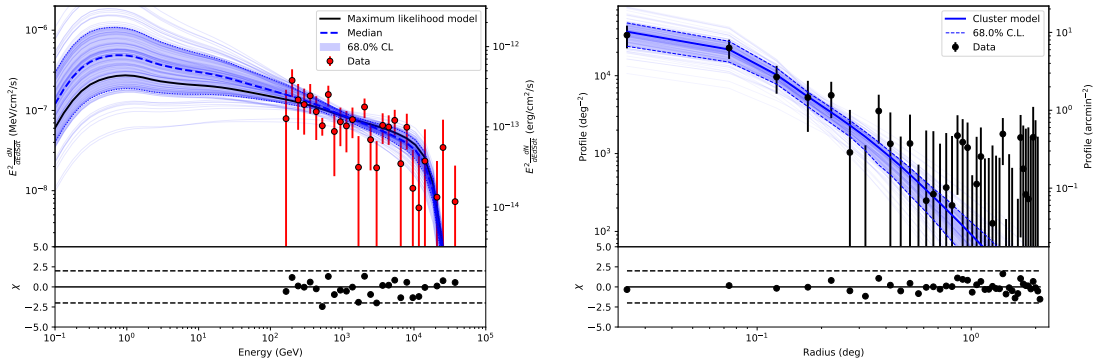

Figure 3.6: Expected CTA constraints on the CRp distribution in the Perseus cluster. **Top:** recovered spectral energy distribution (left) and profile (right) in the case of the baseline model. Extracted from CTA collaboration (forthcoming).

AGNs) and address how well the CRp properties can be measured. This is illustrated in Figure 3.6. The expected constraints on the cluster spectrum and profile are reported for the baseline model. In this scenario, $\alpha_{\rm CRp}$ will be constrained to about 10% and $\eta_{\rm CRp}$ to 25%, which would lead to a considerable step forward for cluster CR physics. However, this analysis has also revealed that CTA data are affected by degeneracies between the CRp parameters. They are particularly strong for a faint signal, especially for the slope and the normalization, since CTA only probes the high energy part of the spectrum. This limits CTA's capability to precisely quantify the cluster CRp energy budget. The presence of NGC 1275, which has a very soft spectrum ($\propto E^{-3.6}$) is prohibitive at low energies, where the point spread function increases. For a low S/N ratio, steep CRp spectrum, and compact CRp morphology, the signal is highly degenerate with NGC 1275 and cannot be distinguished unless strong priors are available from lower energy (e.g., with *Fermi-LAT*).

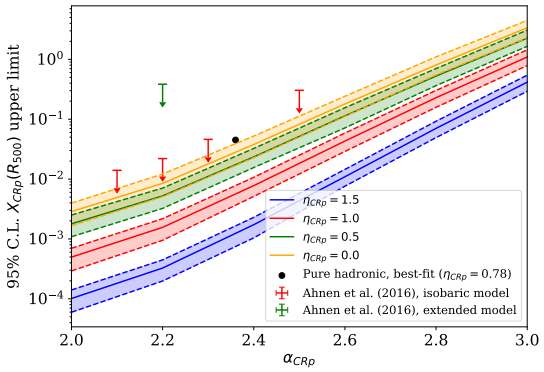

Figure 3.7: Upper limit on the normalization, $X_{\rm CRp}(R_{500})$, as a function of the spectral slope $\alpha_{\rm CRp}$ and the spatial scaling $\eta_{\rm CRp}$. The limits obtained by Ahnen et al. (2016) using isobaric and extended models are reported. They roughly match our $\eta_{\rm CRp} = 1$ and $\eta_{\rm CRp} = 0.5$ models, respectively. Extracted from CTA collaboration (forthcoming).

We also estimated the exclusion limits that can be set in the case of non-detection. This is illustrated in Figure 3.7, which gives the 95% exclusion limits in the parameter space. The huge new parameter space volume accessible with CTA will certainly be a game-changer in the search

for diffuse cluster scale γ-ray emission. Because numerical simulations already predict that the signal should be at the detection limit of the current instrument, a non-detection should seriously challenge current CRp acceleration models. However, the CTA sensitivity drops as the CRp spatial distribution flattens and its spectral slope increases, leaving room for models with gentle acceleration and/or significant CRp diffusion and streaming to remain inaccessible.

In summary, CTA will be able to improve current constraints by about one order of magnitude. A non-detection will likely recast our current view of CR physics in the ICM. In the case of detection, CTA will be able to constrain the spectral energy distribution of CRp, which is intimately connected to their acceleration process. The shape of the profile can be measured as well and will inform us about the transport of CRp in the ICM.

3.4 Conclusion and outlook

The measurement of the diffuse γ-ray emission from galaxy clusters is nearly the only way to directly access the CRp population, which is key to understanding the diffuse radio emission in these systems. However, after more than 20 years of searches, with several generations of ground-based and space-based facilities, such a signal remain elusive. While the emission is expected to be at the detection limit of current observations, its prediction is affected by large uncertainty due to the very complex underlying physics, and the CR properties are still poorly known to date.

Nevertheless, the last few years have seen significant advances in the field. Some of them have been reviewed in the present document. The main conclusions are summarized as follows.

- We developed a new publicly available software, `MINOT`, to provide a self-consistent framework for modeling the physical state of the ICM and its diffuse emission from radio to γ-rays.
- A significant γ-ray emission is observed in the direction of the Coma cluster with *Fermi-LAT*. Diffuse emission models associated with the ICM agree very well with the expectations, but alternative origins of the signal cannot be excluded (e.g., AGNs, star-forming galaxies).
- The joint analysis of the radio and γ-ray emission from the Coma cluster shows that giant radio halos, at least for Coma, cannot be explained in the framework of the pure hadronic model. The turbulent reacceleration model, on the other hand, is in excellent agreement with the data.
- CTA is expected to improve current state-of-the-art limits by about an order of magnitude. A non-detection would exclude a pure hadronic origin of the mini-halo and should severely challenge current models. The data will be sensitive to the energy spectrum and the profile of CRp, which will allow us to better understand CR acceleration and transport physics in galaxy clusters.

The signal observed in the direction of the Coma cluster may indicate that the hadronic emission associated with massive nearby clusters is close to the limit of the *Fermi-LAT* sensitivity, renewing the interest in such searches towards other targets. In fact, combining *Fermi-LAT* data with radio observations at very low frequencies (e.g., LOw Frequency ARray, LOFAR) may be very helpful in constraining turbulent reacceleration models and understanding the role of CRp, given the leverage they provide in the case of steep-spectrum radio halos. Nevertheless, it is unlikely that *Fermi-LAT* analysis will unambiguously detect ICM induced γ-ray. Given its sensitivity and angular resolution, CTA should allow us to push the searches to the next step. Beyond the Perseus cluster key science project, there are several opportunities to constrain the CR physics in clusters. For instance, the extragalactic survey might be used to perform stacking or cross-correlation analysis, taking advantage of available data at other wavelengths. Alternatively, several AGNs that should be observed are associated with BCG in cool-core clusters for which AGN-ICM interactions are clear (e.g., M87 in the Virgo cluster, or the central galaxy of the Hydra-A cluster). The detection of such cavities in γ-rays could tell us a lot about the feedback mechanisms at play in clusters.

4 Perspectives

Contents

The ICM is a fundamental component of galaxy clusters. Its properties reflect the rich physics associated with galaxy formation processes and the dynamics induced by structure formation. Thanks to observational and theoretical achievements, major advances have been made during the last decades regarding our understanding of thermal and non-thermal ICM physics. In this document, we have overviewed the aims, the developments, and the results obtained over the last few years via resolved observations of the SZ effects with the NIKA and NIKA2 cameras, and the quest for the ICM diffuse γ-ray emission both with *Fermi-LAT* from space and the preparation of CTA from the ground. In light of these achievements, many new opportunities are opening to address new timely questions related to the ICM thermal and non-thermal physics. In this section, we briefly discuss, in a non-exhaustive way, some of these possibilities and challenges.

4.1 Future opportunities with resolved Sunyaev-Zel'dovich observations

Building on the results presented in Chapter 2, many new opportunities are opening with resolved SZ observations, as already highlighted in Section 2.6. Here we discuss further two possibilities to push the use of such data: exploring the regime where the ICM establishes and probing the non-thermal ICM contribution via multi-wavelength analyses.

4.1.1 Probing the intra-cluster medium establishment from very high-redshift thermal Sunyaev-Zel'dovich observations

The thermodynamical state of galaxy clusters is now routinely accessible from resolved tSZ data up to intermediate redshifts. The combination with X-ray photometry may even be safely used to characterize the full thermodynamical state of the clusters. Currently, a census of the cluster population at $0.5 \lesssim z \lesssim 1$ is being made by the LPSZ. At higher redshifts ($1 \lesssim z \lesssim 2$, or even higher), however, we start entering a very new regime in which the ICM is being established. In fact, some tSZ and X-ray observations have shown that virialized gas may already exist early up to $z \sim 2$ (Mantz et al. 2018; Gobat et al. 2019; Mantz et al. 2020; Andreon et al. 2021). Characterizing this population will be key for understanding cluster physics and evolution up to the time of their formation. On the other hand, this is also a regime where *Euclid*[1] should detect thousands of clusters (Euclid Collaboration et al. 2019), which will have to be well-understood if one wants to use them for cosmological purpose. A large observing program aiming at characterizing this early ICM phase of cluster formation would therefore be extremely valuable, and complete well the LPSZ at lower redshifts. A selection of such sources from current X-ray or tSZ surveys is not possible for a reliable statistical sample, although it might be in the future (e.g., with CMB-Stage4). Nevertheless, the *Euclid* survey should start soon, and ongoing optical surveys may already be an excellent starting point (e.g., with the Massive and Distant Clusters of *WISE* Survey, Gonzalez et al. 2019), which, in addition, will provide a cluster selection independent from the gas content. Finally, one should note that NIKA2 observations might allow us to probe not only the diffuse thermal gas at 150 GHz via the tSZ effect, but also the star formation in cluster galaxies that is more active in this regime.

4.1.2 Combining deep resolved Sunyaev-Zel'dovich and radio observations: an opportunity to address the non-thermal cluster physics?

The key strength of NIKA2 tSZ data relies on the mapping of the ICM pressure. This allows us to recover the cluster thermal pressure profile, as shown in many analyses (Adam et al. 2015, 2016; Ruppin et al. 2017, 2018; Ricci et al. 2020; Kéruzoré et al. 2020), but may provide much more information if a sufficient S/N ratio is available. In addition to the global morphology, compression and discontinuities can give access to merger events and shocks (Adam et al. 2018b), and tSZ fluctuations might inform us about pressure fluctuations and thus turbulence. These features are connected with the non-thermal components and the HSE mass bias but are currently not well-characterized. On the other hand, shocks and turbulence are likely to be connected to the diffuse radio emission from galaxy clusters, which origin is still not completely understood. Consequently, analyzing jointly high S/N ratio resolved tSZ data and diffuse radio data might be an interesting route to address the physics of the non-thermal cluster component and better understand particle acceleration.

Turbulence The pressure fluctuation spectrum is an excellent diagnosis of the turbulent ICM (Schuecker et al. 2004). On the one hand, turbulence is believed to play an important contribution to the reacceleration of CR, which might be responsible for some of the diffuse radio emissions seen in clusters (in particular giant radio halos, Brunetti and Jones 2014). On the other hand, turbulence is expected to dominate the non-thermal contribution and encapsulate most of the HSE mass bias (Pratt et al. 2019). The tSZ fluctuation spectrum normalization is proportional to the 3D Mach number and proportional to the non-thermal contribution. For instance, Khatri and Gaspari (2016) have used the *Planck* data to extract the pressure spectrum in the Coma cluster and obtained a value

[1] And/Or LSST, to some extent.

from $b_{\rm HSE} = 0.15$ in the core to $b_{\rm HSE} = 0.45$ in the outskirt. The tSZ fluctuations can also give access to the nature of the fluctuations by comparison to X-ray (e.g., isobaric, adiabatic).

Given its high angular resolution, NIKA2 can in principle be used to infer the ICM turbulence up to a relatively high redshift. Recently, we have started investigating to which extent this was possible given the characteristics of the data. Indeed, this is not obvious because of the large-scale filtering involved in the data processing, or the noise properties. We computed the power spectrum of the tSZ fluctuations after subtracting a smooth model from the data (similarly to Khatri and Gaspari 2016, for the Coma cluster). Preliminary results are highlighted in Figure 4.1 in the case of MACS J0717.5+3745, a cluster that hosts the most powerful radio halo known to date. Although this methodology deserves to be further investigated, as it might be affected by various systematic effects (e.g., the definition of the center, the choice of the smooth model), the results indicate that significant information relative to the tSZ fluctuations can be extracted from high S/N ratio NIKA-like data. The validation of the recovery of the signal was done by applying the same analysis to the simulated RHAPSODY-G clusters used in Adam et al. (2018b). Connecting the recovered tSZ fluctuation spectrum to the underlying pressure fluctuation spectrum and its non-thermal energy contribution is ongoing. The comparison of the fluctuation amplitudes to the diffuse radio emission could tell us about the connection between these two tracers of the non-thermal ICM.

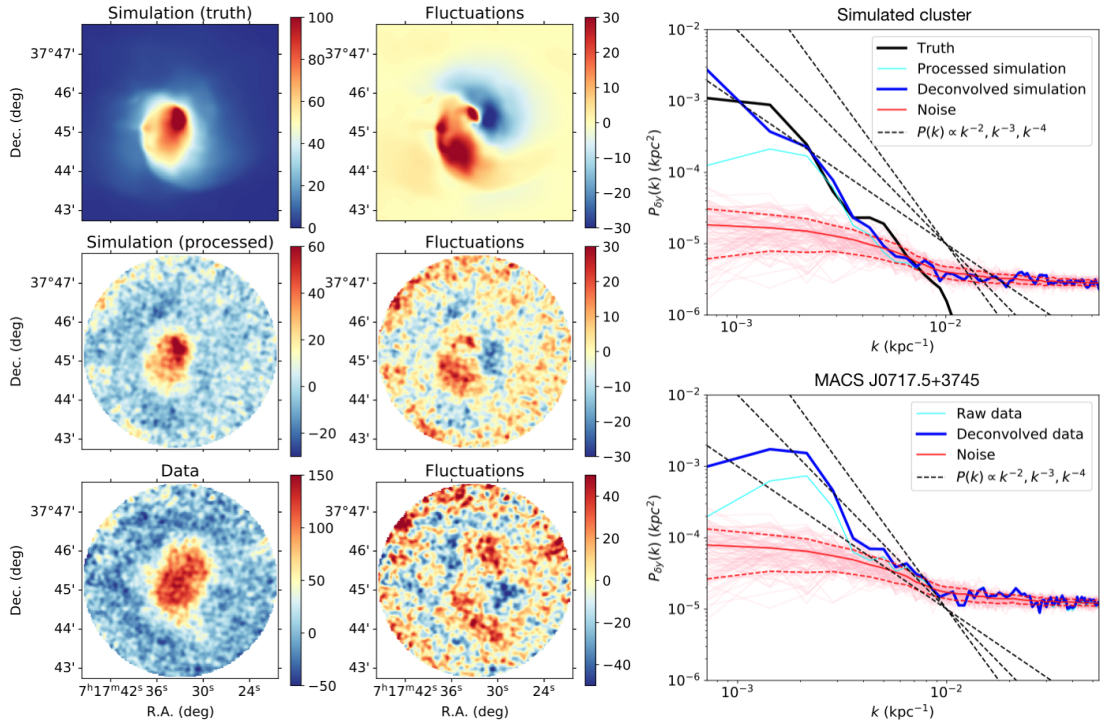

Figure 4.1: Preliminary measurement of the tSZ fluctuations. **Left**: Compton parameter images, in units of $10^6 y$, of the tSZ signal and the fluctuations for a RHAPSODY-G cluster at $z = 0.54$ (top), the same cluster processed through the analysis pipeline (middle), and the NIKA cluster MACS J0717.5+3745 (bottom). The noise level of the simulated cluster was normalized so that the S/N ratio is similar to that of the real data. **Right**: Power spectrum of the tSZ fluctuations for the simulated RHAPSODY-G cluster (top) and MACS J0717.5+3745 (bottom). The signal recovered after data processing is shown in cyan, the signal deconvolved from the transfer function in blue, and the true input in the case of the simulation in black. In both cases, the contribution from the noise is computed using Monte Carlo noise realizations as shown in red together with their median and 68% confidence interval.

Shocks The tSZ data are sensitive to shocks via pressure discontinuities provided enough sensitivity and angular resolution are available. Given the tension that was reported between the Mach numbers inferred from X-ray and radio data (Akamatsu et al. 2017), complementing the analysis using tSZ information is likely to be relevant. It may help to better constrain the shock geometry, test the underlying assumptions, discriminate between shocks and cold front, and even give an infall velocity estimate if the kSZ effect is measured. At high redshifts, the tSZ signal might even be the only way to directly measure ICM shocks given the drop of the X-ray surface brightness, even if angular resolution might become a major limiting factor.

The characterization of shocks from ground-based high-resolution tSZ observations was made with MUSTANG (Korngut et al. 2011) and ALMA (Basu et al. 2016; Di Mascolo et al. 2019). Although discontinuities were investigated as part of the morphological characterization of the NIKA clusters (Adam et al. 2018b), we did not attempt to directly measure shock Mach numbers yet. Nonetheless, this is a point we have started exploring recently. For instance, several NIKA and NIKA2 clusters present indications for the presence of shocks that also correlate with the presence of diffuse radio emission. Further investigation might help understand better the connections between particle acceleration and ICM shocks.

Spatial comparison of the thermal and non-thermal emission The point-to-point correlation between the diffuse radio emission associated with halos and thermal ICM tracers, including the tSZ signal, can tell us about the underlying acceleration physics (Govoni et al. 2001; Feretti et al. 2001; Hoang et al. 2019; Xie et al. 2020; Botteon et al. 2020; Bruno et al. 2021). For instance, the Coma cluster giant radio halo (at 352 MHz) and the tSZ signal are quasi-linearly correlated with a small intrinsic scatter (Planck Collaboration et al. 2013b), implying either a much flatter magnetic field profile than expected or a nearly flat CRe energy density. This disfavors the pure hadronic model.

We started investigating how the tSZ signal correlates with diffuse radio emission in the NIKA clusters. Among them, CL J1226.9+3332 is appealing because it hosts the most distant radio halo known to date such that huge leverage can be obtained when testing processes that evolve in redshift. Figure 4.2 presents the comparison of the tSZ and radio signal in CL J1226.9+3332 ($z \sim 0.9$). We can observe that the western extension of the halo coincides with the substructure seen in tSZ, the probable shock front, and the region of higher temperature (Adam et al. 2015, 2018b). Although CL J1226.9+3332 is nearly a Coma twin at high redshift, the preliminary comparison seems to indicate that the radio synchrotron emission is more compact relative to the tSZ signal. Further investigation may tell us about the physics of giant radio halo across cluster formation history.

Application to cluster samples The thermal to non-thermal emission correlation applied to statistical samples offers an interesting route to address the origin of the radio-emitting CRe. For instance, the scaling between the tSZ flux and the radio power in giant halos can be used to discriminate between pure hadronic or reacceleration models (Basu 2012). In the turbulent reacceleration framework, the amount of ICM fluctuations should correlate with the radio power. The correlation between the X-ray fluctuation and the radio signal reported in Eckert et al. (2017c) indicates that the radio power and the turbulent energy are roughly proportional. Such correlation may also help characterize the non-thermal component and the HSE mass bias, which is essential for cluster cosmology. Indeed, the interpretation of the tSZ flux - mass scaling relation and its scatter could be improved with extra information about the giant radio halo power. It might also open up the possibility to use future radio surveys sensitive to both the tSZ and radio synchrotron signal (e.g., SKA, Prandoni and Seymour 2014; Acero et al. 2017) to build very high-quality mass proxies by correcting the tSZ flux via the information on the non-thermal contribution. Nonetheless, given

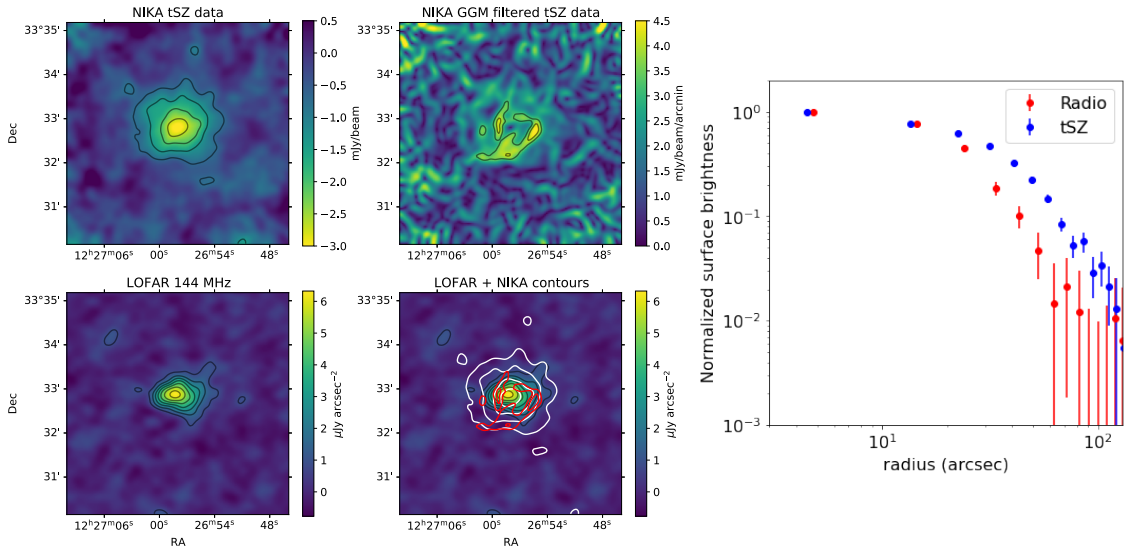

Figure 4.2: Preliminary comparison of the tSZ and radio diffuse emission in CL J1226.9+3332. **Left**: sky maps of the cluster including the NIKA deconvolved data (contours are in units of 3σ), the GGM filtered map (contours are 4 and 5σ), the LOFAR image (contours are in units of 3σ), and the comparison between LOFAR and NIKA. **Right**: surface brightness radial profile comparison of NIKA and LOFAR data. The LOFAR map was taken from https://lofar-surveys.org/planck_dr2.html.

the complexity of the non-thermal physics and the freedom involved in (re)acceleration models, it might be challenging to define tests that could unambiguously discriminate different physics.

Thanks to the advance in radio facilities (and in particular LOFAR, Shimwell et al. 2022), more than 10 clusters of the LPSZ already have available radio data counterparts (Botteon et al. 2022). This opens up the possibility to perform statistical correlations of the LPSZ products to diffuse radio data and start investigating the aforementioned physics. Beyond the LPSZ, the statistical analysis of a high S/N ratio resolved tSZ cluster sample at lower redshifts may also be very prolific because of the better access to the small-scale ICM features and the better diffuse radio emission data available in the more local Universe.

4.2 Towards the full exploitation of CTA capabilities for galaxy cluster physics

The work related to CTA presented in Chapter 3 essentially discussed the CTA sensitivity to cluster CR physics based on the Perseus key science project. In fact, several other key science projects will produce data that are very relevant for cluster science. For instance, the extragalactic and galactic surveys will cover more than 25% of the sky in about 1500 hours, reaching an integrated sensitivity of $\sim$6 mCrab above 125 GeV (equivalent to about 3 hours effective observation time, Cherenkov Telescope Array Consortium et al. 2019). The AGN program may also be relevant because some of the target sources are cluster member galaxies (e.g., M87 is the central galaxy of the Virgo cluster, with 100 hours of observing time foreseen). To fully exploit the CTA capabilities to constrain cluster physics, we have started to investigate several opportunities. These ongoing activities are discussed hereafter.

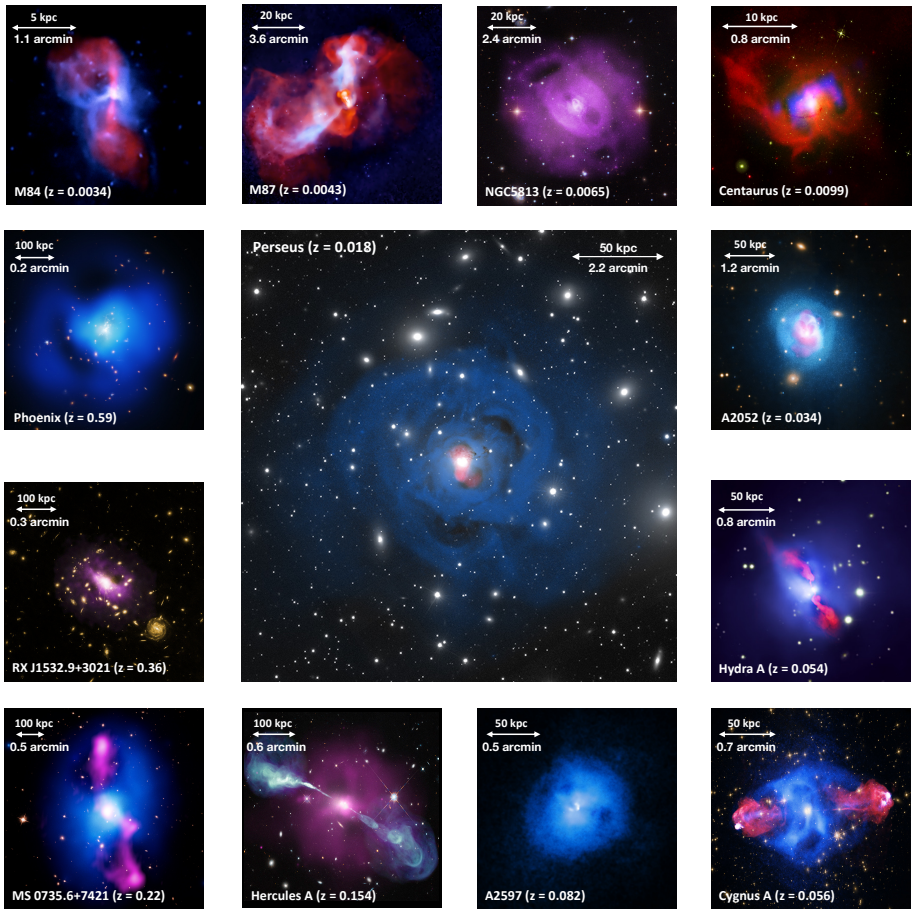

Figure 4.3: Sample of clusters hosting X-ray cavities filled with radio jets, highlighting the radio mode AGN feedback. It includes the most relevant system for CTA observations. For reference, the CTA point spread function is about 3 arcmin at 1 TeV. Extracted from Hlavacek-Larrondo et al. (2022).

4.2.1 The cosmic rays content of active galactic nuclei driven cavities

Several AGNs located in the core of galaxy clusters are responsible for well-known cluster scale X-ray cavities filled with radio emitting plasma. For instance, the Perseus, Virgo (M87), Hydra A, and MS 0735.6+7421 clusters present clear cavities in the X-ray (Shin et al. 2016); see also Figure 4.3. Fruitful CTA observations require not only the emission to be sufficiently bright for detection, but also that the signal is well-resolved to disentangle the different components. Because of its orientation in the sky, its relatively simple geometry, its coordinates and distance, and the power released by its AGN, the central galaxy of the Hydra-A cluster is one of the best candidates to search for γ-ray emission associated with radio bubbles (Nulsen et al. 2005; Wise et al. 2007). It was already targeted by imaging atmospheric Cherenkov telescopes, but the signal remained undetected (HESS Collaboration et al. 2012). Using simple modeling of the cavities, with the help of radio and X-ray data and assumptions on the magnetic field, we started investigating the sensitivity of CTA to constrain the CRp content of the bubbles. This was done during the internship of Marin Fontaine, who showed that for reasonable observing time (a few tens of hours), detection will be possible. Note that such constraints in the γ-ray, sensitive to the CRp pressure, complement well the ones already obtained for another cluster via the tSZ effect (MS 0735.6+7421, see Abdulla et al. 2019). Fortunately, such efforts will provide a definitive answer about the nature of the pressure support in AGN-driven cavities in cluster cores, and inform us about AGN feedback mechanisms.

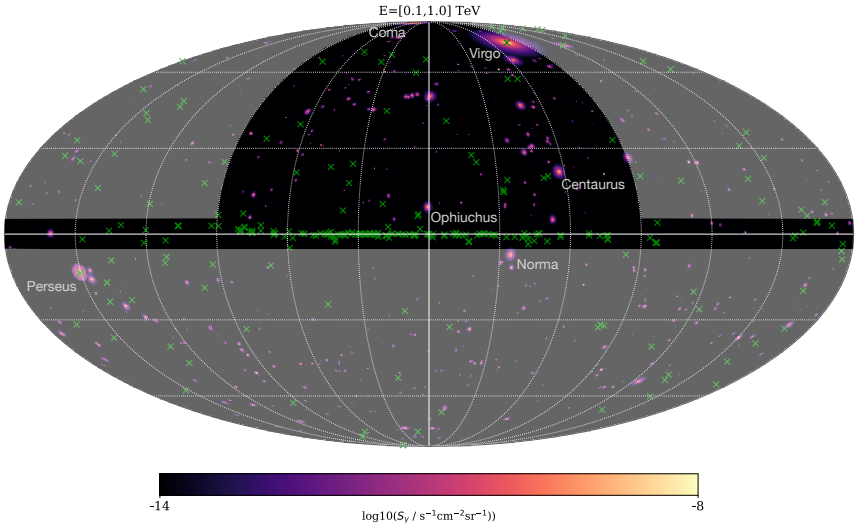

Figure 4.4: Prediction of the full sky hadronic γ-ray emission associated with galaxy clusters, integrated between 100 GeV and 1 TeV. The names of the brightest clusters are indicated. Regions outside the CTA galactic and extragalactic survey area are shaded. The location of currently known TeV sources extracted from the TeVCat catalog are reported as green crosses (essentially AGNs for sources away from the galactic plane, Wakely and Horan 2008).

4.2.2 Statistical analysis of CTA survey data

The CTA extragalactic (and potentially galactic) survey data may be used to constrain the CR content of clusters in two complementary ways: the stacking of the data at the location of known clusters identified at other wavelengths (see, e.g., results using *Fermi-LAT* data, Huber et al. 2013), or the direct cross-correlation with maps produced at other wavelengths (Shirasaki et al. 2020).

The sensitivity of CTA in the case of stacking was investigated during the internship of Elsa Deville and Yanis Pianko. As a starting point, we considered the HIFLUGCS catalog (Reiprich and Böhringer 2002) because it is X-ray flux-limited. Indeed, given the expected scaling between the X-ray and γ-ray flux ($F_\gamma \propto L_{\rm X}^{1.2}/D_L^2$), we expect all the relevant γ-ray targets to be present in our sample. Bright clusters near the galactic plane, in the zone of avoidance, were considered separately. The mass and redshift of the clusters, together with the assumption of universality, were used to define the thermal model based on the results from (Arnaud et al. 2010) and (Ghirardini et al. 2019a). Thanks to `MINOT`, these models were easily validated by comparison to *Planck* tSZ integrated fluxes (and maps) and X-ray temperatures, and the associated systematic effects were quantified. The γ-ray models were finally produced accounting for the CTA response function and using different CRp scaling relative to the thermal gas and different power-law spectral indices. The expected CTA limits were computed by stacking the signal either using On-Off techniques with the formalism of Li and Ma (1983) or via Monte Carlo realization. In the end, Yanis and Elsa have shown that this approach could yield limits on the mean CRp content that are above, but comparable to that obtained for the Perseus key science project. Note that this effort is now being pursued in the context of the CTA data challenge, which aims at producing realistic mock data. These data will then be used to reproduce our preliminary constraints by accounting for the AGN contamination and benefiting from a more realistic observation strategy. As an illustration, Figure 4.4 presents a full-sky model of the γ-ray emission expected between 100 GeV and 1 TeV. In this case, clusters from the NORAS, REFLEX and CIZA catalog were considered (using the MCXC meta-catalog, Piffaretti et al. 2011) and imposing a X-ray flux limit of $L_{\rm X} > 5 \times 10^{-12}$ erg s^{-1} cm^{-2}. The CRp spatial distribution was assumed to follow that of the thermal gas, with a

power-law spectral index $\alpha_{\rm CRp} = 2.2$, and normalized to 1% of the thermal energy. The thermal model was established as follows: the pressure profile was computed from Arnaud et al. (2010), the density was derived according to the polytropic relation measured in Ghirardini et al. (2019b), and we accounted for the dynamical state, when available, according to the cluster core entropy (Cavagnolo et al. 2009).

Cross correlations with tracers of the thermal gas, in particular X-ray and tSZ data, should be particularly sensitive to the CRp content and distribution. The cross-correlation with radio surveys might inform us about the underlying acceleration mechanism (e.g., turbulent reacceleration in radio halos). On the other hand, future optical surveys should provide weak lensing data that could be used as a direct tracer of the dark matter, and thus be relevant for indirect dark matter searches in the γ-rays. Whatsoever, the cross-correlation analysis is expected to be more complicated to perform than the stacking. Indeed, it is not clear at this stage how well the diffuse emission can be recovered and the (complicated) background controlled. Moreover, the signal arising from the AGN population, which should dominate in the γ-rays, will also generally affect the other wavelengths to be used for cross-correlation, such that precise modeling of this component will be important.

In the future, CTA is likely to be the only relevant γ-ray instrument for cluster science. Indeed, although *Fermi-LAT* may be close to the detection limit, its sensitivity will not significantly improve in a short amount of time because it has already been collecting data for more than 12 years. From the ground, the sensitivity of the current imaging atmospheric Cherenkov telescopes is not sufficient to detect the diffuse cluster emission. As discussed in this document, CTA should lead to a huge step forward regarding the physics of CR in clusters, especially if the signal is detected. Nevertheless, its sensitivity will at best allow us to constrain well the CRp in the Perseus cluster. Consequently, CTA will remain limited and the understanding of cluster scale CR physics will require using other routes, for instance, at lower wavelengths.

4.3 The future scene of the intra-cluster medium science

In addition to the ongoing theoretical and simulation effort needed to better address the ICM thermal and non-thermal physics, many starting or planned facilities are likely to lead to a major improvement in our understanding of the ICM. A (most likely) non-exhaustive panorama of relevant experiments is briefly overviewed in the following.

Ongoing and upcoming facilities Beyond *Fermi-LAT* and CTA, water Cherenkov detectors (e.g., HAWC, LHAASO, SWGO, Abeysekara et al. 2013; Cao et al. 2019; Hinton and SWGO Collaboration 2022) are observing or starting the observations of very high energies γ-rays ($\gtrsim$TeV). However, they are not the best-suited instrument for cluster studies because, in addition to their poor angular resolution, photons at these energies are absorbed by the extragalactic background light when traveling through the Universe. From space, instruments like *e-ASTROGAM* could be very relevant to search both for the inverse Compton and the hadronically induced γ-rays in the MeV-GeV region, but the project schedule is still to be defined.

In the X-rays, the *eROSITA* observations have started, providing an unprecedented view of the X-ray sky and the detection of many clusters (Merloni et al. 2012). Future missions are also being prepared, such as *XRISM* (XRISM Science Team 2020), *Athena* (Nandra et al. 2013) and *Lynx* (Gaskin et al. 2019), which should revolutionize the study of ICM motions thanks to their great sensitivity and spectral resolutions.

Although they are not probing the ICM, future galaxy surveys (e.g., LSST, *Euclid*, LSST Science Collaboration et al. 2009; Laureijs et al. 2011) will allow for the definition of mass-selected

statistical cluster samples thanks to weak lensing measurements, independently from their ICM content. Moreover, the detection of clusters at very high redshifts, and their follow-up at other wavelengths, will open a new window onto the epoch of cluster formation.

Planed CMB satellites essentially focus on CMB polarization (e.g., Matsumura et al. 2014) and will provide limited cluster science outcomes. On the other hand, many effort are being pursued to develop ground-based experiments including: MUSTANG2 (Dicker et al. 2014), NIKA2 (Adam et al. 2018a), instruments at the Large Millimeter Telescope[2], CMB-Stage4 (Abazajian et al. 2016), the Atacama Large Aperture Submillimeter Telescope (Klaassen et al. 2020), ALMA[3], CONCERTO (Monfardini et al. 2021), or instruments at the Sardinia Radio Telescope[4]. The improved sensitivity, frequency coverage, and angular resolution will push the limits of SZ detections, ICM studies, and will also provide CMB cluster lensing masses.

Among the upcoming facilities, special attention should certainly be given to the Square Kilometer Array (SKA)[5], as already advertised by its precursors and pathfinders: e.g., GMRT[6], LOFAR (Shimwell et al. 2022), MeerKAT[7]. Indeed, SKA should lead to a change of paradigm in our understanding of the ICM physics, going from a situation where only the tip of the radio cluster scale emission is accessible, to a full census of the cluster population and its non-thermal components. Thanks to its sensitivity, angular resolution, and frequency coverage, huge improvements are expected in many areas, in addition, and complementing the study of the cluster scale radio synchrotron emission (Cassano et al. 2015; Ferrari et al. 2015). For instance, SKA will provide extremely valuable information on the cluster magnetic fields via Faraday rotation measure (Bonafede et al. 2015; Govoni et al. 2015; Giovannini et al. 2015; Johnston-Hollitt et al. 2015), so that it can be better disentangled from the synchrotron signal and inform us on particle acceleration physics. SKA should also allow us to study the feedback from AGNs and their relation to radio mini-halos (Gitti et al. 2015). In addition, high-frequency observations with SKA should give access to the thermal content via the measurement of the tSZ signal at high angular resolution (Grainge et al. 2015). Finally, SKA might even give access to the cluster lensing, providing a mass proxy that is independent of the underlying ICM physics (Brown et al. 2015; McKean et al. 2015).

Last but not least: a major challenge to anticipate A vast crowd of new facilities from radio to γ-rays, relevant to ICM studies and the physics of large-scale structures, is planned for the future. This, together with the simple extrapolation of the rate of discoveries based on the past ten 20-30 years, might indicate that the future of ICM physics will be bright. Nonetheless, the limit to the growth of human societies was also established a few decades ago (Meadows et al. 1972). Some of these limits have now been reached. For instance, the production peak of many non-renewable key resources has passed by now[8], and major growth-related nuisances are already affecting us (e.g., the destruction of biodiversity, the global warming, and its consequences, IPBES 2019; IPCC 2022a,b). A decline phase is now likely to arise soon, whether it is anticipated or uncontrolled. As part of human activities, research largely benefits in many ways from the growth of resource consumption. While it is always difficult to predict the future, the forthcoming changes in our societies will likely severely affect research in astronomy and beyond.

Let us think about it as well!

[2] http://lmtgtm.org/
[3] www.almaobservatory.org
[4] http://www.srt.inaf.it/
[5] https://www.skatelescope.org/
[6] http://www.ncra.tifr.res.in/ncra/gmrt
[7] https://www.sarao.ac.za/gallery/meerkat/
[8] E.g., the peak of conventional oil production occurred around 2005-2008 (https://www.iea.org).

Bibliography

Abazajian, K. N., Adshead, P., Ahmed, Z., et al. (2016). CMB-S4 Science Book, First Edition. *arXiv e-prints*, page arXiv:1610.02743.

Abdo, A. A., Ackermann, M., Ajello, M., et al. (2010). Detection of Gamma-Ray Emission from the Starburst Galaxies M82 and NGC 253 with the Large Area Telescope on Fermi. *ApJ*, 709(2):L152–L157.

Abdollahi, S., Acero, F., Ackermann, M., et al. (2020). Fermi Large Area Telescope Fourth Source Catalog. *ApJS*, 247(1):33.

Abdulla, Z., Carlstrom, J. E., Mantz, A. B., et al. (2019). Constraints on the Thermal Contents of the X-Ray Cavities of Cluster MS 0735.6+7421 with Sunyaev-Zel'dovich Effect Observations. *ApJ*, 871(2):195.

Abeysekara, A. U., Alfaro, R., Alvarez, C., et al. (2013). Sensitivity of the high altitude water Cherenkov detector to sources of multi-TeV gamma rays. *Astroparticle Physics*, 50:26–32.

Abramowski, A., Acero, F., Aharonian, F., et al. (2012). Search for Dark Matter Annihilation Signals from the Fornax Galaxy Cluster with H.E.S.S. *ApJ*, 750(2):123.

Acciari, V. A., Ansoldi, S., Antonelli, L. A., et al. (2018). Constraining dark matter lifetime with a deep gamma-ray survey of the Perseus galaxy cluster with MAGIC. *Physics of the Dark Universe*, 22:38–47.

Acero, F., Acquaviva, J. T., Adam, R., et al. (2017). French SKA White Book - The French Community towards the Square Kilometre Array. *arXiv e-prints*, page arXiv:1712.06950.

Acero, F., Aharonian, F., Akhperjanian, A. G., et al. (2009). Detection of Gamma Rays from a Starburst Galaxy. *Science*, 326(5956):1080.

Ackermann, M., Ajello, M., Albert, A., et al. (2014). Search for Cosmic-Ray-induced Gamma-Ray Emission in Galaxy Clusters. *ApJ*, 787(1):18.

Ackermann, M., Ajello, M., Albert, A., et al. (2016). Search for Gamma-Ray Emission from the Coma Cluster with Six Years of Fermi-LAT Data. *ApJ*, 819(2):149.

Ackermann, M., Ajello, M., Albert, A., et al. (2015). Search for Extended Gamma-Ray Emission from the Virgo Galaxy Cluster with FERMI-LAT. *ApJ*, 812(2):159.

Ackermann, M., Ajello, M., Allafort, A., et al. (2010). Constraints on dark matter annihilation in clusters of galaxies with the Fermi large area telescope. *JCAP*, 2010(5):025.

Adam, R. (2015). *Observation des amas de galaxies par effet Sunyaev-Zel'dovich et de la polarisation du fond diffus cosmologique : de Planck à NIKA*. Theses, Université Grenoble Alpes.

Adam, R., Adane, A., Ade, P. A. R., et al. (2018a). The NIKA2 large-field-of-view millimetre continuum camera for the 30 m IRAM telescope. *A&A*, 609:A115.

Adam, R., Arnaud, M., Bartalucci, I., et al. (2017a). Mapping the hot gas temperature in galaxy clusters using X-ray and Sunyaev-Zel'dovich imaging. *A&A*, 606:A64.

Adam, R., Bartalucci, I., Pratt, G. W., et al. (2017b). Mapping the kinetic Sunyaev-Zel'dovich effect toward MACS J0717.5+3745 with NIKA. *A&A*, 598:A115.

Adam, R., Comis, B., Bartalucci, I., et al. (2016). High angular resolution Sunyaev-Zel'dovich observations of MACS J1423.8+2404 with NIKA: Multiwavelength analysis. *A&A*, 586:A122.

Adam, R., Comis, B., Macías-Pérez, J. F., et al. (2015). Pressure distribution of the high-redshift cluster of galaxies CL J1226.9+3332 with NIKA. *A&A*, 576:A12.

Adam, R., Comis, B., Macías-Pérez, J. F., et al. (2014). First observation of the thermal Sunyaev-Zel'dovich effect with kinetic inductance detectors. *A&A*, 569:A66.

Adam, R., Goksu, H., Brown, S., Rudnick, L., and Ferrari, C. (2021). γ-ray detection toward the Coma cluster with Fermi-LAT: Implications for the cosmic ray content in the hadronic scenario. *A&A*, 648:A60.

Adam, R., Goksu, H., Leingärtner-Goth, A., et al. (2020). MINOT: Modeling the intracluster medium (non-)thermal content and observable prediction tools. *A&A*, 644:A70.

Adam, R., Hahn, O., Ruppin, F., et al. (2018b). Substructure and merger detection in resolved NIKA Sunyaev-Zel'dovich images of distant clusters. *A&A*, 614:A118.

Aghanim, N., Douspis, M., Hurier, G., et al. (2019). PACT. I. Combining ACT and Planck data for improved extraction of tSZ signal. *A&A*, 632:A47.

Aharonian, F., Akhperjanian, A. G., Anton, G., et al. (2009). Constraints on the multi-TeV particle population in the Coma galaxy cluster with HESS observations. *A&A*, 502(2):437–443.

Aharonian, F. A., Kelner, S. R., and Prosekin, A. Y. (2010). Angular, spectral, and time distributions of highest energy protons and associated secondary gamma rays and neutrinos propagating through extragalactic magnetic and radiation fields. *Phys. Rev. D*, 82(4):043002.

Ahnen, M. L., Ansoldi, S., Antonelli, L. A., et al. (2016). Deep observation of the NGC 1275 region with MAGIC: search of diffuse γ-ray emission from cosmic rays in the Perseus cluster. *A&A*, 589:A33.

Akamatsu, H., Mizuno, M., Ota, N., et al. (2017). Suzaku observations of the merging galaxy cluster Abell 2255: The northeast radio relic. *A&A*, 600:A100.

Akino, D., Eckert, D., Okabe, N., et al. (2022). HSC-XXL: Baryon budget of the 136 XXL groups and clusters. *PASJ*, 74(1):175–208.

Alam, S., Ata, M., Bailey, S., et al. (2017). The clustering of galaxies in the completed SDSS-III Baryon Oscillation Spectroscopic Survey: cosmological analysis of the DR12 galaxy sample. *MNRAS*, 470(3):2617–2652.

Aleksić, J., Alvarez, E. A., Antonelli, L. A., et al. (2012). Constraining cosmic rays and magnetic fields in the Perseus galaxy cluster with TeV observations by the MAGIC telescopes. *A&A*, 541:A99.

Aleksić, J., Antonelli, L. A., Antoranz, P., et al. (2010). MAGIC Gamma-ray Telescope Observation of the Perseus Cluster of Galaxies: Implications for Cosmic Rays, Dark Matter, and NGC 1275. *ApJ*, 710(1):634–647.

Allen, S. W., Evrard, A. E., and Mantz, A. B. (2011). Cosmological Parameters from Observations of Galaxy Clusters. *ARA&A*, 49(1):409–470.

AMI Consortium, Rodríguez-Gonzálvez, C., Shimwell, T. W., et al. (2012). Detailed Sunyaev-Zel'dovich study with AMI of 19 LoCuSS galaxy clusters: masses and temperatures out to the virial radius. *MNRAS*, 425(1):162–203.

Anbajagane, D., Chang, C., Jain, B., et al. (2022). Shocks in the stacked Sunyaev-Zel'dovich profiles of clusters II: Measurements from SPT-SZ + Planck Compton-y map. *MNRAS*, 514(2):1645–1663.

Anderson, M. E., Gaspari, M., White, S. D. M., Wang, W., and Dai, X. (2015). Unifying X-ray scaling relations from galaxies to clusters. *MNRAS*, 449(4):3806–3826.

Andreon, S., Romero, C., Castagna, F., et al. (2021). Thermodynamic evolution of the z = 1.75 galaxy cluster IDCS J1426.5+3508. *MNRAS*, 505(4):5896–5909.

Ansarifard, S., Rasia, E., Biffi, V., et al. (2020). The Three Hundred Project: Correcting for the hydrostatic-equilibrium mass bias in X-ray and SZ surveys. *A&A*, 634:A113.

Arlen, T., Aune, T., Beilicke, M., et al. (2012). Constraints on Cosmic Rays, Magnetic Fields, and Dark Matter from Gamma-Ray Observations of the Coma Cluster of Galaxies with VERITAS and Fermi. *ApJ*, 757(2):123.

Arnaud, K. A. (1996). *XSPEC: The First Ten Years*, volume 101 of *Astronomical Society of the Pacific Conference Series*, page 17.

Arnaud, M., Pratt, G. W., Piffaretti, R., et al. (2010). The universal galaxy cluster pressure profile from a representative sample of nearby systems (REXCESS) and the Y_{SZ} - M_{500} relation. *A&A*, 517:A92.

Artis, E., Adam, R., Ade, P., et al. (2022). PSZ2 G091: A massive double cluster at z 0.822 observed by the NIKA2 camera. In *European Physical Journal Web of Conferences*, volume 257 of *European Physical Journal Web of Conferences*, page 00003.

Ata, M., Baumgarten, F., Bautista, J., et al. (2018). The clustering of the SDSS-IV extended Baryon Oscillation Spectroscopic Survey DR14 quasar sample: first measurement of baryon acoustic oscillations between redshift 0.8 and 2.2. *MNRAS*, 473(4):4773–4794.

Babyk, I. V., McNamara, B. R., Nulsen, P. E. J., et al. (2018). A Universal Entropy Profile for the Hot Atmospheres of Galaxies and Clusters within R $_{2500}$. *ApJ*, 862(1):39.

Bagchi, J., Enßlin, T. A., Miniati, F., et al. (2002). Evidence for shock acceleration and intergalactic magnetic fields in a large-scale filament of galaxies ZwCl 2341.1+0000. *New Astr.*, 7(5):249–277.

Bahar, Y. E., Bulbul, E., Clerc, N., et al. (2022). The eROSITA Final Equatorial-Depth Survey (eFEDS). X-ray properties and scaling relations of galaxy clusters and groups. *A&A*, 661:A7.

Baldwin, J. E. and Elsmore, B. (1954). Radio Emission from the Perseus Cluster. *Nature*, 173(4409):818.

Ballet, J., Burnett, T. H., Digel, S. W., and Lott, B. (2020). Fermi Large Area Telescope Fourth Source Catalog Data Release 2. *arXiv e-prints*, page arXiv:2005.11208.

Bartalucci, I., Arnaud, M., Pratt, G. W., Démoclès, J., and Lovisari, L. (2019). The Most Massive galaxy Clusters (M2C) across cosmic time: link between radial total mass distribution and dynamical state. *A&A*, 628:A86.

Bartalucci, I., Arnaud, M., Pratt, G. W., et al. (2017). Resolving galaxy cluster gas properties at z 1 with XMM-Newton and Chandra. *A&A*, 598:A61.

Basu, K. (2012). A Sunyaev-Zel'dovich take on cluster radio haloes - I. Global scaling and bi-modality using Planck data. *MNRAS*, 421(1):L112–L116.

Basu, K., Sommer, M., Erler, J., et al. (2016). ALMA-SZ Detection of a Galaxy Cluster Merger Shock at Half the Age of the Universe. *ApJ*, 829(2):L23.

Bennett, J. S. and Sijacki, D. (2020). Resolving shocks and filaments in galaxy formation simulations: effects on gas properties and star formation in the circumgalactic medium. *MNRAS*, 499(1):597–615.

Bertone, S., Vogt, C., and Enßlin, T. (2006). Magnetic field seeding by galactic winds. *MNRAS*, 370(1):319–330.

Bertschinger, E. (1985). Self-similar secondary infall and accretion in an Einstein-de Sitter universe. *ApJS*, 58:39–65.

Béthermin, M., Daddi, E., Magdis, G., et al. (2012). A Unified Empirical Model for Infrared Galaxy Counts Based on the Observed Physical Evolution of Distant Galaxies. *ApJ*, 757:L23.

Betoule, M., Kessler, R., Guy, J., et al. (2014). Improved cosmological constraints from a joint analysis of the SDSS-II and SNLS supernova samples. *A&A*, 568:A22.

Bhattacharya, S. and Kosowsky, A. (2007). Cosmological Constraints from Galaxy Cluster Velocity Statistics. *ApJ*, 659(2):L83–L86.

Biffi, V., Borgani, S., Murante, G., et al. (2016). On the Nature of Hydrostatic Equilibrium in Galaxy Clusters. *ApJ*, 827(2):112.

Biffi, V., Mernier, F., and Medvedev, P. (2018). Enrichment of the Hot Intracluster Medium: Numerical Simulations. *Space Sci. Rev.*, 214(8):123.

Birkinshaw, M. (1999). The Sunyaev-Zel'dovich effect. *Phys. Rep.*, 310(2-3):97–195.

Birkinshaw, M., Gull, S. F., and Hardebeck, H. (1984). The Sunyaev-Zeldovich effect towards three clusters of galaxies. *Nature*, 309:34–35.

Blasi, P. and Colafrancesco, S. (1999). Cosmic rays, radio halos and nonthermal X-ray emission in clusters of galaxies. *Astroparticle Physics*, 12(3):169–183.

Blasi, P., Gabici, S., and Brunetti, G. (2007). Gamma Rays from Clusters of Galaxies. *International Journal of Modern Physics A*, 22(4):681–706.

Bleem, L. E., Stalder, B., de Haan, T., et al. (2015). Galaxy Clusters Discovered via the Sunyaev-Zel'dovich Effect in the 2500-Square-Degree SPT-SZ Survey. *ApJS*, 216(2):27.

Blumenthal, G. R. and Gould, R. J. (1970). Bremsstrahlung, Synchrotron Radiation, and Compton Scattering of High-Energy Electrons Traversing Dilute Gases. *Reviews of Modern Physics*, 42(2):237–271.

Bocquet, S., Saro, A., Dolag, K., and Mohr, J. J. (2016). Halo mass function: baryon impact, fitting formulae, and implications for cluster cosmology. *MNRAS*, 456(3):2361–2373.

Bocquet, S., Saro, A., Mohr, J. J., et al. (2015). Mass Calibration and Cosmological Analysis of the SPT-SZ Galaxy Cluster Sample Using Velocity Dispersion σ_v and X-Ray Y $_X$ Measurements. *ApJ*, 799(2):214.

Böhringer, H. and Werner, N. (2010). X-ray spectroscopy of galaxy clusters: studying astrophysical processes in the largest celestial laboratories. *A&A Rev.*, 18(1-2):127–196.

Bonafede, A., Feretti, L., Murgia, M., et al. (2010). The Coma cluster magnetic field from Faraday rotation measures. *A&A*, 513:A30.

Bonafede, A., Intema, H. T., Bruggen, M., et al. (2014). A giant radio halo in the cool core cluster CL1821+643. *MNRAS*, 444:L44–L48.

Bonafede, A., Vazza, F., Brüggen, M., et al. (2015). Unravelling the origin of large-scale magnetic fields in galaxy clusters and beyond through Faraday Rotation Measures with the SKA. In *Advancing Astrophysics with the Square Kilometre Array (AASKA14)*, page 95.

Bonafede, A., Vazza, F., Brüggen, M., et al. (2013). Measurements and simulation of Faraday rotation across the Coma radio relic. *MNRAS*, 433(4):3208–3226.

Bonamente, M., Joy, M. K., LaRoque, S. J., et al. (2006). Determination of the Cosmic Distance Scale from Sunyaev-Zel'dovich Effect and Chandra X-Ray Measurements of High-Redshift Galaxy Clusters. *ApJ*, 647(1):25–54.

Borgani, S. and Kravtsov, A. (2011). Cosmological Simulations of Galaxy Clusters. *Advanced Science Letters*, 4(2):204–227.

Botteon, A., Brunetti, G., van Weeren, R. J., et al. (2020). The Beautiful Mess in Abell 2255. *ApJ*, 897(1):93.

Botteon, A., Gastaldello, F., and Brunetti, G. (2018). Shocks and cold fronts in merging and massive galaxy clusters: new detections with Chandra. *MNRAS*, 476(4):5591–5620.

Botteon, A., Shimwell, T. W., Cassano, R., et al. (2022). The Planck clusters in the LOFAR sky. I. LoTSS-DR2: New detections and sample overview. *A&A*, 660:A78.

Briel, U. G., Henry, J. P., and Boehringer, H. (1992). Observation of the Coma cluster of galaxies with ROSAT during the all-sky-survey. *A&A*, 259:L31–L34.

Brown, M., Bacon, D., Camera, S., et al. (2015). Weak gravitational lensing with the Square Kilometre Array. In *Advancing Astrophysics with the Square Kilometre Array (AASKA14)*, page 23.

Brunetti, G. and Blasi, P. (2005). Alfvénic reacceleration of relativistic particles in galaxy clusters in the presence of secondary electrons and positrons. *MNRAS*, 363(4):1173–1187.

Brunetti, G. and Jones, T. W. (2014). Cosmic Rays in Galaxy Clusters and Their Nonthermal Emission. *International Journal of Modern Physics D*, 23(4):1430007–98.

Brunetti, G. and Lazarian, A. (2007). Compressible turbulence in galaxy clusters: physics and stochastic particle re-acceleration. *MNRAS*, 378(1):245–275.

Brunetti, G. and Lazarian, A. (2011). Acceleration of primary and secondary particles in galaxy clusters by compressible MHD turbulence: from radio haloes to gamma-rays. *MNRAS*, 410(1):127–142.

Brunetti, G., Setti, G., Feretti, L., and Giovannini, G. (2001). Particle reacceleration in the Coma cluster: radio properties and hard X-ray emission. *MNRAS*, 320(3):365–378.

Brunetti, G., Zimmer, S., and Zandanel, F. (2017). Relativistic protons in the Coma galaxy cluster: first gamma-ray constraints ever on turbulent reacceleration. *MNRAS*, 472(2):1506–1525.

Bruno, L., Rajpurohit, K., Brunetti, G., et al. (2021). The LOFAR and JVLA view of the distant steep spectrum radio halo in MACS J1149.5+2223. *A&A*, 650:A44.

Bulbul, E., Markevitch, M., Foster, A., et al. (2014). Detection of an Unidentified Emission Line in the Stacked X-Ray Spectrum of Galaxy Clusters. *ApJ*, 789(1):13.

Bulbul, G. E., Hasler, N., Bonamente, M., et al. (2011). The effect of helium sedimentation on galaxy cluster masses and scaling relations. *A&A*, 533:A6.

Buote, D. A. (2001). On the Origin of Radio Halos in Galaxy Clusters. *ApJ*, 553(1):L15–L18.

Burbidge, G. R. (1958). Possible Sources of Radio Emission in Clusters of Galaxies. *ApJ*, 128:1.

Burn, B. J. (1966). On the depolarization of discrete radio sources by Faraday dispersion. *MNRAS*, 133:67.

Bykov, A. M., Kaastra, J. S., Brüggen, M., et al. (2019). Editorial to the topical collection on clusters of galaxies: Physics and cosmology. *Space Science Reviews*, 215(3):27.

Bykov, A. M., Vazza, F., Kropotina, J. A., Levenfish, K. P., and Paerels, F. B. S. (2019). Shocks and Non-thermal Particles in Clusters of Galaxies. *Space Sci. Rev.*, 215(1):14.

Byrd, G. and Valtonen, M. (1990). Tidal Generation of Active Spirals and S0 Galaxies by Rich Clusters. *ApJ*, 350:89.

Cadena, S. H. (2017). Searching dark matter signatures from the Virgo cluster with HAWC. In *6th International Symposium on High Energy Gamma-Ray Astronomy*, volume 1792 of *American Institute of Physics Conference Series*, page 060010.

Cao, Z., della Volpe, D., Liu, S., et al. (2019). The Large High Altitude Air Shower Observatory (LHAASO) Science Book (2021 Edition). *arXiv e-prints*, page arXiv:1905.02773.

Casey, C. M., Cooray, A., Capak, P., et al. (2015). A Massive, Distant Proto-cluster at z = 2.47 Caught in a Phase of Rapid Formation? *ApJ*, 808(2):L33.

Cassano, R., Bernardi, G., Brunetti, G., et al. (2015). Cluster Radio Halos at the crossroads between astrophysics and cosmology in the SKA era. In *Advancing Astrophysics with the Square Kilometre Array (AASKA14)*, page 73.

Cassano, R., Ettori, S., Giacintucci, S., et al. (2010). On the Connection Between Giant Radio Halos and Cluster Mergers. *ApJ*, 721(2):L82–L85.

Castagna, F. and Andreon, S. (2019). PreProFit: Pressure Profile Fitter for galaxy clusters. *A&A*, 632:A22.

Castagna, F. and Andreon, S. (2020). JoXSZ: Joint X-SZ fitting code for galaxy clusters. *A&A*, 639:A73.

Catalano, A., Calvo, M., Ponthieu, N., et al. (2014). Performance and calibration of the NIKA camera at the IRAM 30 m telescope. *A&A*, 569:A9.

Cataneo, M. and Rapetti, D. (2018). Tests of gravity with galaxy clusters. *International Journal of Modern Physics D*, 27(15):1848006–936.

Cavagnolo, K. W., Donahue, M., Voit, G. M., and Sun, M. (2009). Intracluster Medium Entropy Profiles for a Chandra Archival Sample of Galaxy Clusters. *ApJS*, 182(1):12–32.

Cherenkov Telescope Array Consortium, Acharya, B. S., Agudo, I., et al. (2019). *Science with the Cherenkov Telescope Array*.

Chisari, N. E., Richardson, M. L. A., Devriendt, J., et al. (2018). The impact of baryons on the matter power spectrum from the Horizon-AGN cosmological hydrodynamical simulation. *MNRAS*, 480(3):3962–3977.

Chiu, I., Mohr, J. J., McDonald, M., et al. (2018). Baryon content in a sample of 91 galaxy clusters selected by the South Pole Telescope at 0.2 <z < 1.25. *MNRAS*, 478(3):3072–3099.

Chiu, I. N., Ghirardini, V., Liu, A., et al. (2022). The eROSITA Final Equatorial-Depth Survey (eFEDS). X-ray observable-to-mass-and-redshift relations of galaxy clusters and groups with weak-lensing mass calibration from the Hyper Suprime-Cam Subaru Strategic Program survey. *A&A*, 661:A11.

Churazov, E., Forman, W., Jones, C., and Böhringer, H. (2003). XMM-Newton Observations of the Perseus Cluster. I. The Temperature and Surface Brightness Structure. *ApJ*, 590(1):225–237.

Churazov, E., Forman, W., Jones, C., Sunyaev, R., and Böhringer, H. (2004). XMM-Newton observations of the Perseus cluster - II. Evidence for gas motions in the core. *MNRAS*, 347(1):29–35.

Churazov, E., Vikhlinin, A., Zhuravleva, I., et al. (2012). X-ray surface brightness and gas density fluctuations in the Coma cluster. *MNRAS*, 421(2):1123–1135.

Clowe, D., Bradač, M., Gonzalez, A. H., et al. (2006). A Direct Empirical Proof of the Existence of Dark Matter. *ApJ*, 648(2):L109–L113.

Combet, C., Maurin, D., Nezri, E., et al. (2012). Decaying dark matter: Stacking analysis of galaxy clusters to improve on current limits. *Phys. Rev. D*, 85(6):063517.

Concerto Collaboration, Ade, P., Aravena, M., et al. (2020). A wide field-of-view low-resolution spectrometer at APEX: Instrument design and scientific forecast. *A&A*, 642:A60.

Cooray, A. R., Grego, L., Holzapfel, W. L., Joy, M., and Carlstrom, J. E. (1998). Radio Sources in Galaxy Clusters at 28.5 GHz. *AJ*, 115(4):1388–1399.

Cowie, L. L. and McKee, C. F. (1977). The evaporation of spherical clouds in a hot gas. I. Classical and saturated mass loss rates. *ApJ*, 211:135–146.

Croston, J. H., Pratt, G. W., Böhringer, H., et al. (2008). Galaxy-cluster gas-density distributions of the representative XMM-Newton cluster structure survey (REXCESS). *A&A*, 487(2):431–443.

CTA collaboration (forthcoming). Prospect for γ-ray observations of the Perseus galaxy cluster with CTA.

Czakon, N. G., Sayers, J., Mantz, A., et al. (2015). Galaxy Cluster Scaling Relations between Bolocam Sunyaev-Zel'dovich Effect and Chandra X-Ray Measurements. *ApJ*, 806(1):18.

de Graaff, A., Cai, Y.-C., Heymans, C., and Peacock, J. A. (2019). Probing the missing baryons with the Sunyaev-Zel'dovich effect from filaments. *A&A*, 624:A48.

de Haan, T., Benson, B. A., Bleem, L. E., et al. (2016). Cosmological Constraints from Galaxy Clusters in the 2500 Square-degree SPT-SZ Survey. *ApJ*, 832(1):95.

Dennison, B. (1980). Formation of radio halos in clusters of galaxies from cosmic-ray protons. *ApJ*, 239:L93–L96.

Di Gennaro, G., van Weeren, R. J., Brunetti, G., et al. (2021). Fast magnetic field amplification in distant galaxy clusters. *Nature Astronomy*, 5:268–275.

Di Mascolo, L., Mroczkowski, T., Churazov, E., et al. (2019). An ALMA+ACA measurement of the shock in the Bullet Cluster. *A&A*, 628:A100.

Dicker, S. R., Ade, P. A. R., Aguirre, J., et al. (2014). MUSTANG2: a large focal plan array for the 100 meter Green Bank Telescope. In Holland, W. S. and Zmuidzinas, J., editors, *Millimeter, Submillimeter, and Far-Infrared Detectors and Instrumentation for Astronomy VII*, volume 9153 of *Society of Photo-Optical Instrumentation Engineers (SPIE) Conference Series*, page 91530J.

Dicker, S. R., Battistelli, E. S., Bhandarkar, T., et al. (2021). Observations of compact sources in galaxy clusters using MUSTANG2. *MNRAS*, 508(2):2600–2612.

Dicker, S. R., Romero, C. E., Di Mascolo, L., et al. (2020). The Massive and Distant Clusters of WISE Survey. X. Initial Results from a Sunyaev-Zeldovich Effect Study of Massive Galaxy Clusters at z > 1 Using MUSTANG2 on the GBT. *ApJ*, 902(2):144.

Dietrich, J. P., Bocquet, S., Schrabback, T., et al. (2019). Sunyaev-Zel'dovich effect and X-ray scaling relations from weak lensing mass calibration of 32 South Pole Telescope selected galaxy clusters. *MNRAS*, 483(3):2871–2906.

Dolag, K., Borgani, S., Murante, G., and Springel, V. (2009). Substructures in hydrodynamical cluster simulations. *MNRAS*, 399(2):497–514.

Dolag, K. and Enßlin, T. A. (2000). Radio halos of galaxy clusters from hadronic secondary electron injection in realistic magnetic field configurations. *A&A*, 362:151–157.

Domainko, W., Mair, M., Kapferer, W., et al. (2006). Enrichment of the ICM of galaxy clusters due to ram-pressure stripping. *A&A*, 452(3):795–802.

Donahue, M., Horner, D. J., Cavagnolo, K. W., and Voit, G. M. (2006). Entropy Profiles in the Cores of Cooling Flow Clusters of Galaxies. *ApJ*, 643(2):730–750.

Donnert, J., Dolag, K., Lesch, H., and Müller, E. (2009). Cluster magnetic fields from galactic outflows. *MNRAS*, 392(3):1008–1021.

Donnert, J., Vazza, F., Brüggen, M., and ZuHone, J. (2018). Magnetic Field Amplification in Galaxy Clusters and Its Simulation. *Space Sci. Rev.*, 214(8):122.

Dwek, E. and Krennrich, F. (2013). The extragalactic background light and the gamma-ray opacity of the universe. *Astroparticle Physics*, 43:112–133.

Eckert, D., Ettori, S., Pointecouteau, E., et al. (2017a). The XMM cluster outskirts project (X-COP). *Astronomische Nachrichten*, 338(293):293–298.

Eckert, D., Gaspari, M., Gastaldello, F., Le Brun, A. M. C., and O'Sullivan, E. (2021). Feedback from Active Galactic Nuclei in Galaxy Groups. *Universe*, 7(5):142.

Eckert, D., Gaspari, M., Owers, M. S., et al. (2017b). Deep Chandra observations of the stripped galaxy group falling into Abell 2142. *A&A*, 605:A25.

Eckert, D., Gaspari, M., Vazza, F., et al. (2017c). On the Connection between Turbulent Motions and Particle Acceleration in Galaxy Clusters. *ApJ*, 843(2):L29.

Eckert, D., Ghirardini, V., Ettori, S., et al. (2019). Non-thermal pressure support in X-COP galaxy clusters. *A&A*, 621:A40.

Eckert, D., Jauzac, M., Shan, H., et al. (2015a). Warm-hot baryons comprise 5-10 per cent of filaments in the cosmic web. *Nature*, 528(7580):105–107.

Eckert, D., Roncarelli, M., Ettori, S., et al. (2015b). Gas clumping in galaxy clusters. *MNRAS*, 447(3):2198–2208.

Edge, A. C. and Stewart, G. C. (1991). EXOSAT observations of clusters of galaxies - I. The X-ray data. *MNRAS*, 252:414.

Efstathiou, G., Frenk, C. S., White, S. D. M., and Davis, M. (1988). Gravitational clustering from scale-free initial conditions. *MNRAS*, 235:715–748.

Egami, E., Rex, M., Rawle, T. D., et al. (2010). The Herschel Lensing Survey (HLS): Overview. *A&A*, 518:L12.

Enßlin, T., Pfrommer, C., Miniati, F., and Subramanian, K. (2011). Cosmic ray transport in galaxy clusters: implications for radio halos, gamma-ray signatures, and cool core heating. *A&A*, 527:A99.

Ensslin, T. A., Biermann, P. L., Klein, U., and Kohle, S. (1998). Cluster radio relics as a tracer of shock waves of the large-scale structure formation. *A&A*, 332:395–409.

Erler, J., Basu, K., Trasatti, M., Klein, U., and Bertoldi, F. (2015). Evidence for a pressure discontinuity at the position of the Coma relic from Planck Sunyaev-Zel'dovich effect data. *MNRAS*, 447(3):2497–2502.

Ettori, S. and Fabian, A. C. (2006). Effects of sedimented helium on the X-ray properties of galaxy clusters. *MNRAS*, 369(1):L42–L46.

Ettori, S., Fabian, A. C., and White, D. A. (1998). ROSATPSPC observations of the outer regions of the Perseus cluster of galaxies. *MNRAS*, 300(3):837–856.

Euclid Collaboration, Adam, R., Vannier, M., et al. (2019). Euclid preparation. III. Galaxy cluster detection in the wide photometric survey, performance and algorithm selection. *A&A*, 627:A23.

Fabian, A. C. (2012). Observational Evidence of Active Galactic Nuclei Feedback. *ARA&A*, 50:455–489.

Fabian, A. C., Sanders, J. S., Allen, S. W., et al. (2011). A wide Chandra view of the core of the Perseus cluster. *MNRAS*, 418(4):2154–2164.

Fabian, A. C., Sanders, J. S., Allen, S. W., et al. (2003). A deep Chandra observation of the Perseus cluster: shocks and ripples. *MNRAS*, 344:L43–L47.

Feretti, L., Fusco-Femiano, R., Giovannini, G., and Govoni, F. (2001). The giant radio halo in Abell 2163. *A&A*, 373:106–112.

Feretti, L., Giovannini, G., Govoni, F., and Murgia, M. (2012). Clusters of galaxies: observational properties of the diffuse radio emission. *A&A Rev.*, 20:54.

Ferragamo, A., Macías-Pérez, J. F., Pelgrims, V., et al. (2022). Comparison of hydrostatic and lensing cluster mass estimates: A pilot study in MACS J0647.7+7015. *A&A*, 661:A65.

Ferrari, C., Benoist, C., Maurogordato, S., Cappi, A., and Slezak, E. (2005). Dynamical state and star formation properties of the merging galaxy cluster Abell 3921. *A&A*, 430:19–38.

Ferrari, C., Dabbech, A., Smirnov, O., et al. (2015). Non-thermal emission from galaxy clusters: feasibility study with SKA. In *Advancing Astrophysics with the Square Kilometre Array (AASKA14)*, page 75.

Ferrari, C., Govoni, F., Schindler, S., Bykov, A. M., and Rephaeli, Y. (2008). Observations of Extended Radio Emission in Clusters. *Space Sci. Rev.*, 134(1-4):93–118.

Ferrari, C., Intema, H. T., Orrù, E., et al. (2011). Discovery of the correspondence between intra-cluster radio emission and a high pressure region detected through the Sunyaev-Zel'dovich effect. *A&A*, 534:L12.

Fillmore, J. A. and Goldreich, P. (1984). Self-similar gravitational collapse in an expanding universe. *ApJ*, 281:1–8.

Finoguenov, A., Ruszkowski, M., Jones, C., et al. (2008). In-Depth Chandra Study of the AGN Feedback in Virgo Elliptical Galaxy M84. *ApJ*, 686(2):911–917.

Foreman-Mackey, D., Hogg, D. W., Lang, D., and Goodman, J. (2013). emcee: The MCMC Hammer. *PASP*, 125(925):306.

Fujita, Y. and Ohira, Y. (2012). Non-thermal Emissions from Cool Cores Heated by Cosmic Rays in Galaxy Clusters. *ApJ*, 746(1):53.

Gal, R. R. (2006). Optical Detection of Galaxy Clusters. *arXiv e-prints*, pages astro–ph/0601195.

Garon, A. F., Rudnick, L., Wong, O. I., et al. (2019). Radio Galaxy Zoo: The Distortion of Radio Galaxies by Galaxy Clusters. *AJ*, 157(3):126.

Gaskin, J. A., Swartz, D. A., Vikhlinin, A., et al. (2019). Lynx X-Ray Observatory: an overview. *Journal of Astronomical Telescopes, Instruments, and Systems*, 5:021001.

Gatuzz, E., Sanders, J. S., Dennerl, K., et al. (2022). Measuring sloshing, merging, and feedback velocities in the Virgo cluster. *MNRAS*, 511(3):4511–4527.

Gendron-Marsolais, M., Hlavacek-Larrondo, J., van Weeren, R. J., et al. (2017). Deep 230-470 MHz VLA observations of the mini-halo in the Perseus cluster. *MNRAS*, 469(4):3872–3880.

Ghirardini, V., Bulbul, E., Kraft, R., et al. (2021). Evolution of the Thermodynamic Properties of Clusters of Galaxies out to Redshift of 1.8. *ApJ*, 910(1):14.

Ghirardini, V., Eckert, D., Ettori, S., et al. (2019a). Universal thermodynamic properties of the intracluster medium over two decades in radius in the X-COP sample. *A&A*, 621:A41.

Ghirardini, V., Ettori, S., Eckert, D., and Molendi, S. (2019b). Polytropic state of the intracluster medium in the X-COP cluster sample. *A&A*, 627:A19.

Giacintucci, S., Markevitch, M., Cassano, R., et al. (2017). Occurrence of Radio Minihalos in a Mass-limited Sample of Galaxy Clusters. *ApJ*, 841(2):71.

Giodini, S., Lovisari, L., Pointecouteau, E., et al. (2013). Scaling Relations for Galaxy Clusters: Properties and Evolution. *Space Sci. Rev.*, 177(1-4):247–282.

Giovannini, G., Bonafede, A., Brown, S., et al. (2015). Mega-parsec scale magnetic fields in low density regions in the SKA era: filaments connecting galaxy clusters and groups. In *Advancing Astrophysics with the Square Kilometre Array (AASKA14)*, page 104.

Giovannini, G., Tordi, M., and Feretti, L. (1999). Radio halo and relic candidates from the NRAO VLA Sky Survey. *New Astr.*, 4(2):141–155.

Gitti, M., Brunetti, G., and Setti, G. (2002). Modeling the interaction between ICM and relativistic plasma in cooling flows: The case of the Perseus cluster. *A&A*, 386:456–463.

Gitti, M., Tozzi, P., Brunetti, G., et al. (2015). The SKA view of cool-core clusters: evolution of radio mini-halos and AGN feedback. In *Advancing Astrophysics with the Square Kilometre Array (AASKA14)*, page 76.

Gobat, R., Daddi, E., Coogan, R. T., et al. (2019). Sunyaev-Zel'dovich detection of the galaxy cluster Cl J1449+0856 at z = 1.99: The pressure profile in uv space. *A&A*, 629:A104.

Gonzalez, A. H., Gettings, D. P., Brodwin, M., et al. (2019). The Massive and Distant Clusters of WISE Survey. I. Survey Overview and a Catalog of >2000 Galaxy Clusters at $z \simeq 1$. *ApJS*, 240(2):33.

Gould, R. J. (1972). Energy loss of fast electrons and positrons in a plasma. *Physica*, 60(1):145–154.

Govoni, F., Enßlin, T. A., Feretti, L., and Giovannini, G. (2001). A comparison of radio and X-ray morphologies of four clusters of galaxies containing radio halos. *A&A*, 369:441–449.

Govoni, F., Murgia, M., Vacca, V., et al. (2017). Sardinia Radio Telescope observations of Abell 194. The intra-cluster magnetic field power spectrum. *A&A*, 603:A122.

Govoni, F., Murgia, M., Xu, H., et al. (2015). Cluster magnetic fields through the study of polarized radio halos in the SKA era. In *Advancing Astrophysics with the Square Kilometre Array (AASKA14)*, page 105.

Govoni, F., Orrù, E., Bonafede, A., et al. (2019). A radio ridge connecting two galaxy clusters in a filament of the cosmic web. *Science*, 364(6444):981–984.

Grainge, K., Borgani, S., Colafrancesco, S., et al. (2015). The SKA and Galaxy Cluster Science with the Sunyaev-Zel'dovich Effect. In *Advancing Astrophysics with the Square Kilometre Array (AASKA14)*, page 170.

Gunn, J. E. and Gott, J. Richard, I. (1972). On the Infall of Matter Into Clusters of Galaxies and Some Effects on Their Evolution. *ApJ*, 176:1.

Guo, F. and Oh, S. P. (2008). Feedback heating by cosmic rays in clusters of galaxies. *MNRAS*, 384(1):251–266.

Gupta, N., Saro, A., Mohr, J. J., Dolag, K., and Liu, J. (2017). SZE observables, pressure profiles and centre offsets in Magneticum simulation galaxy clusters. *MNRAS*, 469(3):3069–3087.

Hahn, O., Martizzi, D., Wu, H.-Y., et al. (2017). rhapsody-g simulations - I. The cool cores, hot gas and stellar content of massive galaxy clusters. *MNRAS*, 470:166–186.

Hamana, T., Shirasaki, M., Miyazaki, S., et al. (2020). Cosmological constraints from cosmic shear two-point correlation functions with HSC survey first-year data. *PASJ*, 72(1):16.

Hand, N., Addison, G. E., Aubourg, E., et al. (2012). Evidence of Galaxy Cluster Motions with the Kinematic Sunyaev-Zel'dovich Effect. *Phys. Rev. Lett.*, 109(4):041101.

Hasselfield, M., Hilton, M., Marriage, T. A., et al. (2013). The Atacama Cosmology Telescope: Sunyaev-Zel'dovich selected galaxy clusters at 148 GHz from three seasons of data. *JCAP*, 2013(7):008.

Henry, J. P. and Arnaud, K. A. (1991). A Measurement of the Mass Fluctuation Spectrum from the Cluster X-Ray Temperature Function. *ApJ*, 372:410.

HESS Collaboration, Abramowski, A., Acero, F., et al. (2012). Constraints on the gamma-ray emission from the cluster-scale AGN outburst in the Hydra A galaxy cluster. *A&A*, 545:A103.

Hilton, M., Sifón, C., Naess, S., et al. (2021). The Atacama Cosmology Telescope: A Catalog of >4000 Sunyaev-Zel'dovich Galaxy Clusters. *ApJS*, 253(1):3.

Hincks, A. D., Radiconi, F., Romero, C., et al. (2022). A high-resolution view of the filament of gas between Abell 399 and Abell 401 from the Atacama Cosmology Telescope and MUSTANG-2. *MNRAS*, 510(3):3335–3355.

Hinshaw, G., Larson, D., Komatsu, E., et al. (2013). Nine-year Wilkinson Microwave Anisotropy Probe (WMAP) Observations: Cosmological Parameter Results. *ApJS*, 208(2):19.

Hinton, J. and SWGO Collaboration (2022). The Southern Wide-field Gamma-ray Observatory: Status and Prospects. In *37th International Cosmic Ray Conference. 12-23 July 2021. Berlin*, page 23.

Hitomi Collaboration, Aharonian, F., Akamatsu, H., et al. (2018). Atmospheric gas dynamics in the Perseus cluster observed with Hitomi. *PASJ*, 70(2):9.

Hlavacek-Larrondo, J., Li, Y., and Churazov, E. (2022). AGN Feedback in Groups and Clusters of Galaxies. *arXiv e-prints*, page arXiv:2206.00098.

Hlavacek-Larrondo, J., McDonald, M., Benson, B. A., et al. (2015). X-Ray Cavities in a Sample of 83 SPT-selected Clusters of Galaxies: Tracing the Evolution of AGN Feedback in Clusters of Galaxies out to z=1.2. *ApJ*, 805(1):35.

Hoang, D. N., Shimwell, T. W., van Weeren, R. J., et al. (2019). Radio observations of the merging galaxy cluster Abell 520. *A&A*, 622:A20.

Hoang, D. N., Shimwell, T. W., van Weeren, R. J., et al. (2018). Radio observations of the double-relic galaxy cluster Abell 1240. *MNRAS*, 478(2):2218–2233.

Hodgson, T., Johnston-Hollitt, M., McKinley, B., and Hurley-Walker, N. (2022). Searching for the synchrotron cosmic web again: A replication attempt. *PASA*, 39:e013.

Hoekstra, H., Herbonnet, R., Muzzin, A., et al. (2015). The Canadian Cluster Comparison Project: detailed study of systematics and updated weak lensing masses. *MNRAS*, 449(1):685–714.

Huber, B., Tchernin, C., Eckert, D., et al. (2013). Probing the cosmic-ray content of galaxy clusters by stacking Fermi-LAT count maps. *A&A*, 560:A64.

Huchra, J. P., Macri, L. M., Masters, K. L., et al. (2012). The 2MASS Redshift Survey—Description and Data Release. *ApJS*, 199(2):26.

Hurier, G., Adam, R., and Keshet, U. (2019). First detection of a virial shock with SZ data: implication for the mass accretion rate of Abell 2319. *A&A*, 622:A136.

Hurier, G., Aghanim, N., Douspis, M., and Pointecouteau, E. (2014). Measurement of the T_{CMB} evolution from the Sunyaev-Zel'dovich effect. *A&A*, 561:A143.

IPBES (2019). Global assessment report on biodiversity and ecosystem services of the Intergovernmental Science-Policy Platform on Biodiversity and Ecosystem Services.

IPCC (2022a). Climate change 2021: The physical science basis. contribution of working group i to the sixth assessment report of the intergovernmental panel on climate change.

IPCC (2022b). Climate change 2022: Impacts, adaptation, and vulnerability. contribution of working group ii to the sixth assessment report of the intergovernmental panel on climate change.

Iqbal, A., Majumdar, S., Nath, B. B., et al. (2017). Little evidence for entropy and energy excess beyond r_{500} - an end to ICM pre-heating? *MNRAS*, 465(1):L99–L103.

Itoh, N. and Nozawa, S. (2003). Relativistic Corrections to the Sunyaev-Zeldovich Effect for Clusters of Galaxies. V. Numerical Results for High Electron Temperatures. *ArXiv Astrophysics e-prints*.

Johnson, A. R., Rudnick, L., Jones, T. W., Mendygral, P. J., and Dolag, K. (2020). Characterizing the Uncertainty in Cluster Magnetic Fields Derived from Rotation Measures. *ApJ*, 888(2):101.

Johnston-Hollitt, M., Govoni, F., Beck, R., et al. (2015). Using SKA Rotation Measures to Reveal the Mysteries of the Magnetised Universe. In *Advancing Astrophysics with the Square Kilometre Array (AASKA14)*, page 92.

Jones, C. and Forman, W. (1999). Einstein Observatory Images of Clusters of Galaxies. *ApJ*, 511(1):65–83.

Jones, C., Mandel, E., Schwarz, J., et al. (1979). The structure and evolution of X-ray clusters. *ApJ*, 234:L21–L25.

Jones, D. H., Read, M. A., Saunders, W., et al. (2009). The 6dF Galaxy Survey: final redshift release (DR3) and southern large-scale structures. *MNRAS*, 399(2):683–698.

Kafexhiu, E., Aharonian, F., Taylor, A. M., and Vila, G. S. (2014). Parametrization of gamma-ray production cross sections for p p interactions in a broad proton energy range from the kinematic threshold to PeV energies. *Phys. Rev. D*, 90(12):123014.

Kaiser, N. (1986). Evolution and clustering of rich clusters. *MNRAS*, 222:323–345.

Kaiser, N. (1987). Clustering in real space and in redshift space. *MNRAS*, 227:1–21.

Kaiser, N. (1991). Evolution of Clusters of Galaxies. *ApJ*, 383:104.

Kamae, T., Karlsson, N., Mizuno, T., Abe, T., and Koi, T. (2006). Parameterization of γ, $e^{+/-}$, and Neutrino Spectra Produced by p-p Interaction in Astronomical Environments. *ApJ*, 647(1):692–708.

Kang, H., Ryu, D., and Jones, T. W. (2012). Diffusive Shock Acceleration Simulations of Radio Relics. *ApJ*, 756(1):97.

Kelner, S. R., Aharonian, F. A., and Bugayov, V. V. (2006). Energy spectra of gamma rays, electrons, and neutrinos produced at proton-proton interactions in the very high energy regime. *Phys. Rev. D*, 74(3):034018.

Kéruzoré, F. (2021). *Cosmologie à partir des observations Sunyaev-Zeldovich d'amas de galaxies avec NIKA2*. Theses, Université Grenoble Alpes.

Kéruzoré, F., Artis, E., Macías-Pérez, J. F., et al. (2022a). Forecasting the Y_{500} - M_{500} scaling relation from the NIKA2 SZ Large Program. In *European Physical Journal Web of Conferences*, volume 257 of *European Physical Journal Web of Conferences*, page 00025.

Kéruzoré, F., Artis, E., Macías-Pérez, J. F., et al. (2022b). PANCO2: A new software to measure pressure profiles from resolved thermal SZ observations. In *European Physical Journal Web of Conferences*, volume 257 of *European Physical Journal Web of Conferences*, page 00024.

Kéruzoré, F., Mayet, F., Pratt, G. W., et al. (2020). Exploiting NIKA2/XMM-Newton imaging synergy for intermediate-mass high-z galaxy clusters within the NIKA2 SZ large program. Observations of ACT-CL J0215.4+0030 at z $\sim$ 0.9. *A&A*, 644:A93.

Khangulyan, D., Aharonian, F. A., and Kelner, S. R. (2014). Simple Analytical Approximations for Treatment of Inverse Compton Scattering of Relativistic Electrons in the Blackbody Radiation Field. *ApJ*, 783(2):100.

Khatri, R. and Gaspari, M. (2016). Thermal SZ fluctuations in the ICM: probing turbulence and thermodynamics in Coma cluster with Planck. *MNRAS*, 463(1):655–669.

Kilbinger, M., Fu, L., Heymans, C., et al. (2013). CFHTLenS: combined probe cosmological model comparison using 2D weak gravitational lensing. *MNRAS*, 430(3):2200–2220.

Kitayama, T., Ueda, S., Takakuwa, S., et al. (2016). The Sunyaev-Zel'dovich effect at 5": RX J1347.5-1145 imaged by ALMA. *PASJ*, 68(5):88.

Klaassen, P. D., Mroczkowski, T. K., Cicone, C., et al. (2020). The Atacama Large Aperture Submillimeter Telescope (AtLAST). In *Society of Photo-Optical Instrumentation Engineers (SPIE) Conference Series*, volume 11445 of *Society of Photo-Optical Instrumentation Engineers (SPIE) Conference Series*, page 114452F.

Knödlseder, J., Mayer, M., Deil, C., et al. (2016). GammaLib and ctools. A software framework for the analysis of astronomical gamma-ray data. *A&A*, 593:A1.

Köhlinger, F., Viola, M., Joachimi, B., et al. (2017). KiDS-450: the tomographic weak lensing power spectrum and constraints on cosmological parameters. *MNRAS*, 471(4):4412–4435.

Komatsu, E., Matsuo, H., Kitayama, T., et al. (2001). Substructures Revealed by the Sunyaev-Zel'dovich Effect at 150 GHz in a High-Resolution Map of RX J1347-1145. *PASJ*, 53(1):57–62.

Korngut, P. M., Dicker, S. R., Reese, E. D., et al. (2011). MUSTANG High Angular Resolution Sunyaev-Zel'dovich Effect Imaging of Substructure in Four Galaxy Clusters. *ApJ*, 734(1):10.

Kozmanyan, A., Bourdin, H., Mazzotta, P., Rasia, E., and Sereno, M. (2019). Deriving the Hubble constant using Planck and XMM-Newton observations of galaxy clusters. *A&A*, 621:A34.

Kravtsov, A. V. and Borgani, S. (2012). Formation of Galaxy Clusters. *ARA&A*, 50:353–409.

Kravtsov, A. V., Vikhlinin, A., and Nagai, D. (2006). A New Robust Low-Scatter X-Ray Mass Indicator for Clusters of Galaxies. *ApJ*, 650(1):128–136.

Kronberg, P. P., Lesch, H., and Hopp, U. (1999). Magnetization of the Intergalactic Medium by Primeval Galaxies. *ApJ*, 511(1):56–64.

Kunz, M. W., Bogdanović, T., Reynolds, C. S., and Stone, J. M. (2012). Buoyancy Instabilities in a Weakly Collisional Intracluster Medium. *ApJ*, 754(2):122.

Kunz, M. W., Jones, T. W., and Zhuravleva, I. (2022). Plasma physics of the intracluster medium. *arXiv e-prints*, page arXiv:2205.02489.

Large, M. I., Mathewson, D. S., and Haslam, C. G. T. (1959). A High-Resolution Survey of the Coma Cluster of Galaxies at 408 Mc./s. *Nature*, 183(4676):1663–1664.

Larson, R. B., Tinsley, B. M., and Caldwell, C. N. (1980). The evolution of disk galaxies and the origin of S0 galaxies. *ApJ*, 237:692–707.

Laureijs, R., Amiaux, J., Arduini, S., et al. (2011). Euclid Definition Study Report. *arXiv e-prints*, page arXiv:1110.3193.

Le Brun, A. M. C., McCarthy, I. G., Schaye, J., and Ponman, T. J. (2017). The scatter and evolution of the global hot gas properties of simulated galaxy cluster populations. *MNRAS*, 466(4):4442–4469.

Leccardi, A. and Molendi, S. (2008). Radial temperature profiles for a large sample of galaxy clusters observed with XMM-Newton. *A&A*, 486(2):359–373.

Lewis, A., Challinor, A., and Lasenby, A. (2000). Efficient Computation of Cosmic Microwave Background Anisotropies in Closed Friedmann-Robertson-Walker Models. *ApJ*, 538:473–476.

Li, T. P. and Ma, Y. Q. (1983). Analysis methods for results in gamma-ray astronomy. *ApJ*, 272:317–324.

Liddle, A. R. and Lyth, D. H. (2000). *Cosmological Inflation and Large-Scale Structure*.

Limousin, M., Morandi, A., Sereno, M., et al. (2013). The Three-Dimensional Shapes of Galaxy Clusters. *Space Sci. Rev.*, 177(1-4):155–194.

Lin, Y.-T., Partridge, B., Pober, J. C., et al. (2009). Spectral Energy Distribution of Radio Sources in Nearby Clusters of Galaxies: Implications for Sunyaev-Zel'Dovich Effect Surveys. *ApJ*, 694(2):992–1009.

Lindholm, V., Finoguenov, A., Comparat, J., et al. (2021). Clustering of CODEX clusters. *A&A*, 646:A8.

Longair, M. S. (2011). *High Energy Astrophysics*.

Lovisari, L., Ettori, S., Gaspari, M., and Giles, P. A. (2021). Scaling Properties of Galaxy Groups. *Universe*, 7(5):139.

Lovisari, L. and Maughan, B. J. (2022). Scaling relations of clusters and groups, and their evolution. *arXiv e-prints*, page arXiv:2202.07673.

Lovisari, L., Reiprich, T. H., and Schellenberger, G. (2015). Scaling properties of a complete X-ray selected galaxy group sample. *A&A*, 573:A118.

LSST Science Collaboration, Abell, P. A., Allison, J., et al. (2009). LSST Science Book, Version 2.0. *arXiv e-prints*, page arXiv:0912.0201.

Lyth, D. H. D. H. and Riotto, A. A. (1999). Particle physics models of inflation and the cosmological density perturbation. *Phys. Rep.*, 314(1-2):1–146.

Macias-Pérez, J. F., Adam, R., Ade, P., et al. (2017). NIKA2: a mm camera for cluster cosmology. In *Proceedings of the European Physical Society Conference on High Energy Physics. 5-12 July*, page 42.

Mantz, A., Allen, S. W., Battaglia, N., et al. (2019). The Future Landscape of High-Redshift Galaxy Cluster Science. *BAAS*, 51(3):279.

Mantz, A. B., Abdulla, Z., Allen, S. W., et al. (2018). The XXL Survey. XVII. X-ray and Sunyaev-Zel'dovich properties of the redshift 2.0 galaxy cluster XLSSC 122. *A&A*, 620:A2.

Mantz, A. B., Allen, S. W., Morris, R. G., et al. (2020). Deep XMM-Newton observations of the most distant SPT-SZ galaxy cluster. *MNRAS*, 496(2):1554–1564.

Mantz, A. B., Allen, S. W., Morris, R. G., et al. (2016). Weighing the giants- V. Galaxy cluster scaling relations. *MNRAS*, 463(4):3582–3603.

Mantz, A. B., Morris, R. G., Allen, S. W., et al. (2022). Cosmological constraints from gas mass fractions of massive, relaxed galaxy clusters. *MNRAS*, 510(1):131–145.

Markevitch, M. (2010). Intergalactic shock fronts. *arXiv e-prints*, page arXiv:1010.3660.

Markevitch, M., Gonzalez, A. H., David, L., et al. (2002). A Textbook Example of a Bow Shock in the Merging Galaxy Cluster 1E 0657-56. *ApJ*, 567(1):L27–L31.

Markevitch, M., Govoni, F., Brunetti, G., and Jerius, D. (2005). Bow Shock and Radio Halo in the Merging Cluster A520. *ApJ*, 627(2):733–738.

Markevitch, M. and Vikhlinin, A. (2007). Shocks and cold fronts in galaxy clusters. *Phys. Rep.*, 443(1):1–53.

Marulli, F., Veropalumbo, A., Sereno, M., et al. (2018). The XXL Survey. XVI. The clustering of X-ray selected galaxy clusters at z 0.3. *A&A*, 620:A1.

Mathews, W. G. and Brighenti, F. (2007). Creation of X-Ray Cavities in Galaxy Clusters with Cosmic Rays. *ApJ*, 660(2):1137–1145.

Matsumura, T., Akiba, Y., Borrill, J., et al. (2014). Mission Design of LiteBIRD. *Journal of Low Temperature Physics*, 176(5-6):733–740.

Mattox, J. R., Bertsch, D. L., Chiang, J., et al. (1996). The Likelihood Analysis of EGRET Data. *ApJ*, 461:396.

Mayet, F., Adam, R., Ade, P., et al. (2020). Cluster cosmology with the NIKA2 SZ Large Program. In *European Physical Journal Web of Conferences*, volume 228 of *European Physical Journal Web of Conferences*, page 00017.

Mayet, F., Adam, R., Ade, P., et al. (2017). High-resolution SZ imaging of clusters of galaxies with the NIKA2 camera at the IRAM 30-m telescope. *arXiv e-prints*, page arXiv:1709.01255.

Mazzotta, P. and Giacintucci, S. (2008). Do Radio Core-Halos and Cold Fronts in Non-Major-Merging Clusters Originate from the Same Gas Sloshing? *ApJ*, 675(1):L9.

Mazzotta, P., Rasia, E., Moscardini, L., and Tormen, G. (2004). Comparing the temperatures of galaxy clusters from hydrodynamical N-body simulations to Chandra and XMM-Newton observations. *MNRAS*, 354(1):10–24.

McCourt, M., Sharma, P., Quataert, E., and Parrish, I. J. (2012). Thermal instability in gravitationally stratified plasmas: implications for multiphase structure in clusters and galaxy haloes. *MNRAS*, 419(4):3319–3337.

McDonald, M., Allen, S. W., Bayliss, M., et al. (2017). The Remarkable Similarity of Massive Galaxy Clusters from z $\sim$ 0 to z $\sim$ 1.9. *ApJ*, 843(1):28.

McDonald, M., Benson, B. A., Vikhlinin, A., et al. (2014). The Redshift Evolution of the Mean Temperature, Pressure, and Entropy Profiles in 80 SPT-Selected Galaxy Clusters. *ApJ*, 794(1):67.

McDonald, M., Gaspari, M., McNamara, B. R., and Tremblay, G. R. (2018). Revisiting the Cooling Flow Problem in Galaxies, Groups, and Clusters of Galaxies. *ApJ*, 858(1):45.

McKean, J., Jackson, N., Vegetti, S., et al. (2015). Strong Gravitational Lensing with the SKA. In *Advancing Astrophysics with the Square Kilometre Array (AASKA14)*, page 84.

McNamara, B. R., Kazemzadeh, F., Rafferty, D. A., et al. (2009). An Energetic AGN Outburst Powered by a Rapidly Spinning Supermassive Black Hole or an Accreting Ultramassive Black Hole. *ApJ*, 698(1):594–605.

McNamara, B. R. and Nulsen, P. E. J. (2007). Heating Hot Atmospheres with Active Galactic Nuclei. *ARA&A*, 45(1):117–175.

Meadows, D. H., Meadows, D. L., Randers, J., and Behrens III, W. W. (1972). *The Limits to Growth. A Report for the Club of Rome's Project on the Predicament of Mankind*. Universe Books, New York.

Medezinski, E., Battaglia, N., Umetsu, K., et al. (2018). Planck Sunyaev-Zel'dovich cluster mass calibration using Hyper Suprime-Cam weak lensing. *PASJ*, 70:S28.

Mendygral, P. J., Jones, T. W., and Dolag, K. (2012). MHD Simulations of Active Galactic Nucleus Jets in a Dynamic Galaxy Cluster Medium. *ApJ*, 750(2):166.

Merloni, A., Predehl, P., Becker, W., et al. (2012). eROSITA Science Book: Mapping the Structure of the Energetic Universe. *arXiv e-prints*, page arXiv:1209.3114.

Mernier, F., Biffi, V., Yamaguchi, H., et al. (2018). Enrichment of the Hot Intracluster Medium: Observations. *Space Sci. Rev.*, 214(8):129.

Mernier, F., Werner, N., Bagchi, J., et al. (2022). Discovery of inverse-Compton X-ray emission and robust estimation of magnetic field in a galaxy group. *arXiv e-prints*, page arXiv:2207.10092.

Merritt, D. (1983). Relaxation and tidal stripping in rich clusters of galaxies. I. Evolution of the mass distribution. *ApJ*, 264:24–48.

Mihos, J. C. (2004). Interactions and Mergers of Cluster Galaxies. In Mulchaey, J. S., Dressler, A., and Oemler, A., editors, *Clusters of Galaxies: Probes of Cosmological Structure and Galaxy Evolution*, page 277.

Miniati, F., Jones, T. W., Kang, H., and Ryu, D. (2001). Cosmic-Ray Electrons in Groups and Clusters of Galaxies: Primary and Secondary Populations from a Numerical Cosmological Simulation. *ApJ*, 562(1):233–253.

Miyatake, H., Battaglia, N., Hilton, M., et al. (2019). Weak-lensing Mass Calibration of ACTPol Sunyaev-Zel'dovich Clusters with the Hyper Suprime-Cam Survey. *ApJ*, 875(1):63.

Mo, H., van den Bosch, F. C., and White, S. (2010). *Galaxy Formation and Evolution*.

Moliné, Á., Sánchez-Conde, M. A., Palomares-Ruiz, S., and Prada, F. (2017). Characterization of subhalo structural properties and implications for dark matter annihilation signals. *MNRAS*, 466(4):4974–4990.

Molnar, S. M., Hearn, N., Haiman, Z., et al. (2009). Accretion Shocks in Clusters of Galaxies and Their SZ Signature from Cosmological Simulations. *ApJ*, 696(2):1640–1656.

Monfardini, A., Beelen, A., Benoit, A., et al. (2021). CONCERTO at APEX: installation and technical commissioning. *arXiv e-prints*, page arXiv:2106.14028.

Moore, B., Katz, N., Lake, G., Dressler, A., and Oemler, A. (1996). Galaxy harassment and the evolution of clusters of galaxies. *Nature*, 379(6566):613–616.

Morandi, A., Limousin, M., Sayers, J., et al. (2012). X-ray, lensing and Sunyaev-Zel'dovich triaxial analysis of Abell 1835 out to R_{200}. *MNRAS*, 425(3):2069–2082.

More, S., Diemer, B., and Kravtsov, A. V. (2015). The Splashback Radius as a Physical Halo Boundary and the Growth of Halo Mass. *ApJ*, 810(1):36.

Mroczkowski, T., Dicker, S., Sayers, J., et al. (2012). A Multi-wavelength Study of the Sunyaev-Zel'dovich Effect in the Triple-merger Cluster MACS J0717.5+3745 with MUSTANG and Bolocam. *ApJ*, 761(1):47.

Mroczkowski, T., Nagai, D., Basu, K., et al. (2019). Astrophysics with the Spatially and Spectrally Resolved Sunyaev-Zeldovich Effects. A Millimetre/Submillimetre Probe of the Warm and Hot Universe. *Space Sci. Rev.*, 215(1):17.

Muñoz-Echeverría, M., Adam, R., Ade, P., et al. (2022a). Multi-probe analysis of the galaxy cluster CL J1226.9+3332: Hydrostatic mass and hydrostatic-to-lensing bias. In *European Physical Journal Web of Conferences*, volume 257 of *European Physical Journal Web of Conferences*, page 00032.

Muñoz-Echeverría, M., Adam, R., Ade, P., et al. (2022b). The LPSZ-CLASH galaxy cluster sample: Combining lensing and hydrostatic mass estimates. In *European Physical Journal Web of Conferences*, volume 257 of *European Physical Journal Web of Conferences*, page 00033.

Muchovej, S., Leitch, E., Carlstrom, J. E., et al. (2010). Radio Sources from a 31 GHz Sky Survey with the Sunyaev-Zel'dovich Array. *ApJ*, 716(1):521–529.

Muchovej, S., Mroczkowski, T., Carlstrom, J. E., et al. (2007). Observations of High-Redshift X-Ray Selected Clusters with the Sunyaev-Zel'dovich Array. *ApJ*, 663(2):708–716.

Naab, T. and Ostriker, J. P. (2017). Theoretical Challenges in Galaxy Formation. *ARA&A*, 55(1):59–109.

Nagai, D. (2006). The Impact of Galaxy Formation on the Sunyaev-Zel'dovich Effect of Galaxy Clusters. *ApJ*, 650(2):538–549.

Nagai, D., Kravtsov, A. V., and Vikhlinin, A. (2007). Effects of Galaxy Formation on Thermodynamics of the Intracluster Medium. *ApJ*, 668(1):1–14.

Nandra, K., Barret, D., Barcons, X., et al. (2013). The Hot and Energetic Universe: A White Paper presenting the science theme motivating the Athena+ mission. *arXiv e-prints*, page arXiv:1306.2307.

Newman, A. B., Treu, T., Ellis, R. S., and Sand, D. J. (2013a). The Density Profiles of Massive, Relaxed Galaxy Clusters. II. Separating Luminous and Dark Matter in Cluster Cores. *ApJ*, 765(1):25.

Newman, A. B., Treu, T., Ellis, R. S., et al. (2013b). The Density Profiles of Massive, Relaxed Galaxy Clusters. I. The Total Density Over Three Decades in Radius. *ApJ*, 765(1):24.

Nishiwaki, K., Asano, K., and Murase, K. (2021). Particle Reacceleration by Turbulence and Radio Constraints on Multimessenger High-energy Emission from the Coma Cluster. *ApJ*, 922(2):190.

Nulsen, P. E. J. (1982). Transport processes and the stripping of cluster galaxies. *MNRAS*, 198:1007–1016.

Nulsen, P. E. J., McNamara, B. R., Wise, M. W., and David, L. P. (2005). The Cluster-Scale AGN Outburst in Hydra A. *ApJ*, 628(2):629–636.

Nuza, S. E., Gelszinnis, J., Hoeft, M., and Yepes, G. (2017). Can cluster merger shocks reproduce the luminosity and shape distribution of radio relics? *MNRAS*, 470(1):240–263.

Ondaro-Mallea, L., Angulo, R. E., Zennaro, M., Contreras, S., and Aricò, G. (2022). Non-universality of the mass function: dependence on the growth rate and power spectrum shape. *MNRAS*, 509(4):6077–6090.

Orlowski-Scherer, J., Haridas, S. K., Di Mascolo, L., et al. (2022). GBT/MUSTANG-2 9" resolution imaging of the SZ effect in MS0735.6+7421: Confirmation of the SZ Cavities through direct imaging. *arXiv e-prints*, page arXiv:2207.07100.

Oteo, I., Ivison, R. J., Dunne, L., et al. (2018). An Extreme Protocluster of Luminous Dusty Starbursts in the Early Universe. *ApJ*, 856(1):72.

Peacock, J. A. (1999). *Cosmological Physics*.

Pedlar, A., Ghataure, H. S., Davies, R. D., et al. (1990). The radio structure of NGC 1275. *MNRAS*, 246:477.

Peebles, P. J. E. (1993). *Principles of Physical Cosmology*.

Penna-Lima, M., Bartlett, J. G., Rozo, E., et al. (2017). Calibrating the Planck cluster mass scale with CLASH. *A&A*, 604:A89.

Pérez-Romero, J. (2022). Sensitivity of CTA to gamma-ray emission from the Perseus galaxy cluster. In *37th International Cosmic Ray Conference. 12-23 July 2021. Berlin*, page 546.

Perkins, J. S. (2008). VERITAS Observations of the Coma Cluster of Galaxies. In Aharonian, F. A., Hofmann, W., and Rieger, F., editors, *American Institute of Physics Conference Series*, volume 1085 of *American Institute of Physics Conference Series*, pages 569–572.

Perotto, L., Adam, R., Ade, P., et al. (2022). The NIKA2 Sunyaev-Zeldovich Large Program: Precise galaxy cluster physics for an accurate cluster-based cosmology. In *European Physical Journal Web of Conferences*, volume 257 of *European Physical Journal Web of Conferences*, page 00038.

Perotto, L., Adam, R., Ade, P., et al. (2018). NIKA2 Performance and Cosmology Program with Galaxy Clusters. *arXiv e-prints*, page arXiv:1808.10817.

Petrosian, V. (2001). On the Nonthermal Emission and Acceleration of Electrons in Coma and Other Clusters of Galaxies. *ApJ*, 557(2):560–572.

Pfrommer, C., Enßlin, T. A., and Springel, V. (2008). Simulating cosmic rays in clusters of galaxies - II. A unified scheme for radio haloes and relics with predictions of the γ-ray emission. *MNRAS*, 385(3):1211–1241.

Pfrommer, C., Enßlin, T. A., Springel, V., Jubelgas, M., and Dolag, K. (2007). Simulating cosmic rays in clusters of galaxies - I. Effects on the Sunyaev-Zel'dovich effect and the X-ray emission. *MNRAS*, 378(2):385–408.

Pierre, M., Pacaud, F., Adami, C., et al. (2016). The XXL Survey. I. Scientific motivations - XMM-Newton observing plan - Follow-up observations and simulation programme. *A&A*, 592:A1.

Piffaretti, R., Arnaud, M., Pratt, G. W., Pointecouteau, E., and Melin, J. B. (2011). The MCXC: a meta-catalogue of x-ray detected clusters of galaxies. *A&A*, 534:A109.

Pike, S. R., Kay, S. T., Newton, R. D. A., Thomas, P. A., and Jenkins, A. (2014). Cosmological simulations of galaxy clusters with feedback from active galactic nuclei: profiles and scaling relations. *MNRAS*, 445(2):1774–1796.

Pillepich, A., Porciani, C., and Reiprich, T. H. (2012). The X-ray cluster survey with eRosita: forecasts for cosmology, cluster physics and primordial non-Gaussianity. *MNRAS*, 422(1):44–69.

Pinzke, A., Oh, S. P., and Pfrommer, C. (2017). Turbulence and particle acceleration in giant radio haloes: the origin of seed electrons. *MNRAS*, 465(4):4800–4816.

Pinzke, A. and Pfrommer, C. (2010). Simulating the γ-ray emission from galaxy clusters: a universal cosmic ray spectrum and spatial distribution. *MNRAS*, 409(2):449–480.

Plagge, T. J., Marrone, D. P., Abdulla, Z., et al. (2013). CARMA Measurements of the Sunyaev-Zel'dovich Effect in RX J1347.5-1145. *ApJ*, 770(2):112.

Planck Collaboration, Adam, R., Ade, P. A. R., et al. (2016a). Planck 2015 results. X. Diffuse component separation: Foreground maps. *A&A*, 594:A10.

Planck Collaboration, Ade, P. A. R., Aghanim, N., et al. (2014a). Planck 2013 results. XXIX. The Planck catalogue of Sunyaev-Zeldovich sources. *A&A*, 571:A29.

Planck Collaboration, Ade, P. A. R., Aghanim, N., et al. (2014b). Planck 2013 results. XX. Cosmology from Sunyaev-Zeldovich cluster counts. *A&A*, 571:A20.

Planck Collaboration, Ade, P. A. R., Aghanim, N., et al. (2014c). Planck 2013 results. XXI. Power spectrum and high-order statistics of the Planck all-sky Compton parameter map. *A&A*, 571:A21.

Planck Collaboration, Ade, P. A. R., Aghanim, N., et al. (2014d). Planck 2013 results. XXX. Cosmic infrared background measurements and implications for star formation. *A&A*, 571:A30.

Planck Collaboration, Ade, P. A. R., Aghanim, N., et al. (2016b). Planck 2015 results. XIX. Constraints on primordial magnetic fields. *A&A*, 594:A19.

Planck Collaboration, Ade, P. A. R., Aghanim, N., et al. (2013a). Planck intermediate results. V. Pressure profiles of galaxy clusters from the Sunyaev-Zeldovich effect. *A&A*, 550:A131.

Planck Collaboration, Ade, P. A. R., Aghanim, N., et al. (2013b). Planck intermediate results. X. Physics of the hot gas in the Coma cluster. *A&A*, 554:A140.

Planck Collaboration, Ade, P. A. R., Aghanim, N., et al. (2013c). Planck intermediate results. VIII. Filaments between interacting clusters. *A&A*, 550:A134.

Planck Collaboration, Ade, P. A. R., Aghanim, N., et al. (2016c). Planck 2015 results. XXVII. The second Planck catalogue of Sunyaev-Zeldovich sources. *A&A*, 594:A27.

Planck Collaboration, Ade, P. A. R., Aghanim, N., et al. (2016d). Planck 2015 results. XXIV. Cosmology from Sunyaev-Zeldovich cluster counts. *A&A*, 594:A24.

Planck Collaboration, Ade, P. A. R., Aghanim, N., et al. (2016e). Planck intermediate results. XL. The Sunyaev-Zeldovich signal from the Virgo cluster. *A&A*, 596:A101.

Planck Collaboration, Aghanim, N., Akrami, Y., et al. (2020). Planck 2018 results. VI. Cosmological parameters. *A&A*, 641:A6.

Planck Collaboration, Aghanim, N., Arnaud, M., et al. (2016f). Planck 2015 results. XXII. A map of the thermal Sunyaev-Zeldovich effect. *A&A*, 594:A22.

Planelles, S., Borgani, S., Fabjan, D., et al. (2014). On the role of AGN feedback on the thermal and chemodynamical properties of the hot intracluster medium. *MNRAS*, 438(1):195–216.

Pointecouteau, E., Giard, M., Benoit, A., et al. (2001). Extended Sunyaev-Zeldovich Map of the Most Luminous X-Ray Cluster, RX J1347-1145. *ApJ*, 552(1):42–48.

Pointecouteau, E., Santiago-Bautista, I., Douspis, M., et al. (2021). PACT. II. Pressure profiles of galaxy clusters using Planck and ACT. *A&A*, 651:A73.

Pop, A.-R., Hernquist, L., Nagai, D., et al. (2022a). Sunyaev-Zel'dovich effect and X-ray scaling relations of galaxies, groups and clusters in the IllustrisTNG simulations. *arXiv e-prints*, page arXiv:2205.11528.

Pop, A.-R., Hernquist, L., Nagai, D., et al. (2022b). Unifying Sunyaev-Zel'dovich and X-ray predictions from clusters to galaxy groups: the impact of X-ray mass estimates on the $Y - M$ scaling relation. *arXiv e-prints*, page arXiv:2205.11537.

Pope, A., Montaña, A., Battisti, A., et al. (2017). Early Science with the Large Millimeter Telescope: Detection of Dust Emission in Multiple Images of a Normal Galaxy at z > 4 Lensed by a Frontier Fields Cluster. *ApJ*, 838(2):137.

Prandoni, I. and Seymour, N. (2014). Proceedings of 'Advancing Astrophysics with the SKA' (AASKA14) - Continuum Science' Chapters. *arXiv e-prints*, page arXiv:1412.6942.

Pratt, G. W., Arnaud, M., Biviano, A., et al. (2019). The Galaxy Cluster Mass Scale and Its Impact on Cosmological Constraints from the Cluster Population. *Space Sci. Rev.*, 215(2):25.

Pratt, G. W., Arnaud, M., Piffaretti, R., et al. (2010). Gas entropy in a representative sample of nearby X-ray galaxy clusters (REXCESS): relationship to gas mass fraction. *A&A*, 511:A85.

Pratt, G. W., Böhringer, H., Croston, J. H., et al. (2007). Temperature profiles of a representative sample of nearby X-ray galaxy clusters. *A&A*, 461(1):71–80.

Prokhorov, D. A. (2014). An analysis of Fermi-LAT observations of the outskirts of the Coma cluster of galaxies. *MNRAS*, 441(3):2309–2315.

Prokhorov, D. A. and Churazov, E. M. (2014). Counting gamma rays in the directions of galaxy clusters. *A&A*, 567:A93.

Rafferty, D. A., McNamara, B. R., Nulsen, P. E. J., and Wise, M. W. (2006). The Feedback-regulated Growth of Black Holes and Bulges through Gas Accretion and Starbursts in Cluster Central Dominant Galaxies. *ApJ*, 652(1):216–231.

Randall, S. W., Forman, W. R., Giacintucci, S., et al. (2011). Shocks and Cavities from Multiple Outbursts in the Galaxy Group NGC 5813: A Window to Active Galactic Nucleus Feedback. *ApJ*, 726(2):86.

Randall, S. W., Nulsen, P. E. J., Jones, C., et al. (2015). A Very Deep Chandra Observation of the Galaxy Group NGC 5813: AGN Shocks, Feedback, and Outburst History. *ApJ*, 805(2):112.

Rasia, E., Lau, E. T., Borgani, S., et al. (2014). Temperature Structure of the Intracluster Medium from Smoothed-particle Hydrodynamics and Adaptive-mesh Refinement Simulations. *ApJ*, 791(2):96.

Reimer, O., Pohl, M., Sreekumar, P., and Mattox, J. R. (2003). EGRET Upper Limits on the High-Energy Gamma-Ray Emission of Galaxy Clusters. *ApJ*, 588(1):155–164.

Reiprich, T. H. and Böhringer, H. (2002). The Mass Function of an X-Ray Flux-limited Sample of Galaxy Clusters. *ApJ*, 567(2):716–740.

Reiprich, T. H., Veronica, A., Pacaud, F., et al. (2021). The Abell 3391/95 galaxy cluster system. A 15 Mpc intergalactic medium emission filament, a warm gas bridge, infalling matter clumps, and (re-) accelerated plasma discovered by combining SRG/eROSITA data with ASKAP/EMU and DECam data. *A&A*, 647:A2.

Ricci, M. (2018). *Study of the optical properties of X-ray selected galaxy clusters : multi-wavelengths analysis and implications for the future large surveys*. Theses, COMUE Université Côte d'Azur (2015 - 2019).

Ricci, M., Adam, R., Eckert, D., et al. (2020). The XXL Survey. XLIV. Sunyaev-Zel'dovich mapping of a low-mass cluster at z $\sim$ 1: a multi-wavelength approach. *A&A*, 642:A126.

Riseley, C. J., Rajpurohit, K., Loi, F., et al. (2022). A MeerKAT-meets-LOFAR study of MS 1455.0 + 2232: a 590 kiloparsec 'mini'-halo in a sloshing cool-core cluster. *MNRAS*, 512(3):4210–4230.

Roediger, E., Kraft, R. P., Nulsen, P. E. J., et al. (2015). Stripped Elliptical Galaxies as Probes of ICM Physics: I. Tails, Wakes, and Flow Patterns in and Around Stripped Ellipticals. *ApJ*, 806(1):103.

Roettiger, K., Burns, J. O., and Stone, J. M. (1999). A Cluster Merger and the Origin of the Extended Radio Emission in Abell 3667. *ApJ*, 518(2):603–612.

Romero, C., McWilliam, M., Macías-Pérez, J. F., et al. (2018). A multi-instrument non-parametric reconstruction of the electron pressure profile in the galaxy cluster CLJ1226.9+3332. *A&A*, 612:A39.

Rossetti, M., Gastaldello, F., Eckert, D., et al. (2017). The cool-core state of Planck SZ-selected clusters versus X-ray-selected samples: evidence for cool-core bias. *MNRAS*, 468(2):1917–1930.

Rumsey, C., Olamaie, M., Perrott, Y. C., et al. (2016). AMI observations of 10 CLASH galaxy clusters: SZ and X-ray data used together to determine cluster dynamical states. *MNRAS*, 460(1):569–589.

Ruppin, F. (2018). *Cosmologie via les observations d'amas de galaxies par effet Sunyaev-Zel'dovich avec NIKA2*. Theses, Université Grenoble Alpes.

Ruppin, F., Adam, R., Ade, P., et al. (2022). Mapping the intracluster medium temperature in the era of NIKA2 and MUSTANG-2. In *European Physical Journal Web of Conferences*, volume 257 of *European Physical Journal Web of Conferences*, page 00043.

Ruppin, F., Adam, R., Comis, B., et al. (2017). Non-parametric deprojection of NIKA SZ observations: Pressure distribution in the Planck-discovered cluster PSZ1 G045.85+57.71. *A&A*, 597:A110.

Ruppin, F., Mayet, F., Pratt, G. W., et al. (2018). First Sunyaev-Zel'dovich mapping with the NIKA2 camera: Implication of cluster substructures for the pressure profile and mass estimate. *A&A*, 615:A112.

Ruppin, F., McDonald, M., Bleem, L. E., et al. (2021). Stability of Cool Cores during Galaxy Cluster Growth: A Joint Chandra/SPT Analysis of 67 Galaxy Clusters along a Common Evolutionary Track Spanning 9 Gyr. *ApJ*, 918(2):43.

Ruppin, F., McDonald, M., Brodwin, M., et al. (2020). Unveiling the Merger Dynamics of the Most Massive MaDCoWS Cluster at z = 1.2 from a Multiwavelength Mapping of Its Intracluster Medium Properties. *ApJ*, 893(1):74.

Ruppin, F., Sembolini, F., De Petris, M., et al. (2019). Impact of ICM disturbances on the mean pressure profile of galaxy clusters: A prospective study of the NIKA2 SZ large program with MUSIC synthetic clusters. *A&A*, 631:A21.

Rybicki, G. B. and Lightman, A. P. (1986). *Radiative Processes in Astrophysics*.

Ryle, M., Smith, F. G., and Elsmore, B. (1950). A preliminary survey of the radio stars in the Northern Hemisphere. *MNRAS*, 110:508.

Sakr, Z., Ilić, S., Blanchard, A., Bittar, J., and Farah, W. (2018). Cluster counts: Calibration issue or new physics? *A&A*, 620:A78.

Salvati, L., Saro, A., Bocquet, S., et al. (2022). Combining Planck and SPT Cluster Catalogs: Cosmological Analysis and Impact on the Planck Scaling Relation Calibration. *ApJ*, 934(2):129.

Sánchez-Conde, M. A., Cannoni, M., Zandanel, F., Gómez, M. E., and Prada, F. (2011). Dark matter searches with Cherenkov telescopes: nearby dwarf galaxies or local galaxy clusters? *JCAP*, 2011(12):011.

Sanders, J. S., Dennerl, K., Russell, H. R., et al. (2020). Measuring bulk flows of the intracluster medium in the Perseus and Coma galaxy clusters using XMM-Newton. *A&A*, 633:A42.

Sanders, J. S., Fabian, A. C., Russell, H. R., and Walker, S. A. (2018). Hydrostatic Chandra X-ray analysis of SPT-selected galaxy clusters - I. Evolution of profiles and core properties. *MNRAS*, 474(1):1065–1098.

Sanders, J. S., Fabian, A. C., Russell, H. R., Walker, S. A., and Blundell, K. M. (2016). Detecting edges in the X-ray surface brightness of galaxy clusters. *MNRAS*, 460:1898–1911.

Sarazin, C. L. (1988). *X-ray emission from clusters of galaxies*.

Sarazin, C. L. (1999). The Energy Spectrum of Primary Cosmic-Ray Electrons in Clusters of Galaxies and Inverse Compton Emission. *ApJ*, 520(2):529–547.

Sarazin, C. L. (2002). The Physics of Cluster Mergers. In Feretti, L., Gioia, I. M., and Giovannini, G., editors, *Merging Processes in Galaxy Clusters*, volume 272 of *Astrophysics and Space Science Library*, pages 1–38.

Savini, F., Bonafede, A., Brüggen, M., et al. (2019). A LOFAR study of non-merging massive galaxy clusters. *A&A*, 622:A24.

Sayers, J., Czakon, N. G., Mantz, A., et al. (2013a). Sunyaev-Zel'dovich-measured Pressure Profiles from the Bolocam X-Ray/SZ Galaxy Cluster Sample. *ApJ*, 768(2):177.

Sayers, J., Mantz, A. B., Rasia, E., et al. (2022). The Evolution and Mass Dependence of Galaxy Cluster Pressure Profiles at $0.05 \leq z \leq 0.60$ and 4×10^{14} $M_\odot \leq M_{500} \leq 30 \times 10^{14}$ $M_\odot$. *arXiv e-prints*, page arXiv:2206.00091.

Sayers, J., Montaña, A., Mroczkowski, T., et al. (2019). Imaging the Thermal and Kinematic Sunyaev-Zel'dovich Effect Signals in a Sample of 10 Massive Galaxy Clusters: Constraints on Internal Velocity Structures and Bulk Velocities. *ApJ*, 880(1):45.

Sayers, J., Mroczkowski, T., Zemcov, M., et al. (2013b). A Measurement of the Kinetic Sunyaev-Zel'dovich Signal Toward MACS J0717.5+3745. *ApJ*, 778(1):52.

Schellenberger, G., Reiprich, T. H., Lovisari, L., Nevalainen, J., and David, L. (2015). XMM-Newton and Chandra cross-calibration using HIFLUGCS galaxy clusters . Systematic temperature differences and cosmological impact. *A&A*, 575:A30.

Schlickeiser, R., Sievers, A., and Thiemann, H. (1987). The diffuse radio emission from the Coma cluster. *A&A*, 182:21–35.

Schuecker, P., Finoguenov, A., Miniati, F., Böhringer, H., and Briel, U. G. (2004). Probing turbulence in the Coma galaxy cluster. *A&A*, 426:387–397.

Scolnic, D. M., Jones, D. O., Rest, A., et al. (2018). The Complete Light-curve Sample of Spectroscopically Confirmed SNe Ia from Pan-STARRS1 and Cosmological Constraints from the Combined Pantheon Sample. *ApJ*, 859(2):101.

Seeger, C. L., Westerhout, G., and Conway, R. G. (1957). Observations of discrete sources, the Coma cluster, the moon, and the Andromeda nebula at a wave length of 75 cm. *ApJ*, 126:585–587.

Sereno, M. and Ettori, S. (2017). CoMaLit - V. Mass forecasting with proxies: method and application to weak lensing calibrated samples. *MNRAS*, 468(3):3322–3341.

Sereno, M., Ettori, S., Meneghetti, M., et al. (2017). CLUMP-3D: three-dimensional lensing and multi-probe analysis of MACS J1206.2-0847, a remarkably regular cluster. *MNRAS*, 467(4):3801–3826.

Sereno, M., Umetsu, K., Ettori, S., et al. (2018). CLUMP-3D: Testing ΛCDM with Galaxy Cluster Shapes. *ApJ*, 860(1):L4.

Shi, X. (2016). Locations of accretion shocks around galaxy clusters and the ICM properties: insights from self-similar spherical collapse with arbitrary mass accretion rates. *MNRAS*, 461(2):1804–1815.

Shi, X., Komatsu, E., Nelson, K., and Nagai, D. (2015). Analytical model for non-thermal pressure in galaxy clusters - II. Comparison with cosmological hydrodynamics simulation. *MNRAS*, 448(1):1020–1029.

Shimwell, T. W., Hardcastle, M. J., Tasse, C., et al. (2022). The LOFAR Two-metre Sky Survey. V. Second data release. *A&A*, 659:A1.

Shin, J., Woo, J.-H., and Mulchaey, J. S. (2016). A Systematic Search for X-Ray Cavities in Galaxy Clusters, Groups, and Elliptical Galaxies. *ApJS*, 227(2):31.

Shirasaki, M., Macias, O., Ando, S., Horiuchi, S., and Yoshida, N. (2020). Cross-correlation of the extragalactic gamma-ray background with the thermal Sunyaev-Zel'dovich effect in the cosmic microwave background. *Phys. Rev. D*, 101(10):103022.

Sijacki, D., Pfrommer, C., Springel, V., and Enßlin, T. A. (2008). Simulations of cosmic-ray feedback by active galactic nuclei in galaxy clusters. *MNRAS*, 387(4):1403–1415.

Sijacki, D., Springel, V., Di Matteo, T., and Hernquist, L. (2007). A unified model for AGN feedback in cosmological simulations of structure formation. *MNRAS*, 380(3):877–900.

Simionescu, A., Nakashima, S., Yamaguchi, H., et al. (2019a). Constraints on the chemical enrichment history of the Perseus Cluster of galaxies from high-resolution X-ray spectroscopy. *MNRAS*, 483(2):1701–1721.

Simionescu, A., Werner, N., Mantz, A., Allen, S. W., and Urban, O. (2017). Witnessing the growth of the nearest galaxy cluster: thermodynamics of the Virgo Cluster outskirts. *MNRAS*, 469(2):1476–1495.

Simionescu, A., ZuHone, J., Zhuravleva, I., et al. (2019b). Constraining Gas Motions in the Intra-Cluster Medium. *Space Sci. Rev.*, 215(2):24.

Skillman, S. W., O'Shea, B. W., Hallman, E. J., Burns, J. O., and Norman, M. L. (2008). Cosmological Shocks in Adaptive Mesh Refinement Simulations and the Acceleration of Cosmic Rays. *ApJ*, 689(2):1063–1077.

Smith, G. P., Mazzotta, P., Okabe, N., et al. (2016). LoCuSS: Testing hydrostatic equilibrium in galaxy clusters. *MNRAS*, 456(1):L74–L78.

Somerville, R. S. and Davé, R. (2015). Physical Models of Galaxy Formation in a Cosmological Framework. *ARA&A*, 53:51–113.

Sreekumar, P., Bertsch, D. L., Dingus, B. L., et al. (1996). EGRET Observations of the North Galactic Pole Region. *ApJ*, 464:628.

Stuardi, C., Bonafede, A., Lovisari, L., et al. (2021). The intracluster magnetic field in the double relic galaxy cluster Abell 2345. *MNRAS*, 502(2):2518–2535.

Su, Y., Kraft, R. P., Roediger, E., et al. (2017). Deep Chandra Observations of NGC 1404: Cluster Plasma Physics Revealed by an Infalling Early-type Galaxy. *ApJ*, 834(1):74.

Subramanian, K. (2016). The origin, evolution and signatures of primordial magnetic fields. *Reports on Progress in Physics*, 79(7):076901.

Sun, F., Egami, E., Fujimoto, S., et al. (2022). ALMA Lensing Cluster Survey: ALMA-Herschel Joint Study of Lensed Dusty Star-forming Galaxies across $z \simeq 0.5 - 6$. *ApJ*, 932(2):77.

Sunyaev, R. A. and Zeldovich, Y. B. (1970). Small-Scale Fluctuations of Relic Radiation. *Ap&SS*, 7(1):3–19.

Sunyaev, R. A. and Zeldovich, Y. B. (1972). The Observations of Relic Radiation as a Test of the Nature of X-Ray Radiation from the Clusters of Galaxies. *Comments on Astrophysics and Space Physics*, 4:173.

Sunyaev, R. A. and Zeldovich, Y. B. (1980). The velocity of clusters of galaxies relative to the microwave background - The possibility of its measurement. *MNRAS*, 190:413–420.

Tanimura, H., Aghanim, N., Douspis, M., and Malavasi, N. (2022). X-ray emission from cosmic web filaments in SRG/eROSITA data. *arXiv e-prints*, page arXiv:2206.00084.

Tanimura, H., Aghanim, N., Kolodzig, A., Douspis, M., and Malavasi, N. (2020). First detection of stacked X-ray emission from cosmic web filaments. *A&A*, 643:L2.

Tanimura, H., Hinshaw, G., McCarthy, I. G., et al. (2019). A search for warm/hot gas filaments between pairs of SDSS Luminous Red Galaxies. *MNRAS*, 483(1):223–234.

Tarrío, P., Melin, J. B., and Arnaud, M. (2018). A matched filter approach for blind joint detection of galaxy clusters in X-ray and SZ surveys. *A&A*, 614:A82.

Taylor, G. B., Gugliucci, N. E., Fabian, A. C., et al. (2006). Magnetic fields in the centre of the Perseus cluster. *MNRAS*, 368(4):1500–1506.

Tchernin, C., Eckert, D., Ettori, S., et al. (2016). The XMM Cluster Outskirts Project (X-COP): Physical conditions of Abell 2142 up to the virial radius. *A&A*, 595:A42.

Truong, N., Rasia, E., Mazzotta, P., et al. (2018). Cosmological hydrodynamical simulations of galaxy clusters: X-ray scaling relations and their evolution. *MNRAS*, 474(3):4089–4111.

Tucci, M., Toffolatti, L., de Zotti, G., and Martínez-González, E. (2011). High-frequency predictions for number counts and spectral properties of extragalactic radio sources. New evidence of a break at mm wavelengths in spectra of bright blazar sources. *A&A*, 533:A57.

Tulin, S. and Yu, H.-B. (2018). Dark matter self-interactions and small scale structure. *Phys. Rep.*, 730:1–57.

Tully, R. B. and Fisher, J. R. (1977). A new method of determining distances to galaxies. *A&A*, 54:661–673.

Umetsu, K. (2020). Cluster-galaxy weak lensing. *A&A Rev.*, 28(1):7.

Urban, O., Simionescu, A., Werner, N., et al. (2014). Azimuthally resolved X-ray spectroscopy to the edge of the Perseus Cluster. *MNRAS*, 437(4):3939–3961.

Vacca, V., Murgia, M., Govoni, F., et al. (2012). The intracluster magnetic field power spectrum in A2199. *A&A*, 540:A38.

Vacca, V., Oppermann, N., Enßlin, T., et al. (2016). Using rotation measure grids to detect cosmological magnetic fields: A Bayesian approach. *A&A*, 591:A13.

van Weeren, R. J., de Gasperin, F., Akamatsu, H., et al. (2019). Diffuse Radio Emission from Galaxy Clusters. *Space Sci. Rev.*, 215(1):16.

van Weeren, R. J., Röttgering, H. J. A., Brüggen, M., and Hoeft, M. (2010). Particle Acceleration on Megaparsec Scales in a Merging Galaxy Cluster. *Science*, 330(6002):347.

Vazza, F. and Brüggen, M. (2014). Do radio relics challenge diffusive shock acceleration? *MNRAS*, 437(3):2291–2296.

Vazza, F., Brüggen, M., Wittor, D., et al. (2016). Constraining the efficiency of cosmic ray acceleration by cluster shocks. *MNRAS*, 459(1):70–83.

Vazza, F., Brunetti, G., and Gheller, C. (2009). Shock waves in Eulerian cosmological simulations: main properties and acceleration of cosmic rays. *MNRAS*, 395(3):1333–1354.

Vazza, F., Eckert, D., Brüggen, M., and Huber, B. (2015). Electron and proton acceleration efficiency by merger shocks in galaxy clusters. *MNRAS*, 451(2):2198–2211.

Verde, L., Treu, T., and Riess, A. G. (2019). Tensions between the early and late Universe. *Nature Astronomy*, 3:891–895.

VERITAS Collaboration, Acciari, V. A., Aliu, E., et al. (2009). A connection between star formation activity and cosmic rays in the starburst galaxy M82. *Nature*, 462(7274):770–772.

Vernstrom, T., Heald, G., Vazza, F., et al. (2021). Discovery of magnetic fields along stacked cosmic filaments as revealed by radio and X-ray emission. *MNRAS*, 505(3):4178–4196.

Vikhlinin, A., Burenin, R. A., Ebeling, H., et al. (2009). Chandra Cluster Cosmology Project. II. Samples and X-Ray Data Reduction. *ApJ*, 692(2):1033–1059.

Vink, J. and Yamazaki, R. (2014). A Critical Shock Mach Number for Particle Acceleration in the Absence of Pre-existing Cosmic Rays: $M = \sqrt{5}$. *ApJ*, 780(2):125.

Voit, G. M. (2005). Tracing cosmic evolution with clusters of galaxies. *Reviews of Modern Physics*, 77(1):207–258.

Voit, G. M., Kay, S. T., and Bryan, G. L. (2005). The baseline intracluster entropy profile from gravitational structure formation. *MNRAS*, 364(3):909–916.

Völk, H. J., Aharonian, F. A., and Breitschwerdt, D. (1996). The Nonthermal Energy Content and Gamma-Ray Emission of Starburst Galaxies and Clusters of Galaxies. *Space Sci. Rev.*, 75(1-2):279–297.

Völk, H. J. and Atoyan, A. M. (2000). Early Starbursts and Magnetic Field Generation in Galaxy Clusters. *ApJ*, 541(1):88–94.

Wakely, S. P. and Horan, D. (2008). TeVCat: An online catalog for Very High Energy Gamma-Ray Astronomy. In *International Cosmic Ray Conference*, volume 3 of *International Cosmic Ray Conference*, pages 1341–1344.

Walker, S. and Lau, E. (2022). Cluster outskirts and their connection to the cosmic web. *arXiv e-prints*, page arXiv:2202.07056.

Walker, S., Simionescu, A., Nagai, D., et al. (2019). The Physics of Galaxy Cluster Outskirts. *Space Sci. Rev.*, 215(1):7.

Walker, S. A., Hlavacek-Larrondo, J., Gendron-Marsolais, M., et al. (2017). Is there a giant Kelvin-Helmholtz instability in the sloshing cold front of the Perseus cluster? *MNRAS*, 468(2):2506–2516.

Walker, S. A., Mirakhor, M. S., ZuHone, J., et al. (2022). Is There an Enormous Cold Front at the Virial Radius of the Perseus Cluster? *ApJ*, 929(1):37.

Wang, T., Elbaz, D., Daddi, E., et al. (2016). Discovery of a Galaxy Cluster with a Violently Starbursting Core at z = 2.506. *ApJ*, 828(1):56.

Werner, N., Finoguenov, A., Kaastra, J. S., et al. (2008). Detection of hot gas in the filament connecting the clusters of galaxies Abell 222 and Abell 223. *A&A*, 482(3):L29–L33.

Werner, N., McNamara, B. R., Churazov, E., and Scannapieco, E. (2019). Hot Atmospheres, Cold Gas, AGN Feedback and the Evolution of Early Type Galaxies: A Topical Perspective. *Space Sci. Rev.*, 215(1):5.

Werner, N., Urban, O., Simionescu, A., and Allen, S. W. (2013). A uniform metal distribution in the intergalactic medium of the Perseus cluster of galaxies. *Nature*, 502(7473):656–658.

West, M. J., de Propris, R., Bremer, M. N., and Phillipps, S. (2017). Ten billion years of brightest cluster galaxy alignments. *Nature Astronomy*, 1:0157.

Wiener, J., Oh, S. P., and Guo, F. (2013). Cosmic ray streaming in clusters of galaxies. *MNRAS*, 434(3):2209–2228.

Wik, D. R., Hornstrup, A., Molendi, S., et al. (2014). NuSTAR Observations of the Bullet Cluster: Constraints on Inverse Compton Emission. *ApJ*, 792(1):48.

Willson, M. A. G. (1970). Radio observations of the cluster of galaxies in Coma Berenices - the 5C4 survey. *MNRAS*, 151:1.

Wise, M. W., McNamara, B. R., Nulsen, P. E. J., Houck, J. C., and David, L. P. (2007). X-Ray Supercavities in the Hydra A Cluster and the Outburst History of the Central Galaxy's Active Nucleus. *ApJ*, 659(2):1153–1158.

Wittor, D. (2021). On the Challenges of Cosmic-Ray Proton Shock Acceleration in the Intracluster Medium. *New Astr.*, 85:101550.

Wittor, D., Vazza, F., and Brüggen, M. (2017). Testing cosmic ray acceleration with radio relics: a high-resolution study using MHD and tracers. *MNRAS*, 464(4):4448–4462.

Wood, M., Caputo, R., Charles, E., et al. (2017). Fermipy: An open-source Python package for analysis of Fermi-LAT Data. In *35th International Cosmic Ray Conference (ICRC2017)*, volume 301 of *International Cosmic Ray Conference*, page 824.

Wu, H.-Y., Hahn, O., Wechsler, R. H., Mao, Y.-Y., and Behroozi, P. S. (2013). Rhapsody. I. Structural Properties and Formation History from a Statistical Sample of Re-simulated Cluster-size Halos. *ApJ*, 763:70.

Xi, S.-Q., Wang, X.-Y., Liang, Y.-F., et al. (2018). Detection of gamma-ray emission from the Coma cluster with Fermi Large Area Telescope and tentative evidence for an extended spatial structure. *Phys. Rev. D*, 98(6):063006.

Xie, C., van Weeren, R. J., Lovisari, L., et al. (2020). The discovery of radio halos in the frontier fields clusters Abell S1063 and Abell 370. *A&A*, 636:A3.

XRISM Science Team (2020). Science with the X-ray Imaging and Spectroscopy Mission (XRISM). *arXiv e-prints*, page arXiv:2003.04962.

Xu, J. and Han, J. L. (2022). Evidence for Strong Intracluster Magnetic Fields in the Early Universe. *ApJ*, 926(1):65.

Yang, H. Y. K., Gaspari, M., and Marlow, C. (2019). The Impact of Radio AGN Bubble Composition on the Dynamics and Thermal Balance of the Intracluster Medium. *ApJ*, 871(1):6.

Yang, H. Y. K. and Reynolds, C. S. (2016a). How AGN Jets Heat the Intracluster Medium—Insights from Hydrodynamic Simulations. *ApJ*, 829(2):90.

Yang, H. Y. K. and Reynolds, C. S. (2016b). Interplay Among Cooling, AGN Feedback, and Anisotropic Conduction in the Cool Cores of Galaxy Clusters. *ApJ*, 818(2):181.

Yu, L., Nelson, K., and Nagai, D. (2015). The Influence of Mergers on Scatter and Evolution in Sunyaev-Zel'dovich Effect Scaling Relations. *ApJ*, 807(1):12.

Zabalza, V. (2015). naima: a python package for inference of relativistic particle energy distributions from observed nonthermal spectra. *Proc. of International Cosmic Ray Conference 2015*, page 922.

Zandanel, F. and Ando, S. (2014). Constraints on diffuse gamma-ray emission from structure formation processes in the Coma cluster. *MNRAS*, 440(1):663–671.

Zandanel, F., Pfrommer, C., and Prada, F. (2014). On the physics of radio haloes in galaxy clusters: scaling relations and luminosity functions. *MNRAS*, 438(1):124–144.

Zemcov, M., Blain, A., Cooray, A., et al. (2013). HerMES: A Deficit in the Surface Brightness of the Cosmic Infrared Background due to Galaxy Cluster Gravitational Lensing. *ApJ*, 769(2):L31.

Zhang, C., Churazov, E., Forman, W. R., and Lyskova, N. (2019). Runaway merger shocks in galaxy cluster outskirts and radio relics. *MNRAS*, 488(4):5259–5266.

Zhuravleva, I., Allen, S. W., Mantz, A., and Werner, N. (2018). Gas Perturbations in the Cool Cores of Galaxy Clusters: Effective Equation of State, Velocity Power Spectra, and Turbulent Heating. *ApJ*, 865(1):53.

Zhuravleva, I., Churazov, E., Arévalo, P., et al. (2015). Gas density fluctuations in the Perseus Cluster: clumping factor and velocity power spectrum. *MNRAS*, 450(4):4184–4197.

Zubeldia, Í. and Challinor, A. (2019). Cosmological constraints from Planck galaxy clusters with CMB lensing mass bias calibration. *MNRAS*, 489(1):401–419.

ZuHone, J. and Su, Y. (2022). The Merger Dynamics of the X-ray Emitting Plasma in Clusters of Galaxies. *arXiv e-prints*, page arXiv:2202.06712.

ZuHone, J. A., Brunetti, G., Giacintucci, S., and Markevitch, M. (2015). Testing Secondary Models for the Origin of Radio Mini-Halos in Galaxy Clusters. *ApJ*, 801(2):146.

ZuHone, J. A., Markevitch, M., Brunetti, G., and Giacintucci, S. (2013). Turbulence and Radio Mini-halos in the Sloshing Cores of Galaxy Clusters. *ApJ*, 762(2):78.

ZuHone, J. A., Markevitch, M., and Johnson, R. E. (2010). Stirring Up the Pot: Can Cooling Flows in Galaxy Clusters be Quenched by Gas Sloshing? *ApJ*, 717(2):908–928.

ZuHone, J. A., Markevitch, M., Weinberger, R., Nulsen, P., and Ehlert, K. (2021). How Merger-driven Gas Motions in Galaxy Clusters Can Turn AGN Bubbles into Radio Relics. *ApJ*, 914(1):73.

Zuhone, J. A. and Roediger, E. (2016). Cold fronts: probes of plasma astrophysics in galaxy clusters. *Journal of Plasma Physics*, 82(3):535820301.

ECOLE DOCTORALE

Titre: Étude des propriétés thermiques et non-thermiques du plasma diffus dans les amas de galaxies

Mots clés: Amas de galaxies: milieu intra-amas. Mécanismes de radiation: thermique et non-thermique, Techniques: haute résolution angulaire, observations des rayons γ

Résumé: Les amas de galaxies représentent la dernière étape de la formation des structures à grande échelle dans l'Univers. Ils sont reconnus comme l'une des sondes cosmologiques les plus importantes, mais aussi comme des laboratoires cosmiques uniques. Les amas se forment par accrétion de matière environnante et par fusion de sous-amas, lors d'événements très énergétiques, formant finalement une phase gazeuse diffuse dominée par une composante thermique chaude, mais conduisant également à l'accélération de particules jusqu'à de très hautes énergies.
Cette thèse d'habilitation à diriger les recherches résume les efforts déployés au cours des dernières années pour comprendre les mécanismes astrophysiques associés à la formation et à l'évolution du milieu intra-amas. La première partie passe en revue les développements réalisés dans le domaine millimétrique avec les caméras NIKA et NIKA2, et largement complétés par d'autres observations, afin de sonder la physique thermique du gas à haute résolution angulaire et mesurer son évolution en redshift. Dans la deuxième partie, la recherche de l'émission diffuse de rayons γ dans les amas de galaxies, qui trace la physique des rayons cosmiques, est passée en revue. L'accent est mis sur les derniers résultats obtenus avec les données de *Fermi-LAT* et présente les perspectives pour les futures observations de CTA. La troisième partie traite des perspectives futures. Elle se concentre sur des moyens alternatifs pour sonder la physique des rayons cosmiques dand les amas, mais aussi sur la possibilité d'utiliser des observations millimétriques résolues pour mieux comprendre la co-évolution des composantes thermiques et non-thermiques dans les amas.

Title: Thermal and non-thermal properties of the diffuse plasma in galaxy clusters

Keywords: Galaxy clusters: intra-cluster medium. Radiation mechanisms: thermal and non-thermal, Techniques: high angular resolution, γ-ray observations

Abstract: Galaxy clusters represent the last step of the formation of large-scale structures in the Universe. They are recognized as one of the most important cosmological probes and unique cosmic laboratories. Clusters grow by accretion of the surrounding material and from the merging of sub-clusters, in very energetic events, eventually forming a diffuse gas phase dominated by a hot thermal component, but also leading to particle acceleration up to very high energies.
This habilitation thesis summarizes the efforts made over the last few years to understand the astrophysical mechanisms associated with the formation and evolution of the intra-cluster medium. The first part reviews the developments made in the millimeter band with the NIKA and NIKA2 cameras, extensively complemented by other observations, to probe the thermal gas state at high angular resolution and measure its redshift evolution. In the second part, the search for the diffuse γ-ray emission from galaxy clusters, which probes the cosmic ray physics, is reviewed. It highlights the latest results obtained with the *Fermi-LAT* data and presents the expectations for future CTA observations. The third part discusses prospects. It focuses on alternative means to probe the cluster cosmic rays, but also on the possibility to use resolved microwave observations to understand better the coevolution of the thermal and non-thermal cluster components.

Institut Polytechnique de Paris
91120 Palaiseau, France